



Technische Universität München
Fakultät für Maschinenwesen
Lehrstuhl für Mikrotechnik und Medizingerätetechnik
Univ.-Prof. Dr. Tim C. Lüth

Master Thesis

Design Optimization and Characterization of a Double-Arm Endoscopic Mini-Manipulator

Mar Olmeda Palomar

Matr.-Nr.: 03676703

Supervising University Professor: Univ.-Prof. Dr. Tim C. Lüth

Thesis Advisor: Suat Cömert, M. Sc.

Thesis Co-Advisor: Stefan Leonhardt, M. Sc.

Date started: 01.12.2017

Date submitted: 31.05.2017

Own Work Declaration

Hereby I confirm that this is my own work and I referenced all sources and auxiliary means used and acknowledged any help that I have received from others as appropriate.

Garching, May 31st 2017

Mar Olmeda Palomar

Acknowledgements

This thesis has been developed within the framework of the Master's degree in Medical Technology and Engineering at the Institute of Micro Technology and Medical Device Technology (MIMED) at the Technische Universität München.

First and foremost, I would like to thank my thesis advisor Suat Cömert for his knowledge, motivation, patience and great enthusiasm. He would always have time to listen and to give advice, and his guidance helped me throughout writing this thesis.

I would also like to acknowledge Stefan Leonhardt, who, as my co advisor, guided one of the most important parts of my project and for teaching me everything about such an interesting topic.

I am also very grateful to Univ.-Prof. Dr. rer. nat. Dipl.Ing. Tim C. Lüth for giving me the opportunity of writing my master thesis at his department.

I wish to thank all the people who have contributed in some way to the work described in this thesis.

And finally, I would like to express my deepest gratitude to my friends and family, but especially to my parents for their wise counsel and continuous encouragement. Despite the distance, they have always been by my side, making everything easier and supporting every decision I have taken. Thank you.

Garching, May 2017

Mar Olmeda Palomar

Table of Contents

Own Work Declaration	II
Acknowledgements	III
Table of Contents	IV
1 Introduction.....	1
1.1 Problem Definition	2
1.2 State of the Art and Research	5
1.2.1 Compliant Mechanisms.....	5
1.2.2 Flexibility and Strength.....	9
1.2.3 Linear and Nonlinear Deflections	10
1.2.4 Modeling Compliant Mechanisms	14
1.2.5 Processing Techniques	19
1.2.6 Steam Sterilization Method.....	23
1.2.7 Sterilization of Hollow Instruments	25
1.3 Drawbacks of the State of the Art and Research	31
1.3.1 Compliant Mechanisms.....	31
1.3.2 Processing Techniques	32
2 Materials and Methods.....	35
2.1 Preliminary Considerations	35
2.2 Task Description.....	36
2.3 Expected Advantages and Functions of the Solution	37
2.4 Solution Structure	37
2.5 Solution Process.....	38
2.6 Distinctive Features of the Solution	41
2.7 Realization – Mechanical Characterization	42
2.7.1 Definition of the Model.....	42
2.7.2 Compliant Mechanism Test Sample Design	44
2.7.3 Tensile Test	48
2.8 Realization – Medical Processability.....	50
2.8.1 Process Challenge Device Conception.....	50
2.8.2 Processing Steps	53
2.8.3 Validation Process.....	58
3 Experiments	64
3.1 Experiment I – Mechanical Characterization	64
3.1.1 Determination of the Measurement Procedure.....	64
3.1.2 Experiment for Measuring the Advantages.....	66
3.1.3 Summary of the Results	72
3.2 Experiment II – Medical Processability	72
3.2.1 Determination of the Measurement Procedure.....	72
3.2.2 Experiment for Measuring the Advantages.....	74
3.2.3 Summary of the Results	80

4 Summary and Outlook	81
References	82
LIST OF FIGURES	87
LIST OF TABLES	90
Appendix A – Nitinol Material Certificate	91
Appendix B – Stainless Steel Material Certificate	92
Appendix C – Nitinol Tensile Test	93

1 Introduction

With the widespread introduction of minimally invasive surgery (MIS) and its remarkable growth over the last decades, open surgery is being more and more routinely replaced by minimal access techniques (Swanstrom *et al.*, 2005; Gillen *et al.*, 2010). Laparoscopic surgery has become the standard procedure for several interventions thanks to its beneficial clinical outcomes backed up mainly by a reduced surgical trauma and an improved cosmetic result (Antoniu and Bartsch, 2012). This modern surgical concept refers to the way of proceeding through small incisions in the abdomen where the instruments will afterwards be located. Nevertheless, the placement of the ports is known to result in several complications, namely vascular and visceral injuries, port-site hernias and metastases, wound infections and surgical emphysemas among others (Pemberton *et al.*, 2006). For this reason and to further decrease the invasiveness, new and improved instrumentation have been developed in such a way that single-incision and natural orifice access routes could become the preferred approach, combined with MIS approaches when more complex procedures are carried out (Vitiello *et al.*, 2013).

Entering the surgical field via natural orifices for both diagnosis and therapeutic aims means being able to avoid skin incisions, thus emphasizing some of the well-recognized advantages: reduced patient pain and morbidity, shortened recovery time, improved cosmesis and ensured overall cost-effectiveness among others (Vitiello *et al.*, 2013). The development of these scarless and innovative techniques represents a continuous evolution of the traditional surgical instrumentation and, particularly, of the conventional flexible devices, namely endoscopes.

Flexible endoscopic surgery (FES), which was initially limited to the intestinal lumen, has already become a major part of surgery and it is thought to be a potential approach for a wider range of surgical fields (Yoshida *et al.*, 2010). Originally developed for diagnostic purposes, it has over time technically evolved and has made its way also toward therapeutic applications. Nevertheless, this technical evolution has not directly been related with the design of the endoscope itself, but with the introduction of highly sophisticated accessories trying to overcome some of the technical hurdles of the not-yet-further-developed endoscopes. This discordance has led to an inappropriate task performance that cannot be solved until the fundamentals of their design address the existing limitations and evolve in a more procedure-specific manner (Thompson *et al.*, 2009).

Therefore, there is a need of further expanding the capabilities of endoscopic surgeries so as to be incorporated into everyday clinical practice. Some of the well-known limitations of the nowadays FES instrumentation include lack of stability and triangulation of instruments, improper tissue handling and deficient force transmission to properly proceed regarding the singularities of each intervention (Patel *et al.*, 2015). In addition to these shortcomings, limited instrument freedom, insufficient distal dexterity and troublesome access to the surgical field can also be listed, as well as proof of suitability for being sterilized (Shang *et al.*, 2011).

Relevant advances in technology and knowledge have led to the ongoing development of complex medical devices trying to overcome some of the previously mentioned deficiencies to support the delivery of healthcare to patients. However, the way of solving them has led to complicated designs, which are potentially more difficult to clean, disinfect and sterilize. Because such procedures involve contact by medical instruments within the patient's body, it is essential to safely process them in a compatible and effective way. The use of a proper sterilization technique is critical for ensuring that they do not represent a major risk to patients (Rutala and Weber, 2004).

It is then to be outlined that modifications of the current flexible scopes are particularly noteworthy given the ongoing settlement of the endoscopic techniques. During the design and development phases of a medical product, aspects regarding its aptness to be processed have to be yet taken into account. However, there might be some limits if a more procedure-oriented instrumentation is to be obtained, hence leading to improved clinical outcomes. As a result, the scope of natural orifice surgery should be finally optimally standardized.

In light of the previously mentioned limitations posed by these emerging techniques, there is a Double Arm Endoscopic Mini-Manipulator System which is currently being developed at the Institute of Micro Technology and Medical Device Technology at the Technical University of Munich. This novel platform seeks to obtain an intervention-specific way of proceeding that fits properly into the current clinical workflow for Transurethral Resection of Bladder Tumors (TURBT), providing accurate and assorted movements that aim to ensure more efficient and safer clinical outcomes. This particular manipulator, later on further detailed, is going to be the focus of this work. The main goal is to optimize its design regarding mechanical considerations and to characterize its suitability for being medically processed, which is of great relevance for the performance of the required task and a preliminary condition before its commercialization.

The results obtained with the current work can afterwards be generalized for other medical devices, acting thus as general guidelines and representing therefore very useful information when developing new medical devices.

1.1 Problem Definition

As previously outlined, there is a highlighted need for developing new instrumentation specifically engineered to overcome the technical hurdles of the nowadays used instrumentation. When designing new instrumentation or improving the already available one, several factors should be taken into account and many challenges might be faced. Because of the complexity of the currently performed surgical interventions, also the tools used are becoming more complex and there is a demand for miniaturization, which requires additional efforts on the whole process.

Some of these challenges are closely related with the mechanical and technical considerations that such devices should fulfill, for instance the ones regarding flexibility, robustness, fatigue failure or the full coverage of the surgical workspace. Besides, the processability of the new instruments should also be considered, meaning the cleaning, disinfection and sterilization processes that they must be put through before being employed in medical interventions with real-life patients. Attention should be paid to all these aspects, in order for the newly developed system to be suitable for the desired application.

The problems covered by this work are related with the previously mentioned manipulator system based on compliant mechanisms. Surgical instruments based on compliant mechanisms can be of greater interest over conventional MIS instruments and the available robotic platforms: they allow precise and natural hand movements with haptic feedback even in complex interventions (Kota *et al.*, 2005). Nevertheless, the inherent flexibility of these compliant devices makes modeling very complex and specific to the particular engineering applications for which they are developed. For that reason and in order to make use of them, it should be known beforehand how they behave.

As in the previous section already introduced, the present manipulator is going to be applied for the transurethral resection of bladder tumors (TURBT), procedure illustrated in Figure 1.1, which represents the standard procedure for non-muscle invasive bladder cancer (NMIBC); meaning tumors that have not grown into the main muscle layer of the bladder (Smith, 1989). Despite its general practice, conventional TURBT, performed with a resectoscope, is still nowadays associated with patient morbidity due to the high rates of recurrence and progression to invasively growing tumors (Babjuk, 2009). Technological and anatomical constraints are thought to be the main causes for such complications (Goldman *et al.*, 2013; Wilby *et al.*, 2009). The location of the tumor might influence its resectability due to the kinematically impossibility of tracing some challenging areas with the optimal resection angle (Ukai *et al.*, 2000). Piece-meal eradication of the tumor is also believed to influence recurrence rates since it contributes to the seeding of tumor cells all over the bladder (Ray and O'Brien, 2007), so does the use of the cauterization wire loop, which can additionally lead to a later misdiagnosis while staging the tumor (Babjuk, 2009).

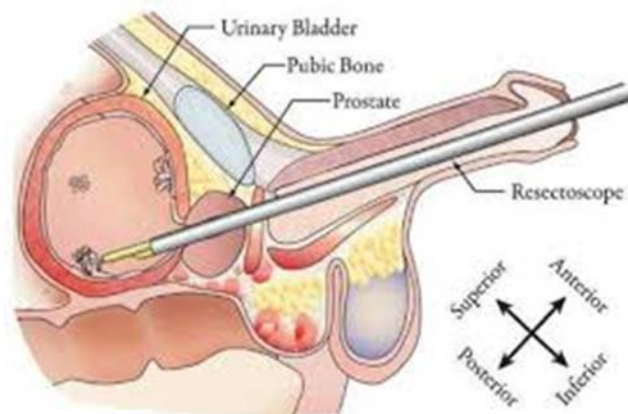


Figure 1.1: Transurethral Resection of Bladder Tumors (TURBT). (Source: Bajo *et al.*, 2013).

In order to address these limitations and considering the increased importance of a proper TURBT with the complete removal of the entire tumor, the current continuum manipulator was developed. It seeks to improve clinical outcomes since it supports the en bloc resection technique (see Figure 1.2), allowing simultaneous use of a grasper forceps and a laser fiber. Laser fibers such as holmium ones provide several benefits compared to the traditional instrumentation. It enables coagulation of the tumor margins and use of the laser on its base, as well as a decrease of the cellular seeding potential (Smith, 1989).

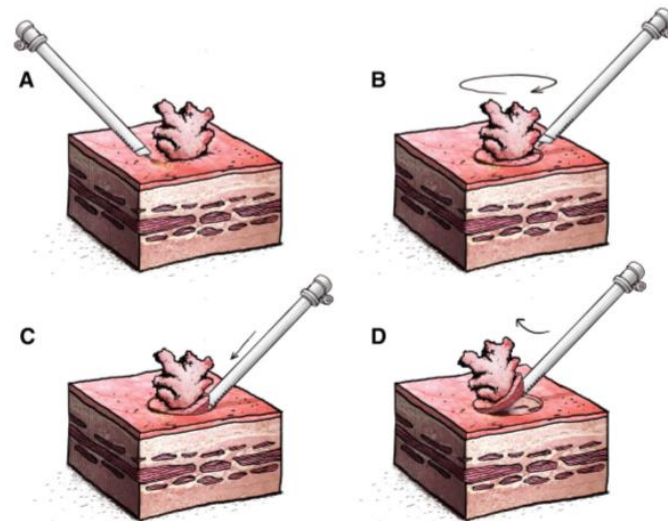


Figure 1.2: En bloc resection technique of a bladder tumor. (A), (B) A superficial circular incision around the tumor is initially made, keeping a margin of the resection site. (C) The tumor is then en bloc resected with the aid of the instruments. (D) Finally the base of the tumor is coagulated by the laser fiber, as well as the remaining adhesions. (Source: Kramer *et al.*, 2015).

Since bladder cancer represents the ninth most common cancer worldwide, with approximately 430.000 new cases and 165.000 deaths in 2012 (Stewart and Wild, 2014), it is then evident the importance of a complete resection of the tumor for adequately diagnosing, staging, and treating it. That means being able to reach all the regions of the urinary bladder, including the most challenging ones such as the ones located behind the bladder neck and in the anterior bladder wall (Herrell *et al.*, 2014). If not properly performed, incomplete resection of the tumor can lead to high recurrence rates (Jurewicz and Soloway, 2014). Hence an optimal design of the compliant mechanisms that form the manipulator is required. Since the manipulator should easily cover the whole surgical workspace, reaching all tumors regardless of their location, the optimal design would be a feasible design capable of achieving a tradeoff between flexibility and strength, providing therefore the largest deflection without reaching failure due to plastic deformation. For that reason, statements about the behavior of compliant mechanisms must be derived, so the optimal geometry for this specific procedure can finally be determined.

Newly developed instruments, on the other hand, have to prove their suitability to be processed before being legally introduced into the market. According to the classification proposed by Dr. E. H. Spaulding, widely accepted and used by the Food and Drug Administration (FDA) among other institutions, patient-care items and equipment should be categorized as critical, semicritical and non-critical regarding the risk of infection involved with their use. These categories specify the extent to which the medical devices should be processed, and whether they need to be finally sterilized or not (British Columbia Ministry of Health, 2011).

As already stated, innovative instrumentation is becoming more complex, as the procedures do, with the subsequent rigorous processing requirements. Given the increasing use of minimally invasive devices, such as endoscopes with narrow lumens of extended lengths and small diameters, or hollow instruments such as catheters and medical devices mainly used in ENT surgery, neurosurgery or ophthalmology (Deutsche Gesellschaft für Sterilgutversorgung, 2006); it raises the question as to whether these complex instruments can be safely sterilized. To that end, there is a need for appropriate testing methods to validate the technology for sterilizing these instruments (Dufresne *et al.*, 2008).

In particular, our snake-like manipulator has on its wall small actuation channels, where the tendon driven actuation needs to be placed, representing the most challenging geometry to be processed; in addition to its two instrument channels. To further research and contribute to this topic, statements about the limits of the geometry which can be properly processed will be made.

Consequently, two different aspects related with the design of the surgical manipulator will be addressed, namely its mechanical characterization and medical processability, for which two different projects will be carried out. The general structure of the present thesis including both parts is organized as follows. In the next section, the state of the art and research are going to be presented, as well as their corresponding drawbacks, introducing some important concepts for a better understanding of the thesis outline. Chapter 2 thoroughly explains the materials and methodology used to perform the experiments and carried out for the realization of the current work. Herein main goals and required tasks will be described, as well as the solution adopted. The description of the experiments lies in Chapter 3, with the presentation of their corresponding results. Finally, Chapter 4 summarizes the most relevant aspects of the work. It also presents major conclusions and states potential future work.

1.2 State of the Art and Research

1.2.1 Compliant Mechanisms

To begin with and before discussing the wider issues relating to the modeling and analysis of compliant mechanisms, some fundamental knowledge should be first introduced:

“A mechanism is a mechanical device that has the purpose of transferring motion and/or force from a source to an output” (Erdman *et al.*, 2001).

Two different major categories of mechanisms are going to be addressed along this chapter, rigid-body mechanisms (RBM) and compliant mechanisms (CM) (Figure 1.3). Conventional rigid-body mechanisms make use of rigid links or pins connected at movable joints and gain all of their motion thanks to the relative movement between their rigid parts through these joints.

Compliant mechanisms, on the other hand, are mechanical devices that achieve motion via elastic deformation. Unlike rigid-link mechanisms, which perceive elastic deformation as an undesired property, compliant mechanisms find their functional principle in their flexibility acting as the source for motion or force transmission, allowing them to perform the specific task. When applying a force, the mechanism will undergo elastic deformation, hence achieving the desired output movement (Frecker *et al.*, 1997).

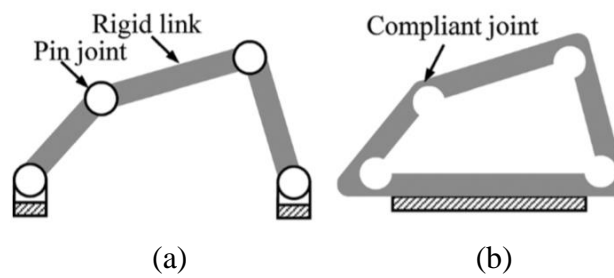


Figure 1.3: Mechanisms. (a) Rigid-body mechanism (RBM). (b) Fully compliant mechanism (CM). (Source: Cao *et al.*, 2015).

These single-piece compliant mechanisms find their application in a wide range of areas in general, and in the engineering design of surgical tools for minimally invasive procedures, in particular.

Some of the already developed instruments for such procedures which make use of compliant mechanisms are, for example, a fully compliant and monolithic kidney gripper and manipulator (Kota *et al.*, 2005), a multifunctional compliant scissors–forceps instrument for MIS (Frecker *et al.*, 2005), a compliant endoscopic suturing device (Cronin *et al.*, 2008), a narrow-gauge compliant forceps for NOTES (Aguirre *et al.*, 2011), and a compliant articulation structure for surgical tool tips used in NOTES procedures (Liu *et al.*, 2013), which can all be seen in the figures below.

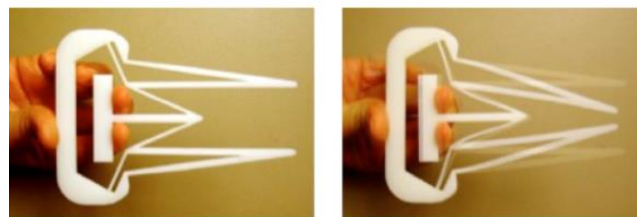


Figure 1.4: Prototype of the fully compliant and monolithic kidney gripper and manipulator in its inactive and gripping mode, respectively. (Source: Kota *et al.*, 2005).

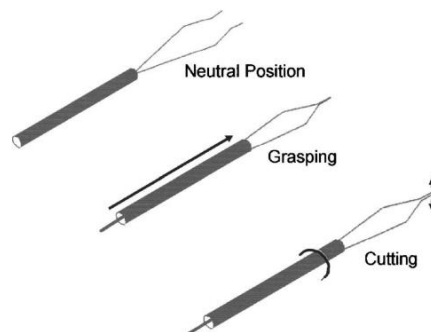


Figure 1.5: The scissors-forceps end-effector design at its neutral, grasping and cutting positions. (Source: Frecker *et al.*, 2005).

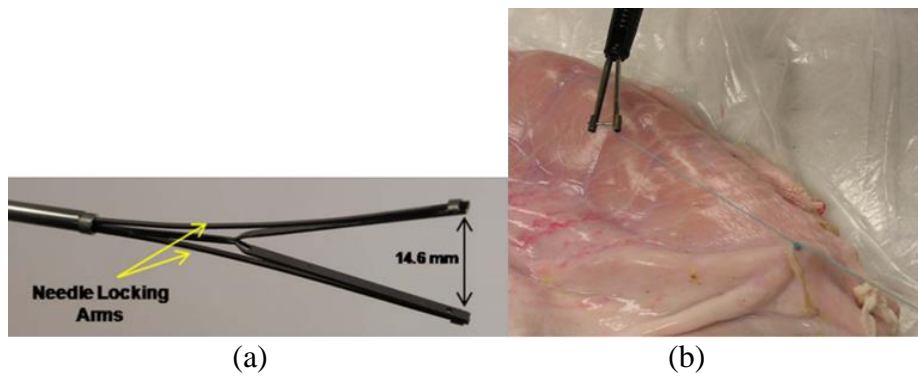


Figure 1.6: Compliant suturing device. (a) Prototype. (b) Suture of a porcine stomach. (Source: Cronin *et al.*, 2008).

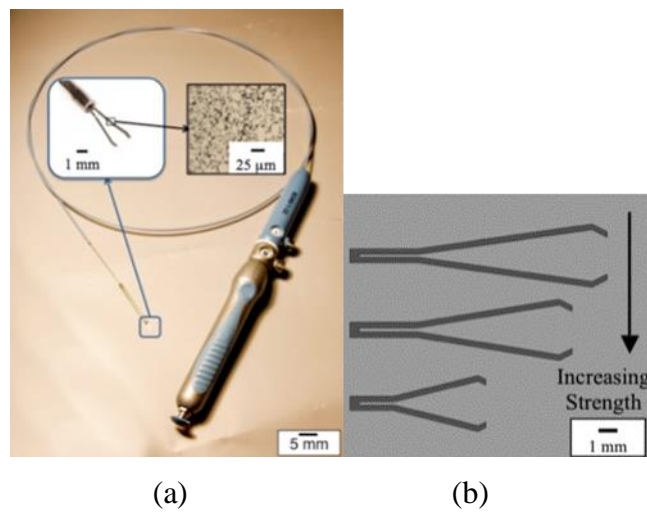


Figure 1.7: Compliant forceps for NOTES. (a) Prototype. (b) Optimal designs. (Source: Aguirre *et al.*, 2011).

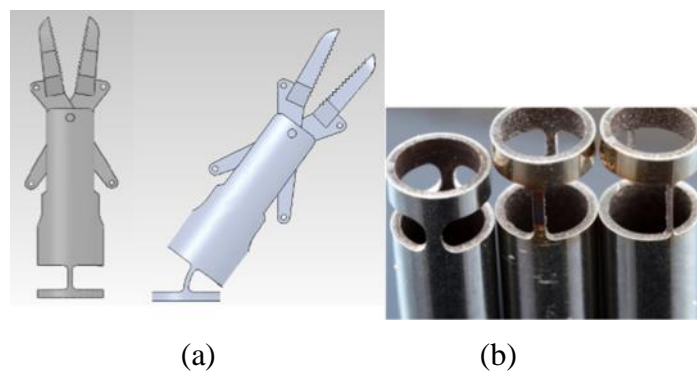


Figure 1.8: Compliant articulation structure. (a) Integration of a surgical tool tip. (b) Designs of the compliant structure to be tested. (Source: Liu *et al.*, 2013).

Several advantages come with the design of a compliant device-based instrument, which can be divided into two different categories regarding cost reduction and increased performance.

Cost reduction advantages derive from the part-count reduction, as well as from the decreased assembly time and the more simplified manufacturing process; which can be dramatically reduced if single-piece compliant mechanisms are used, being this monolithic nature of great interest for small-scale medical applications. Moreover, this property adds further benefits in terms of the sterilization process (Kota *et al.*, 2005). Also important for such minimally invasive procedures is the ease of miniaturization that allows them to be used in medical applications where the workspace is reduced or the tools not easily accessible (Howell, 2001).

On the other hand, the lack of traditional joints leads to an increased performance, highly desired in surgery, in a way that there is no need for lubrication, a reduced wear is achieved and the precision of the tool is enhanced because of the fact that backlash may be reduced or totally eliminated. The increased dexterity is also backed up by the significant reduction of weight when compared with rigid-body mechanisms. The absence of pinch points and crevices and a reduced maintenance are another of the provided benefits.

Because compliant mechanisms are not able to produce the same range of motion as rigid-body mechanisms do (Howell, 2001), nitinol material was chosen for the developed manipulator in order to overcome this limitation. Nitinol represents a metal alloy of Nickel and Titanium. Two different thermomechanical properties, besides its biocompatibility, characterize nitinol as the material of choice for surgical applications requiring enormous flexibility and motion, the *superelasticity* (SE; also called Pseudoelasticity, PE) and the *shape memory effect* (SME), being the former the relevant one for the present study.

Superelasticity refers to the ability of fully recovering of quite unusual large strains, up to 8%, once an applied mechanical stress has been released, provided that permanent deformation was not yet reached. This effect, which is the outcome of a phase transformation between the austenitic and martensitic phases of a crystal, yields a wider range of motion during the task performance and can therefore benefit the operation principle of the compliant mechanisms-based instruments (Lagoudas, 2011).

Nickel-titanium material properties defining the behavior of the alloy significantly depend on factors such as alloy composition and processing conditions, including particular heat treatments previously applied and hot/cold-working, which can produce alterations of the characteristic behavior to a great extent. (Miller and Lagoudas, 2000; Biscarini *et al.*, 2008; Lagoudas, 2011; Wu, 2002). For these reasons, a mechanical characterization of this particular shape memory alloy (SMA) needs to be performed with the corresponding tensile test, in order to obtain distinct quantitative material properties, such as the elastic modulus or the yield strength, required for the execution of the current dissertation.

Besides the previously mentioned beneficial attributes of nitinol, it also presents some other great advantages over the traditionally used stainless steel material such as excellent kink resistance, elastic and thermal deployment, constant unloading stress, biomechanical compatibility, hysteresis, fatigue resistance and uniform plastic deformation among others, which provide its suitability for a wide variety of medical applications (Wu, 2002; Biscarini *et al.*, 2008).

1.2.2 Flexibility and Strength

The behavior of a compliant mechanism will mainly depend on two different properties: flexibility and strength, which are not necessarily related but will, however, determine its characteristic failure reaction.

The term flexibility, opposite to stiffness or rigidity, is related with the amount of deflection a part will experience when a specific load is applied. For equally applied forces, the larger this deflection, the higher the flexibility of the part.

The stiffness or rigidity of a part depends on both material and geometrical properties. The stiffness of a material is usually measured by applying uniaxial loads to the part and measuring afterwards the resulting deformation.

Strength, on the other hand, is just a property of the material and represents the maximum stress that can be withstand before failure by fracture or excessive deformation. The most common stresses compliant mechanisms are subjected to are axial and bending stresses, being respectively defined as:

$$\sigma = \frac{F}{A} \quad (1.1)$$

$$\sigma = \frac{My}{I} \quad (1.2)$$

, where F represents the axial force, A the area of the cross section, M the moment load, y the distance from the neutral axis to the point of interest and I the moment of inertia of the cross section.

For the bending stress, the maximum value occurs at the farthest point from the neutral axis, which will be designated as c , and it can be formulated as follows:

$$\sigma = \frac{Mc}{I} \quad (1.3)$$

For the current thesis, it is of great interest the definition of concepts such as the elastic modulus and the yield strength, being both related with flexibility and strength properties. The so-called tensile test, represented in Figure 1.9, is the experimental test method most widely used to characterize the mechanical properties of materials. This test consists on the gradual application of a uniaxial load until fracture and the measurement of the resulting deformation of the part. Important information concerning the material's elastic properties, the character and extent of plastic deformation, and yield and tensile strength can be obtained (Hertzberg, 1989).

The elastic modulus is characteristic of a specific material and defines its behavior in the elastic region; in other words, the resistance of the material to deform within the linear area. According to Hertzberg (1989), the yield strength, σ_{ys} , is defined as the stress level at which irreversible plastic deformation begins. It can be obtained as the intersection, point A in Figure 1.9, between the characteristic $\sigma - \epsilon$ curve and a 0.2% offset parallel line of the initial proportional range, the one represented with dashed line.

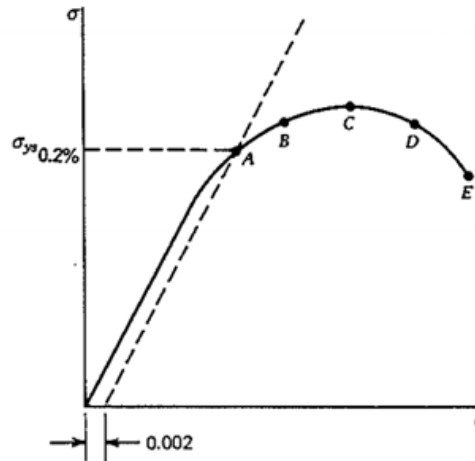


Figure 1.9: Stress-strain diagram of a typical tensile test. (Source: Hertzberg, 1989).

The definition of both properties is necessary for the consequent understanding of the thesis, and provided that both of them will play an important role on the design and analysis of compliant mechanisms.

1.2.3 Linear and Nonlinear Deflections

In most deflection analyses, linear equations can be used considering the following assumptions: the deflection of the structure is small compared with its global dimensions, the material is supposed to be elastic and stresses and strains are proportional. However, there are situations in which these assumptions are no longer valid due to nonlinearities, nor are the provided results with linear equations.

Structural nonlinearities have their source in material and geometric nonlinearities. Material nonlinearities originate when Hooke's law does not apply anymore, for instance, when plasticity, nonlinear elasticity, hyperelasticity or creep are being considered. On the other hand, geometric nonlinearities take place when conditions such as large deflections, stress stiffening or large strains are involved and the resulting deflections change therefore the nature of the problem.

In the following section, the most common methods of designing and analyzing compliant mechanisms will be presented.

Linear Analysis

When considering only small deflections, linear analysis is performed and conventional linear beam theory can be used. The classical beam theory, also known as Bernoulli-Euler beam theory, represents a method of calculating the load-carrying and deflection characteristics of beams, such as the flexible cantilever beam represented in Figure 1.10.

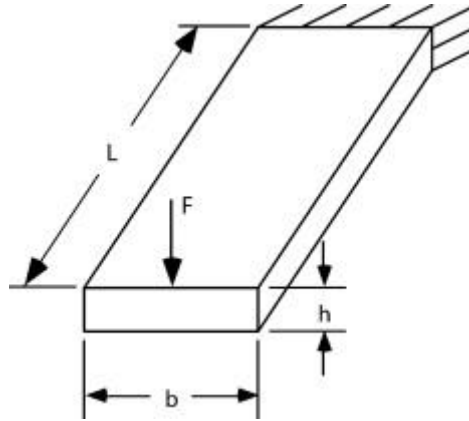


Figure 1.10: Flexible cantilever beam. (Source: Howell, 2013).

The Bernoulli-Euler equation states that the bending moment resulting of laterally loading a beam is proportional to its curvature, and it can be expressed as follows:

$$M = EI \frac{d\theta}{ds} \quad (1.4)$$

, representing M the bending moment; $d\theta/ds$ the rate of change in angular deflection along the beam, in other words, the beam's curvature; E the Young's modulus of the material and I the beam moment of inertia. For a better understanding, it can be applied to a cantilever beam, like the one shown in Figure 1.11. The curvature of the beam can be defined in terms of the transverse deflection, y , and the coordinate along the undeflected beam axis, x , like:

$$\frac{d\theta}{ds} = \frac{d^2y/dx^2}{[1 + (dy/dx)^2]^{3/2}} \quad (1.5)$$

Because linear analysis is being considered, only small deflections occur. It can therefore be assumed that the term represented by $(dy/dx)^2$ can be neglected when compared to unity, yielding the classical linear beam moment-curvature equation:

$$M = EI \frac{d^2y}{dx^2} \quad (1.6)$$

, with its correspondent beam angle, or slope, equation,

$$\theta = \frac{dy}{dx} \quad (1.7)$$

If we consider the cantilever beam with a vertical bending moment at its free end, as the one in Figure 1.11, the equation that provides the deflected angle can be easily obtained by substituting Equation (1.7) into Equation (1.6) and integrating it:

$$\theta = \frac{dy}{dx} = \frac{Fx}{2EI}(2L - x) \quad (1.8)$$

, having previously rewritten the bending moment as $M = F(L - x)$. Equation (1.8) provides information about the deflected angle of a cantilever beam when a moment is being applied at one of its free ends.

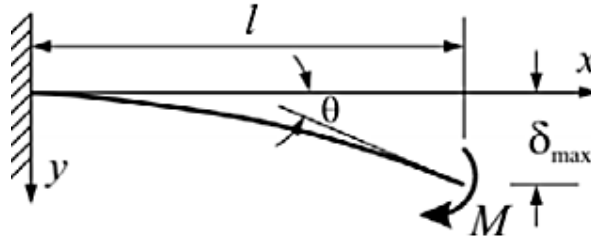


Figure 1.11: Flexible cantilever beam with a moment applied at its free end. (Source: Beam Deflection Formulae).

Nonlinear Analysis

Because compliant mechanisms rely on flexible members to perform their task, large deflections are therefore experienced by these mechanisms, entailing the need for nonlinear equations accounting for geometric nonlinearities (Howell, 2001).

The difference in analysis between linear and nonlinear considerations lies in the treatment of the Bernoulli-Euler beam equation (refer to Equation (1.4)), particularly in the assumption made about the slope of the beam. When large-deflection analysis applies, the slope of the beam is no longer small and nor is the validity of such assumption.

In this case, and following with the cantilever beam example (Figure 1.12), on the basis of Equation (1.4) the chain rule of differentiation has to be used to rewrite the equation into the following one:

$$\frac{M_0}{EI} = \frac{d\theta}{ds} = \frac{d\theta}{dy} \frac{dy}{ds} \quad (1.9)$$

Separating variables and making the appropriate arrangements to the equation results in,

$$\int_0^b dy = \frac{EI}{M_0} \int_0^{\theta_0} \sin \theta d\theta \quad (1.10)$$

Integrating the former equation yields,

$$\frac{b}{L} = \frac{1 - \cos \theta_0}{\theta_0} \quad (1.11)$$

, or

$$\frac{a}{L} = \frac{\sin \theta_0}{\theta_0} \quad (1.12)$$

, where the deflected angle of the beam end, θ_0 , can be found and expressed in terms of the nondimensionalized vertical or horizontal beam deflection respectively, as represented in Figure 1.12.

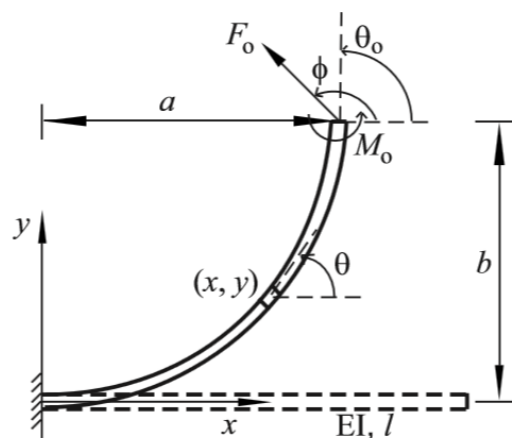


Figure 1.12: Large deflection of a cantilever beam. (Source: Su, 2009).

1.2.4 Modeling Compliant Mechanisms

Derivation of closed-form solutions are much more difficult for structures with large deflections and more complex loading conditions than the one illustrated in the previous section. For this reason different solution techniques of approaching the design and analysis of compliant mechanisms are also available and the most common used ones will now be introduced.

Elliptic Integral Solutions

Elliptic integrals are functions where an input is introduced and an output calculated by a series expansion or a table is returned. They can be divided into first, second and third kind and they may require one, two or even three independent variables as inputs. The method is widely used to solve large-deflection problems with different and more complex loading conditions, being able to provide exact, closed-form solutions by solving second-order, nonlinear differential equations using these elliptic integrals.

The elliptic integrals used in large-deflection analyses are the ones of first and second kinds, which are defined as follows:

$$F(\phi, k) = \int_0^{\phi} \frac{d\theta}{\sqrt{1 - k^2 \sin^2 \theta}} \quad (1.13)$$

$$E(\phi, k) = \int_0^{\phi} \sqrt{1 - k^2 \sin^2 \theta} \, d\theta \quad (1.14)$$

, where ϕ is known as the amplitude and k the modulus of the elliptic integral.

The way of proceeding consists of three different steps:

- 1) Obtaining the equations to be solved. These equations involve integral terms which cannot be solved by usual methods,
- 2) Arrangement of the integral terms in such a way that elliptic integrals can be used,
- 3) Choose an available and appropriate form in the elliptic function tables

This particular method provides the background needed for the development of another approximate methods for helping in the analysis and design of compliant mechanisms, for instance the one introduced by (Shoup and McLarnan, 1971) and (Shoup, 1972), who applied the equations of the undulating and nodal elastica for the analysis of flexible-link mechanisms. The method they came up with required solving a set of nonlinear equations for which they made use of elliptic integrals.

Numerical Methods

Numerical techniques such as nonlinear finite element analysis or the chain algorithm are common alternatives to elliptic integral solutions.

Finite Element Analysis (FEA) refers to the method used to discretize the object being modeled into several smaller elements. A wide range of forms such as beam elements, plane elements or three-dimensional elements can represent each element. That way, they can be separately analyzed and when putting them together, a large system of equations is obtained:

$$\{f\} = [K]\{u\} \quad (1.15)$$

, being $\{f\}$ defined as the force vector, $[K]$ the global stiffness matrix, and $\{u\}$ the displacement vector. The previous set of equations takes normally the shape of an optimization problem, optimization between force and deflection of the mechanism, which can be solved through methods such as the genetic algorithm (GA) or the sequential linear programming (SLP).

Aguirre *et al.* (2011) and Cronin *et al.* (2008) both developed a design method for surgical instruments based on compliant mechanisms implementing a finite element analysis solution into an optimization routine to maximize tool performance. Once the optimization problem has been formulated, including all required variables and their specific constraints, it is then executed in the finite element method (refer to Figure 1.13). The results provided information about the largest blocked forces that could be supplied by the mechanisms. They afterwards validated the results with fabricated prototypes.

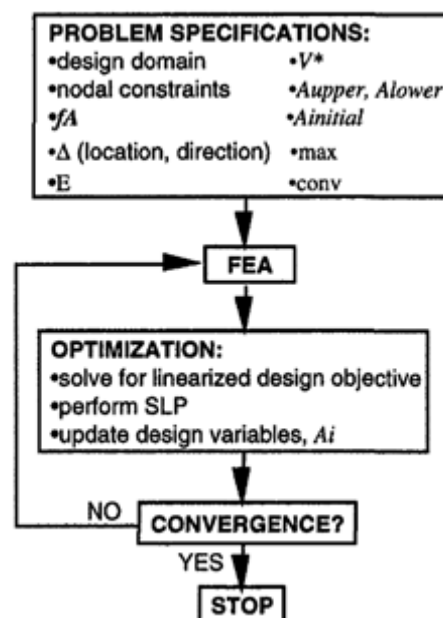


Figure 1.13: Basic computational procedure. (Source: Frecker *et al.*, 1997).

On the other hand, the so-called chain algorithm represents a finite element type algorithm that uses a different approach to combine and solve the resulting system of equations. It models each of the discretized elements as beams, as shown in Figure 1.14, and analyzes them in succession. The different deflections of the elements are found by determining the internal and

equivalent external loads at the free end of the element that is being analyzed, represented as a single cantilever beam. Once they have been calculated, rigid-body translations and rotations are carried out to the remaining elements, so that the angles between the end of one beam and the beginning of the following one are compatible. The way of proceeding with the next beam is exactly the same as with the previous one, and so continues the sequence until the final element of the chain. At the end, deflections of each element are known, as well as the total deflection of the mechanism.

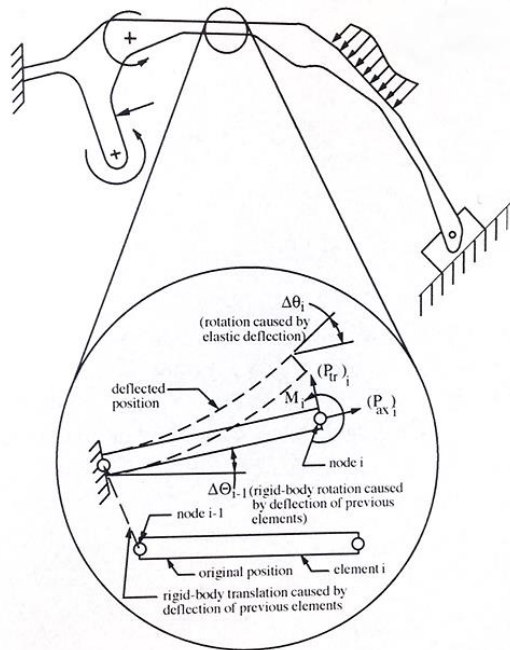
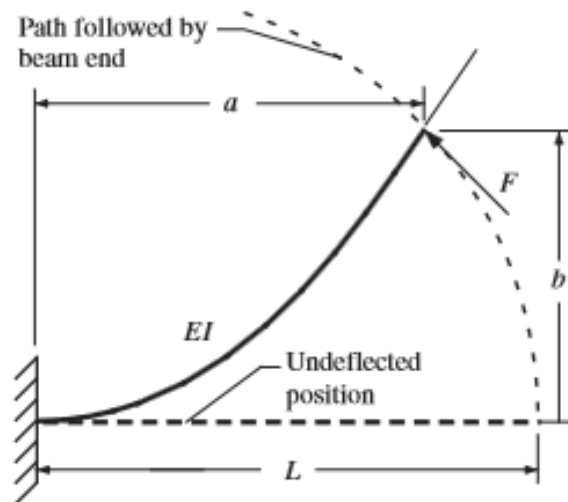


Figure 1.14: Illustration of a general compliant mechanism and the beam element used for its discretization by the chain algorithm. (Source: Howell, 2001, p. 261).

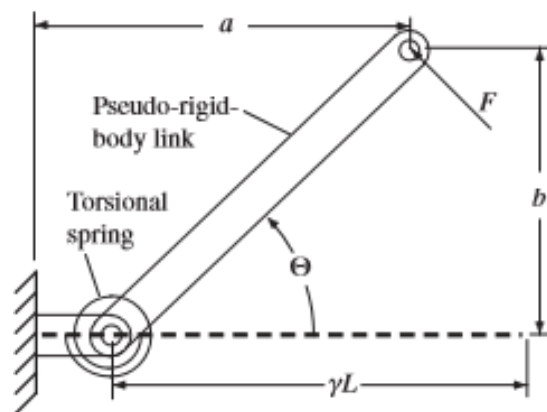
Pseudo-Rigid-Body Model

The pseudo-rigid-body model seeks to provide a simple method of analyzing systems where large, nonlinear deflections are being considered. It is derived from an optimization process that ends up with exact solutions of nonlinear equations solved with elliptic integrals or other numerical methods (Howell *et al.*, 2013). Basically, this method uses rigid body components to model the deflection of flexible members and uses their corresponding kinematics to analyze them. These components have an equivalent force-deflection relationship as the ones being modeled. Depending on the characteristics of each flexible segment, there is a wide range of different pseudo-rigid-body models that can be applied.

In order to accurately model their motion, rigid links are introduced and attached at pin joints and springs are added to symbolize the load–displacement relations of the segments. The beam’s resistance to deflection is introduced via a torsional spring constant, K_{θ} , known as the stiffness coefficient. This coefficient helps the determination of such spring constant’s value of each particular pseudo-rigid-body model, combined with material and geometry properties.



(a)



(b)

Figure 1.15: (a) Cantilever beam element with a force applied at one of its ends. (b) Representation of the beam element with the pseudo-rigid-body model. (Source: Howell, 2001, p.146).

Because all the previously enunciated differences between rigid-body mechanisms and compliant mechanisms, their ways of being analyzed and synthesized do differ one from another. The analysis and synthesis of compliant mechanisms represents a greater challenge and one of the difficulties when designing instruments based on those single-piece mechanisms. Knowledge regarding both, mechanism analysis and synthesis methods and the particular way the elastic members deflect must be well-known beforehand (Howell, 2001).

Besides the already above mentioned design and modeling methods, some other contributions have also been made to the matter in question.

Frecker *et al.* (1997) presented a new multi-criteria automated method for topological synthesis of single-piece compliant mechanisms based on its required deflection. Given a specific input force and output deflection values, it provides the optimal structural form of a compliant mechanism that requires flexibility and stiffness. Once the numerical solution of the optimization problem is found, it can be further implemented in a finite element analysis. The structural form it provides uses a truss ground structure. Since they are two opposed design objectives, the

problem is solved by combining them and using multi-criteria optimization for its resolution. This study is thought to be a great contribution to the automated design of compliant mechanisms with general specified force-deflection relationships. The solutions obtained differ from the conventional method because of the inclusion of the mutual potential energy.

Lu and Kota (2005) developed a genetic algorithm (GA)-based synthesis approach, the ‘load path representation’, schematically represented in Figure 1.16. They state that every compliant mechanism can be represented through three different ‘essential ports’, namely input points for actuation, fixed points to ground the structure and output points to interact with the surroundings, which should be connected by load paths. These connections, represented by rectangular beam elements, create a functionally valid compliant mechanism and transmit forces from the input points until the output ones. Additionally, and what is more important, they ensure structural connectivity between them and make the mesh configurations variable, without an initial discretization mesh.

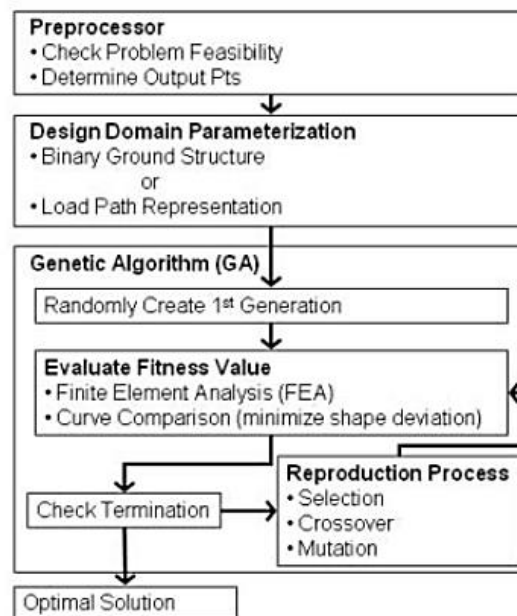


Figure 1.16: Schematic illustration for the ‘load path representation’ procedure. (Source: Lu and Kota, 2005).

Cao *et al.* (2015) proposed a type and dimensional synthesis approach that can be useful for rigid body mechanisms as well as for compliant mechanisms, unifying the way of designing them. By means of this approach, module optimization, elements of both mechanisms can be represented through a combination of different modules such as compliant links, rigid links, pin joints, compliant joints and rigid joints (Figure 1.17), which can in turn be modeled as beam and hinge elements in a geometrically nonlinear finite-element solver. This model seeks to extend the topology optimization technique by introducing the hinge element, and results in the obtaining of a mechanism, namely rigid body, partially compliant or fully compliant mechanism without any previous type prescription. The new beam-hinge model introduces two new features compared with the traditional topology optimization method: the join stiffness between the beams can be controlled and is no longer as rigid modeled; and the angle between them can as well be suitably modified.

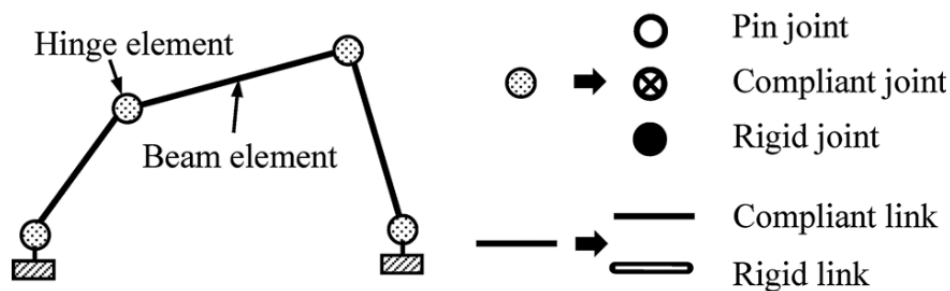


Figure 1.17: Module optimization model of a four-bar mechanism. (Source: Cao *et al.*, 2015).

1.2.5 Processing Techniques

The term processing is defined in draft international standard E EN ISO 17664:2016-06 as the “activity including cleaning, disinfection and sterilization (if necessary and applicable), to prepare a new or used healthcare product for its intended use”. This standard specifies the information to be provided by the medical device manufacturer regarding the processing requirements and the steps needed to be performed when sterilizing a surgical device.

Pursuant to European Directive 93/42/EEC (Richtlinie 93/42/EWG), the most important guideline to make proof of the safety and medical-technical performance of a surgical device, medical and surgical instrumentation require previous processing before being used with human patients. Regarding the processing of surgical instrumentation, and since they are generally in literature often confused, the meaning of some well-known terms should be initially clarified. The sterilization process itself can be defined as “a process that destroys or eliminates all forms of microbial life and is carried out in health-care facilities by physical or chemical methods”. On the other hand, disinfection is described as “a process that eliminates many or all pathogenic microorganisms, except bacterial spores, on inanimate objects” (Rutala *et al.*, 2008). The main difference between both processes lies in their sporicidal action; unlike sterilization, disinfection is not sporicidal.

In light of the previous statement and when developing new instruments or for the currently available ones, attention should be paid to the different accessible techniques to process or re-process them, if non-single-use item considered. In order to select the most suitable processing procedure and not to interfere in its effectiveness, material, functional and structural properties of the instrument have to be considered, as well as its intended use, depending on which the device will be categorized according to the Spaulding Scheme (Kommission für Krankenhaushygiene und Infektionsprävention (KRINKO) and Bundesinstitutes für Arzneimittel und Medizinprodukte (BfArM), 2012).

Spaulding (1957) proposed a classification of the medical devices based on which they have to be categorized as noncritical, semi-critical or critical items regarding their potential for transmitting infections (Table 1.1), which in turn also depends on its intended use.

Table 1.1: Spaulding classification of medical devices.

Classification	Contact	Level of Processing	Examples
Critical	Sterile tissues/ cavities	Sterilization	- Surgical instruments - Cardiac and urinary catheters - Implants - Cystoscopes ¹
Semi-critical	Non-intact skin or mucous membranes	High-level disinfection (Sterilization preferred)	- Respiratory equipment - Laryngoscope blades - Endoscopes - Cystoscopes ¹
Noncritical	Intact skin	Low-level disinfection	- Bedpans - Blood pressure cuffs - Crutches - Computers

¹Cystoscopes – 2012 appear in Critical and Semi-critical classification section. The preferred level of (re)processing is sterilization.

(Rutala *et al.*, 2008; British Columbia Ministry of Health, 2011; EN ISO 17664:2016-06)

In case of doubt relating the classification of a medical device, such as the cystoscopes in the previous table, which appear in both critical and semi-critical risk levels, it needs to be categorized to the higher one to be on the safe side (Kommission für Krankenhaushygiene und Infektionsprävention (KRINKO) and Bundesinstitutes für Arzneimittel und Medizinprodukte (BfArM), 2012).

The processing of a surgical instrument generally embraces following phases:

1. Pre-treatment
2. Preparation
3. **Cleaning**
4. **Disinfection**
5. **Drying**
6. Inspection, maintenance and functionality testing
7. Packaging
8. **Sterilization**
9. Storage
10. Transport

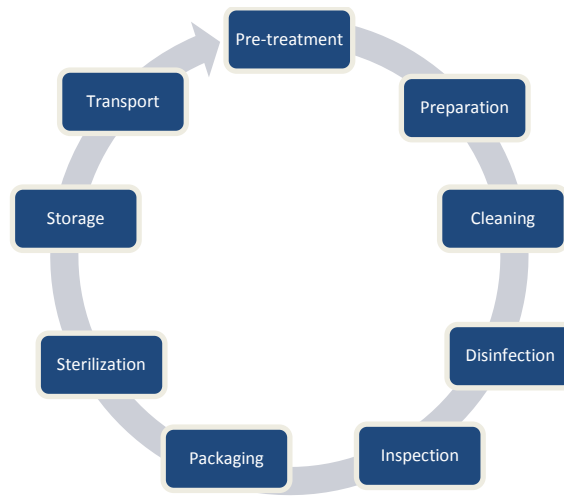


Figure 1.18: Processing steps for a medical product or device.

Pre-treatment and preparation refer to the actions that involve the removal of the gross contamination, disassembly of the different parts of an instrument, pre-cleaning and transport to the processing site. On the other hand, inspection, maintenance and functionality testing seek to verify the cleanliness and integrity of the instrument, as well as maintenance of its functionality. Cleaning, disinfection, drying and sterilization are the most relevant aspects of the whole procedure and where the current master thesis is going to be focused at, particularly at the sterilization one.

Briefly introduced in Table 1.2 are the most commonly used sterilization methods for the processing or reprocessing of surgical instrumentation in healthcare facilities. They can be divided into high or low temperature, depending on the temperatures they reach during their respective cycles. High temperature techniques include moist heat (steam) or dry heat (air), while low temperature ones include ethylene oxide (EtO), hydrogen peroxide gas plasma (HPGP) and ozone sterilizers among others.

Table 1.2: Summary of advantages of commonly used sterilization technologies.

Sterilization method	Characteristics	Advantages
Steam	Moist heat in the form of saturated steam under pressure Denaturation and hydrolysis reactions	Nontoxic, inexpensive Short cycle duration Capable of penetrating packaging and instrument lumens Rapidly microbicidal and sporicidal Easy to control and monitor Little waste
EtO	Gas sterilization technique Microbicidal activity of EtO capable of alkylation of proteins, DNA, and RNA	Capable of penetrating packaging and instrument lumens Suitable for heat- and moisture-sensitive items Easy to control and monitor Compatible with most medical materials
HPGP <i>Examples include: Sterrad—by Advanced Sterilization Products</i>	Production of free radicals within a plasma field that are capable of disrupting the metabolism of microorganisms	Simple to operate, install and monitor Short cycle duration Nontoxic, no aeration phase Suitable for heat- and moisture-sensitive items Compatible with most medical devices
Ozone <i>Examples include: TSO3</i>	Strong oxidizing properties capable of destroying a wide range of pathogens	Nontoxic, no aeration phase Suitable for heat- and moisture-sensitive items

EtO: Ethylene Oxide; HPGP: Hydrogen Peroxide Gas Plasma

(Rutala and Weber, 1998; Fraise *et al.*, 2004; British Columbia Ministry of Health, 2011)

1.2.6 Steam Sterilization Method

Because steam sterilization method is going to be the one selected for the experiments, as in following sections explained, more detailed information about this technique is about to be provided so that the reader can have a better understanding of the whole procedure.

Steam sterilizers, also known as autoclaves, rely on the principle of steam's direct contact with every surface. They can be subcategorized into gravity displacement and dynamic air removal (DAR), commonly known as pre-vacuum autoclaves, regarding the way they remove air from the chamber. They both have however the same phases conforming the whole cycle, which are represented in Figure 1.19:

- Conditioning Phase
- Exposure (Sterilization) Phase
- Exhaust Phase
- Drying Phase

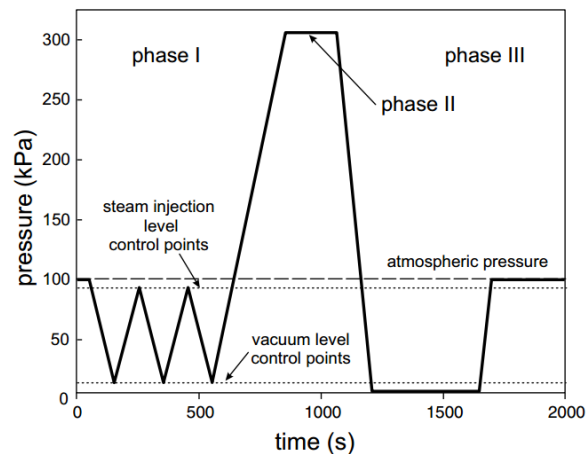


Figure 1.19: Schematic illustration of the pressure inside a sterilization chamber. Phase I: removal of air and penetration of steam. Phase II: sterilization. Phase III: exhaust and drying. (Source: van Doornmalen *et al.*, 2013).

In the former phase, air is actively removed using a series of vacuums and steam is injected into the sterilizer chamber, conditioning phase or phase I. Sterilization phase, or phase II, consists on exposing the item to the correct temperature and maintaining it during a certain period of time. Once the prescribed time has expired, the steam is exhausted from the chamber through the drain, pressure is brought to atmospheric and drying phase starts, procedures of which phase III is conformed (van Doornmalen *et al.*, 2013).

Six different factors are necessary to ensure the effectiveness of the steam sterilization procedure (Dion and Parker, 2013), which are:

- Time
- Temperature
- Moisture
- Direct steam contact
- Air removal
- Drying

In order to monitor the effectiveness of the sterilization process, meaning that the previous factors occur and take place as they should, the so-called indicators are currently used (Rutala *et al.*, 2008; Fraise *et al.*, 2004; Dion and Parker, 2013):

- Mechanical Indicators (MIs)
- Chemical Indicators (CIs)
- Biological Indicators (BIs)

Mechanical indicators, also known as physical indicators, include charts, graphs or displays that provide information about the physical parameters of the sterilization cycle such as pressure, temperature or time. They indicate whether the cycle did perform correctly or not.

Chemical indicators, on the other hand, indicate that the item being tested has been exposed to the sterilization process, which can be proved both externally and internally. There are several types, depending on the method of sterilization:

- External autoclave tapes located on the packages showing the process occurred
- Chemical integrators correlated with time and temperature
- Temperature sensors placed in hard-to-reach places

Usually, these chemical indicators are heat- or chemical-sensitive inks that change color when the parameter being monitored reaches a specific value, or they simply measure a particular parameter in a certain location. However, chemical indicators cannot be used to validate the lethality of a given sterilization process, but just as a complementary indicator of sterilizing conditions (Fraise *et al.*, 2004).

Biological indicators, which consist of resistant bacterial strains, are actually the ones capable of measuring the microbial killing power of the sterilizing agent. If the biological indicator gets inactivated, and because they have been chosen due to their high resistance to the sterilization process employed, it also means that other existing microorganisms did as well get killed. In order to provide valid results, spores used as biological indicators should be more resistant than the bioburden possibly found on the medical devices being processed. The most common biological indicators used for the validation and monitoring of sterilization processes are:

- Inoculated spore test strips. The strips have already been inoculated with spores of the corresponding bacterial strain that is going to be tested. Once the sterilization process is finished, these strips have to be aseptically transferred to the corresponding medium, let them incubate and analyze whether growth takes place.
- Self-contained biological indicators (SCBIs). They do not need to be aseptically transferred to the growth medium, in which they already are. Instead, they already contain both the spore-coated strip and the growth media.
- Suspensions. Usually used when other indicators are not suitable, because of structural constraints such as lack of space or because particular F_{Bio} -values are required and they cannot be found in form of other indicators. An example is the validation of hollow instruments. The suspension needs to be applied to the worst-case location and after sterilization the item is put into a culture media and let it incubating for possible growth of the bacterial strains.

When qualifying the performance of a particular sterilization technique, biological indicators are used to ensure steam penetration and direct contact between steam and the item to be sterilized and they should be located in areas representing the greatest challenge. The selection of

the adequate biological indicator depends on the sterilizing agent and its resistance against it (Fraise *et al.*, 2004).

1.2.7 Sterilization of Hollow Instruments

Processing and reprocessing of hollow instruments represents one of the greatest challenges nowadays in order to render a used medical device safe for reuse. Some research has been carried out in this particular topic. Since it is not feasible to test each and every single instrument available in the market for sterility, special items are used to validate this requisite, the so-called Process Challenge Devices (PCDs).

According to draft international standard E EN ISO 17664:2016-06, Process Challenge Devices (PCDs) are devices which present a defined challenge to a sterilization process and should be used to assess the performance of such processes. Comparison of everyday used medical instruments featuring geometries similar to these PCDs provides information about their processability. These models have two different purposes; on one hand, they furnish proof of the suitability to process already in the past developed instruments which are currently being used; on the other hand, the results they provide can be used as general guidelines for the design of new instrumentation with optimized preconditions for processing.

Regarding new legislation, the existing wide range of medical instruments has to be taken into account, for which different models of constructive characteristics have to be designed and subsequently tested. These critical constructive characteristics represent the most challenging surfaces the steam has to make contact with, thus influencing or even impeding the sterilization process. For that reason, PCDs should represent as closely as possible the structural features encountered among available medical instruments, which usually have several of them at once. This can be illustrated in Figure 1.20 with a MIS scissors already dismantled for the processing procedure.

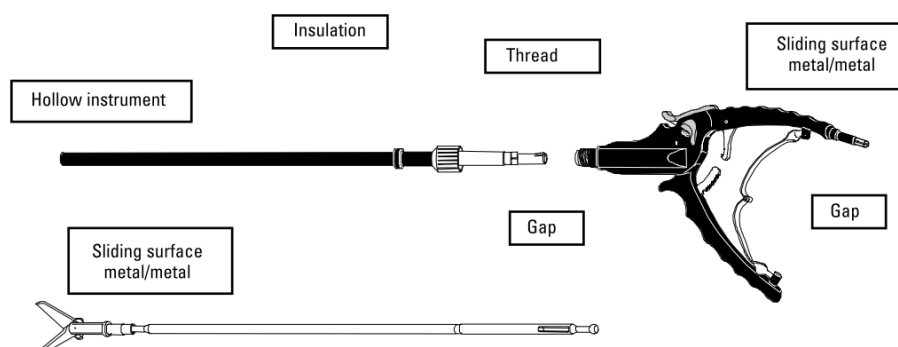


Figure 1.20: Representation of different critical features of a MIS scissors including: hollow instrument, sliding metal/metal surface, insulation, thread and gap features (Source: Working Group Instrument Preparation, 2001a).

One of the most common design features seen in medical devices which represents a challenge for the sterilization process in terms of air removal, steam penetration and drying is the hollow instrument (Working Group Instrument Preparation, 2001a), which includes through and blind

holes. Hollow cavity, also referred as lumen, can be described as the narrow internal surfaces of a medical device that does not allow complete visual inspection from the outside (Carter *et al.*, 2013). They are representative for tubes, cannulas, tubular instruments, devices and equipment parts with open or dead-end lumens, which cover a wide range of the surgical instrumentation requiring sterilization.

When used for the monitoring or validation of a steam sterilization technique, their purpose is to simulate steam penetration (Hoyos and Kopinga, 2015). Monitoring temperature and pressure alone does not provide sufficient information to ensure steam penetration. According to standard EN 867-5 there is a Hollow A device test that small sterilizers, Type B and S, need to pass in order to validate their capability of processing hollow instruments, for which a PCD for hollow instrument loads (hollow load process challenge device) is used. The Hollow Load Process Challenge Device (HLPCD) described in EN 867-5 consists of a 1500 mm long PTFE tube with a 2 mm internal diameter, a 0.5 mm wall thickness and fitted at one end with a 10 g PTFE capsule for accommodating indicators.

PCDs for the Hollow test are commercially available, Figure 1.21, and they are supposed to simulate the penetration requirements of complex hollow, minimal invasive surgical (MIS) instruments, tubes and solid instruments. They consist of a plastic case with small stainless steel tubes placed inside, which have different sizes regarding length and inner diameter, and a capsule or receptacle containing an indicator at one of their ends. Usually these PCDs can be found helix-shaped in a way that they offer greater resistance to the steam penetration. A detailed representation of a Helix PCD can be shown in Figure 1.22.

For a successful sterilization process, the sterilizing agent, in this case the steam, must contact all the surfaces of the goods to be sterilized, which means being able to reach the place where the indicator is located, the most challenging one inside the load. Once the process has taken place, the indicator can be analyzed and information about the ability of processing hollow instruments can be provided.

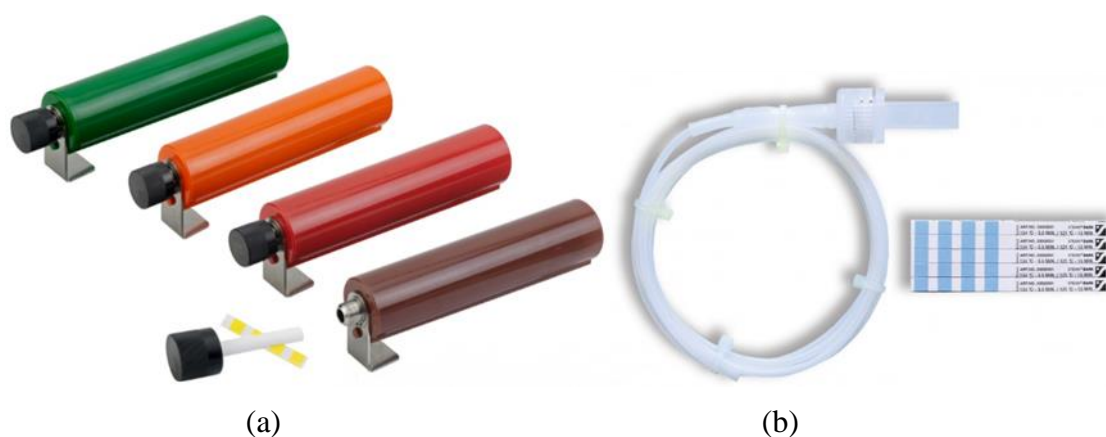


Figure 1.21: Commercially available Process Challenge Devices (PCDs). (a) Steri-Record® Compact-PCD® provided by gke GmbH. (b) ISP® Helix Test System provided by Sentry Medical.

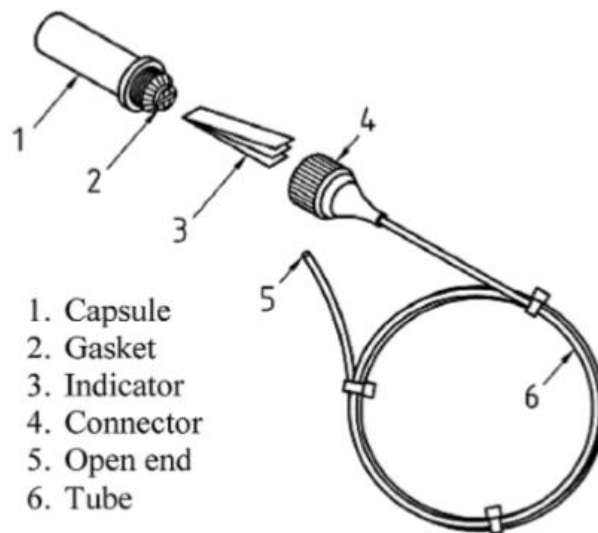


Figure 1.22: Schematic illustration of a Helix PCD with its components: 1. Capsule where the indicator is hosted. 2. Gasket to close the capsule. 3. Chemical or biological indicator. 4. Connector between the tube and the capsule. 5. Open end where the steam enters. 6. Tube along which the steam penetration takes place. (Source: de Bruijn and van Drongelen, 2005).

Working Group Instrument Preparation (2001) designed a hollow PCD instrument (Figure 1.23) to simulate the critical feature of this specific geometry for the steam to penetrate it through the entire length. The selected geometry for the tests was a 500 mm long tube with an internal diameter of 0.5 mm. The results they obtained proved that even such small inner diameters could be sterilized under the specified conditions:

- Steam sterilization with 3-fold prevacuum
- Temperature: 134 °C
- Hold time: > 5 minutes
- Drying time: 15 minutes

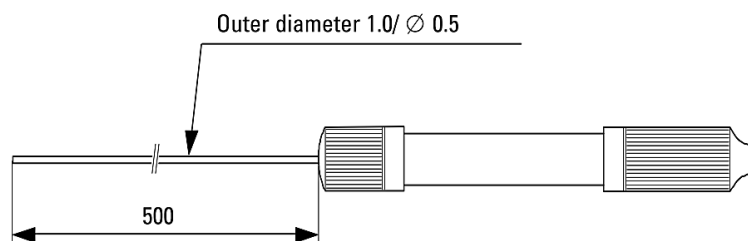


Figure 1.23: “Hollow PCD Instrument” simulating lumens accessible from one or both ends with a length of 500 mm and a 0.5 mm inner diameter. (Source: Working Group Instrument Preparation, 2001a).

Sterilization of hollow devices can only occur when air inside it is properly removed, so that the injected steam, the sterilizing agent, can enter the lumen and contact every inner surface of the goods to be sterilized. Because of the widespread use of steam sterilizers to process medical instruments with narrow channels, some research regarding the qualitative and quantitative behavior of air removal and steam penetration into narrow lumens has already been carried out.

In order to get information about its behavior, the measurement of the steam penetration into different dead-ended channels (PCDs) were performed with a chemical indicator placed in a receptacle at the dead end of the channel. Results proved that currently used Process Challenge Devices that make use of this small receptacle at the end of their length may no longer be representative for the penetration of steam in channels of the available medical instruments (Hoyos and Kopinga, 2015). Neither is the Hollow A PCD suggested by EN 867-5 standards (Kirk *et al.*, 2016). This is due to the fact that they both introduce an additional volume, the one for the chamber hosting the indicator, which facilitates somehow the penetration of the steam through the whole length (Hoyos and Kopinga, 2015). Besides, the existent surgical instruments generally have channels of different diameters and lengths than the ones these PCDs have, being therefore no longer a realistic standard steam penetration test for every hollow instrument. To the same conclusion came also (Kirk *et al.*, 2016), who indicated that some of the currently available PCDs cannot be trustworthy since they are sometimes not able to detect process failures, thus mistakenly releasing surgical instrumentation as sterile.

Concerning the suitability of the PCDs to assess the performance of the sterilizers, de Bruijn and van Drongelen (2005) carried out some experiments with four different commercial helical PCDs. They showed that factors such as the type of PCD, the type of load (empty, partial or full load) and sterilizer cycle did affect the results of the tests. They also found out that, although claiming to be compliant with EN 867-5, the tubular PCDs did not meet the specifications given by the European standard regarding the ratio of the internal volume of the tube and the free volume of the receptacle containing the indicator. The free capsule volumes were either too large, what might result in early positive results because of the enhancement of this free volume for the steam penetration, or too small. Moreover, no information was supplied by manufacturers about the conformity of the devices with the reference one. The change in material of the chamber hosting the indicator also influenced the results because of differences in heat transmission characteristics.

Kremmel *et al.* (2011) performed some tests with fourteen different PCDs, some of them commercially available. Normal tests were conducted as well as tests which introduced some of the most common sterilization deficiencies. When exposed to the correct cycle, they all passed the test, but when the sterilization cycles included simulated faults, results concluded that 40% of the devices were not capable of detecting not even a single fault and only 27% of the introduced faults were clearly identified. Authors also revealed that the shape of the PCD was not relevant, since some of the PCDs with a different shape than the one the EN 867-5 proposes, did detect all faulty cycles. This might lead to the thought that available PCDs are not in equivalence with standards, and consequently to the fact that further work is needed to confirm to which extent the results provided by nowadays used PCDs can be applied to everyday instrumentation.

Regarding the effect of the geometric parameters of a tube in terms of its processability, some controversial affirmations exist. According to Young (1993) and Hoyos and Kopinga (2015), small diameters are harder to sterilize than larger ones, considering the same length of the tube. One of the explanations could be the convective displacement of air due to density differences (Young, 1993) or the increasing effect of the viscosity of the air-vapour mixture (Hoyos and Kopinga, 2015). On the contrary, (Kaiser and Gömann, 1998; Kaiser *et al.*, 2006), who also

researched the air removal and steam penetration into narrow lumens, demonstrated that the wider the inner diameter of the tube, the harder for the steam to penetrate it. Same material, wall thickness and length of the tubes were considered for the previous statement. The experiments were conducted with several PTFE tubes of different lengths (500 to 4500 mm) and different inner diameters (1 to 5 mm). They developed the so-called “Hollow Penetration Resistance” (HPR), which reflects the level of air removal difficulty expressed as the product of tube length (L) and inner diameter (d):

$$\text{HPR} = L \cdot d \quad (1.16)$$

Similar results were obtained by (Borchers and Mielke, 2004). The effect of the internal diameter of the tube yielded a decreasing log reduction in the following order: 1 = 4, 2, 6 = 8 mm. Again being the larger diameters the most difficult ones to sterilize.

The effect of the wall thickness of the tube was also investigated by Borchers and Mielke (2004), resulting in a complex effect on the sterilization process. The spore log reduction reached by different wall thicknesses listed from highest to lowest was: 0.25, 2.0, 0.5 and 1 mm.

Dufresne *et al.* (2008) conducted experiments using stainless steel tubes to obtain information about the maximum lumen length and the smallest lumen diameter that could be processed with a new ozone sterilizer (TSO₃ 125L), already cleared by FDA in August 2003 as a validated sterilization technique for reusable medical devices. The tubes used for the tests had several lengths and different inner diameters of 0.5 mm, 1 mm, 2 mm, 3 mm and 4 mm. The results they obtained about the limits on the geometry that could be processed are show in Table 1.3. They demonstrated the efficacy of these results by sterilizing the ACMI ureteroscope (Table 1.4), which represents a very challenging instruments in terms of sterilizing agent penetration, being one of the longest and smallest for-use lumen ACMI endoscopes. Some other real instruments have also been processed with the available techniques in order to test the claims of the manufacturers (Table 1.4).

Table 1.3: Summary of data regarding limiting geometric values obtained with different processing techniques.

	Diameter x Length (mm)	Description	Reference
EtO Mixture			
HCFC-EtO	3 x 400	Straight stainless steel tubes	(Rutala and Weber, 1998)
HPGP			
STERRAD® 100S	6 x 310	Metal and non-metal lumened instruments	(ASP, Johnson & Johnson)
STERRAD® 100S	3 x 400	Medical device with only a single stainless steel lumen	(ASP, Johnson & Johnson)
STERRAD® NX™ Standard cycle	2 x 400	Single channel stainless steel lumened instruments	(ASP, Johnson & Johnson)
STERRAD® NX™ Standard cycle	1 x 150	Single channel stainless steel lumened instruments	(ASP, Johnson & Johnson)
STERRAD® NX™ Advanced cycle	1 x 500	Single channel stainless steel lumened instruments	(ASP, Johnson & Johnson)
STERRAD 100NX®	0.7 x 500	Single-channel stainless steel lumens	(ASP, Johnson & Johnson)
Ozone			
	2 x 250		
TSO ₃ 125L	3 x 470 4 x 600	Rigid lumened devices	(Dufresne <i>et al.</i> , 2004)
TSO ₃ 125L	0.5 x 450 4 x 700	Stainless steel lumened devices	(Dufresne <i>et al.</i> , 2008)
Steam			
3-fold pre vacuum steam sterilizer	0.5 x 500	Single channel lumened instrument	(Working Group Instrument Preparation, 2001b)

EtO: Ethylene Oxide; HPGP: Hydrogen Peroxide Gas Plasma

Table 1.4: Processing of real surgical instruments tested with different sterilization techniques.

Instrument Channel	Diameter x Length (mm)	Sterilizer	Reference
Ureteroscope	1.7 x 485		
Laparoscope	5 x 330	HPGP	(Borneff-Lipp <i>et al.</i> , 2008)
Gastroscope	2.8 x 1160		
Flexible Endoscope	1 x 500	HPGP	(Deutsche Gesellschaft für Sterilgutversorgung, 2006)
Ureteroscope	0.8 x 505	Ozone	(Dufresne <i>et al.</i> , 2008)
	1.1 x 505		

EtO: Ethylene Oxide; HPGP: Hydrogen Peroxide Gas Plasma

Finally, Goemann *et al.*, 2001 and Kaiser and Gömann, 1998 demonstrated that the procedure used to remove the air does affect the processability results, being only fractionated vacuum sterilizers effective at removing air from long lumens (Kaiser and Gömann, 1998). Trans-atmospheric air-removal procedure, on the contrary, was proven not to be able to achieve sufficient air removal to allow steam penetration (Goemann *et al.*, 2001).

1.3 Drawbacks of the State of the Art and Research

1.3.1 Compliant Mechanisms

Elliptic Integral Solutions

The Elliptic Integral method involves derivations quite complicated and they only provide a solution when the geometry and the loading conditions are relatively simple. Besides, some assumptions are made in order to obtain a solution such as the consideration of linear material properties or inextensible members. An alternative technique is required for analyzing more general flexible components (Howell, 2001).

Numerical Methods

Both nonlinear finite element analysis and the chain algorithm are numerical solutions which are mostly used for further refinement of a previously required initial design. They are useful when validating or refining designs already created with other method, which is not always required. They can be used to assist in the design of complex structures with non-regular geometries, but it is highly difficult to design them only making use of these techniques (Howell, 2001).

Another disadvantage of the conventional finite element analysis used for considering large deflections is the computation time needed to obtain a convergent solution capable of solving the resulting system of equations (Howell and Midha, 1994). Very large, powerful computer algorithms and hardware are needed in complex problems due to the many iterations accounting for nonlinearities.

Pseudo-Rigid-Body Model

As a general drawback of this method, it should not be used with mechanisms of complex shapes, since it cannot accurately model them analytically. The decisive point of using rigid-body mechanisms to model the behavior of compliant mechanisms lies in choosing a proper and accurate pseudo-rigid link to represent the compliant link. Using this method will be worthwhile as long as its advantages in simplicity are greater than the disadvantages derived from the loss of accuracy.

One of the greatest challenges of this model is knowing where to put the joints and which value should take the constant of the spring. Another disadvantage is derived from the introduction of springs accounting for the force-deflection relationships of the flexible members. These will impede any stiffness variation of the join and will introduce some direction error motions (Howell *et al.*, 2013).

Although easier to analyze than compliant mechanisms, the pseudo-rigid-body model can still be more complex than rigid-body skeleton diagrams. Because of all the choices to be done and the different elements to consider, such as the rigid links, kinematic pairs and springs, this solution can become cumbersome, when trying to determine the load-displacement relationship of the model. Hence, additional techniques to determine the load-displacements relationships are required.

1.3.2 Processing Techniques

Several options regarding processability techniques for surgical instruments are available. However, and depending mostly on the material and geometry selected, not all of them present the same characteristics, having each their own disadvantages (Table 1.5), which need to be taken into account when selecting a sterilization technique for a concrete medical device.

Table 1.5: Summary of disadvantages of commonly used sterilization technologies.

Sterilization method	Disadvantages
Steam	Nonsuitable for heat- and moisture-sensitive items
	May leave instruments wet, causing them to rust
	Potential for burns
	Damage of microsurgical instruments by repeated exposure
EtO	Safety concerns (environmental and personnel)
	Time-consuming
	Non cost-effective
	Minor microbicidal effectivity in instruments within inner lumens
HPGP	Comparatively high costs of the sterilant and packaging
	Comparatively poor penetration of the sterilant (long narrow lumens)
	Reduced number of lumens being processed in one cycle
	Small sterilization chamber (3.5 ft ³)
Ozone	Small sterilization chamber

EtO: Ethylene Oxide; HPGP: Hydrogen Peroxide Gas Plasma

(Rutala and Weber, 1998; Fraise *et al.*, 2004; British Columbia Ministry of Health, 2011; Dufresne *et al.*, 2008; Borneff-Lipp *et al.*, 2008; Rutala *et al.*, 2008)

As previously stated, and taking into consideration only the steam sterilization technique, there are some drawbacks about the methods used to evaluate the behavior of the steam when penetrating narrow lumens. This concerns the receptacle placed at one of the ends of the PCD, which is hosting the biological indicator needed to validate the sterilization procedure. However, although this small receptacle placed at the closed end of the tube being considered as inappropriate to accurately simulate air removal and steam penetration into narrow lumens, conventional thermoelectric measurements for the control of steam penetration commonly used in the experiments (Goemann *et al.*, 2001) are also no longer possible since the measuring probes cannot be introduced through such narrow lumens (Deutsche Gesellschaft für Sterilgutversorgung, 2006). Moreover, such small channels cannot host traditional biological indicators such as spore strips or self-contained indicators (Dufresne *et al.*, 2008). For all the previously stated reasons, the validation of the sterilization process of narrow lumens has indeed become a complex issue.

In relation to the effect of the geometry, opposing statements have been made, as in previous section already presented. This disconformity brings to light the cumbersome-to-explain behavior of the air removal and steam penetration into narrow lumens, where different physical mechanisms are involved, and demands further research and work in this specific topic.

In addition to that, it has also been proved that several factors play a relevant role in the steam sterilization procedure, such as the method used to remove the air in the chamber hence turning it into a complex field of study full of several unknowns still to be addressed.

To conclude with, it can be highlighted that no conclusive information about steam penetration into narrow lumens can be found in literature, neither is provided by manufacturers, leading to no information about processing methods for small-inner-diameter and thin-walled instruments.

2 Materials and Methods

2.1 Preliminary Considerations

As a first step, and once the medical application for the surgical manipulator has already been confirmed, meaning it can be used for the transurethral resection of the bladder tumors, a preliminary experiment regarding its suitability for being able to completely reach the whole surface of the urinary bladder needed to be performed. The results of such experiment will reveal whether the initial design does allow for an entire coverage of the surgical workspace or if, on the contrary, it still needs to be further improved.

In order to carry out the experiment, some research about the human bladder was initially done. Findings revealed that a human bladder can hold up to 600 ml urine (Hole, 1981) and assuming that full bladder, which is how TURBT is performed, takes a spherical shape, a half-spherical 10 cm diameter phantom was designed and additively manufactured (Figure 2.2). As already mentioned, the main purpose was to reach the entire surgical field, what could be ensured by dividing the phantom into several segments and by touching all of them. Because it is symmetrical, marking only the segments in the right lower hand side was sufficient.

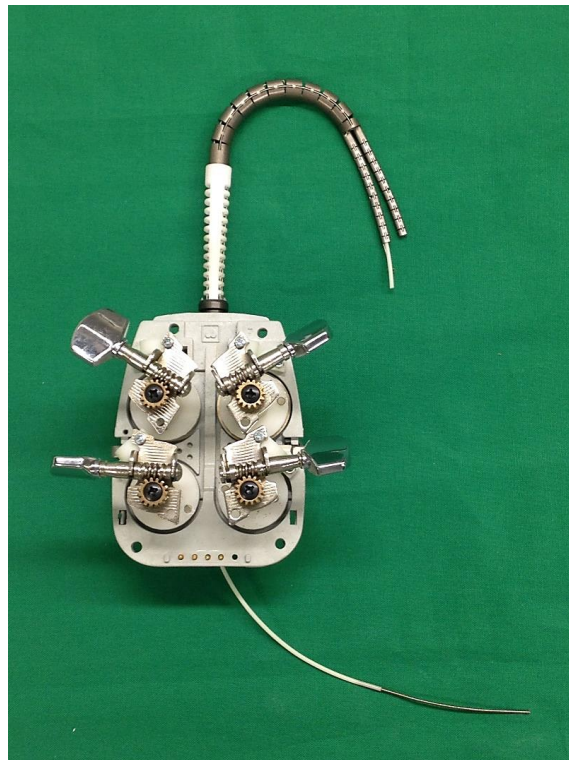


Figure 2.1: Surgical manipulator attached to the actuation unit used to reproduce the movements at the preliminary experiment about surgical workspace coverage.

The da Vinci actuation box unit (Intuitive Surgical, USA) was used to manually simulate the real movement of the manipulator, as shown in Figure 2.1. It accommodates an adaptor at one of its ends through which the tool can be placed. The manipulator was guided until reaching every sector of the phantom. When reached, the marking was done using a brown colored silicone injected through the flexible tube by an injector at the proximal end of the actuation unit.

The experimental setup with one of the marking configurations as well as the results can be seen in Figure 2.2.

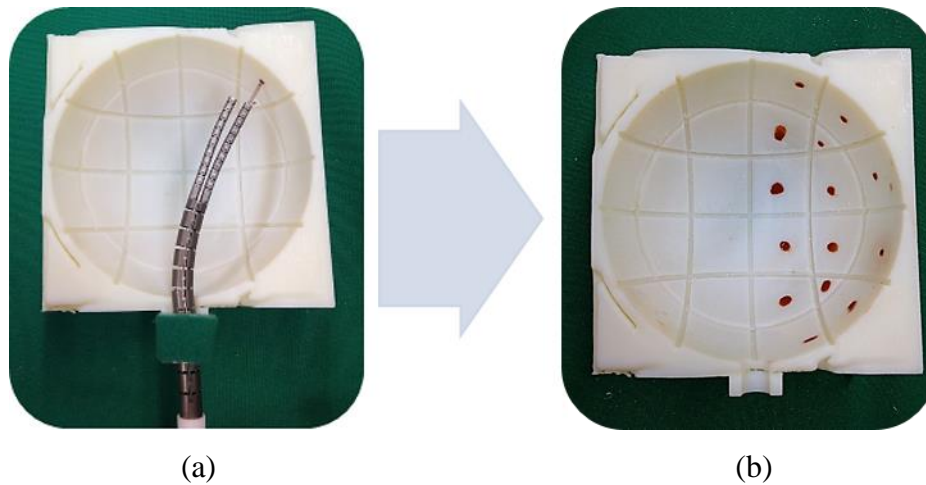


Figure 2.2: Experimental setup with the first marking configuration (a) and the final one (b).

From the previous illustration deducible, all of the segments were marked by the manipulator, thus being able to reach even the most challenging areas of the bladder. However, they were reached by making use of S-bends, meaning bending both the arms and the overtube of the manipulator. The main purpose is to be able to reach them by only C-bending the manipulator, which is done with the overtube, so its arms can meanwhile treat the surgical field. In order to make it feasible, the design of the actual manipulator needs to be modified so it will not experience plastic deformation when just C-bending is taking place to fully cover the entire bladder, getting thus more reliable and safer medical outcomes. For this reason, further work needs to be done. The following section will take a close look on what exactly is needed to be done.

2.2 Task Description

Within the framework of the current thesis two different tasks are going to be performed regarding the design optimization and characterization of a surgical instrument.

1. Experimental definition of a model applied to predict **nitinol compliant mechanism's** behavior in terms of **flexibility** and **strength**. The influence of different parameters of the structure is going to be tested in the model. Such parameters refer to the length, L ; width, b ; and thickness, h , of the compliant mechanism. The resulting model will give information about the maximum deflected angle that the mechanism can achieve before reaching failure, in this particular case meaning plastic deformation.
2. Design of a guideline in terms of **steam sterilization processing techniques** for stainless steel **hollow thin-walled instruments** with the most common structural configurations in the nowadays used medical instrumentation. This guideline will provide information regarding processable lumen length of a specific inner diameter.

2.3 Expected Advantages and Functions of the Solution

Through the realization of the previously described tasks several benefits can be deduced. Generally speaking, both tasks can conclude with the design of general Guidelines that will answer the question as to whether an instrument can fulfill mechanical requirements needed to perform its prescribed task, and whether it can be properly processed with a steam sterilization technique.

If referred to the particular double-arm continuum surgical manipulator, the one the current thesis is focused at and which represents also the baseline of the performed experiments, several advantages can be derived. On one hand, the present model will enable the determination of the optimal geometry of the different compliant mechanisms that conform the device, hence refining the prior design. This geometry will allow them to perform their required task, meaning the transurethral en bloc resection of the bladder tumors, without reaching failure due to plastic deformation. The resulting model is capable of providing a tradeoff between flexibility, permitting the mechanism to loosely cover the entire surgical workspace, and strength, thus avoiding yielding. Additionally, it can also help to predict the behavior of the mechanisms when changing one of the beam parameters or, the other way around, provided a certain required angle, be able to choose the adequate geometric values. On the other hand, regarding the instrument's processability, the guideline will give information about whether the small holes as well as the instrument channels built into its design can be properly sterilized.

Additionally, this information can be extrapolated to different surgical platforms and devices, either instruments made of nitinol and based on compliant mechanisms regarding the descriptive model or stainless steel instruments that need to be processed as one of their last steps before being used in healthcare facilities. Some of the benefits deduced from both guidelines can be expressed as no more trial and error efforts, since the information is provided beforehand, which is considerably useful when designing new instruments or improving the available ones. That also leads to no more uncertainty about the safety of the surgical tools to be used, regardless their category, critical, semicritical or noncritical, thus being on the safe side. Cost reduction and a less time-consuming design are also from both Guidelines deducible.

2.4 Solution Structure

The solution structure aims to provide information about the best geometry of an instrument regarding both mechanical characterization and medical processability. In the former one, the user needs information about the specific geometry for which the model needs to be experimentally defined. A determined compliant structure is to be designed with a CAD software in relation to the selected geometry. The realization of the experiments will yield relevant data, which will be used for the definition of the model. The step in between is performed by a curve fitting method, considering the classic beam theory as the baseline equation. The model will be now capable of predicting the behavior of the compliant structure, thus providing the best geometry for it not to be plastically deformed.

In order to assess the medical processability of the surgical instrument and regarding its material and geometric parameters, the conception of the so-called PCDs will be carried out, with which the experiments will be performed. A sterilization technique will be used, in this case the steam sterilization technique, and important information will be provided concerning the suitability of this technique for such geometries. In order to validate the procedure and to ensure reliable

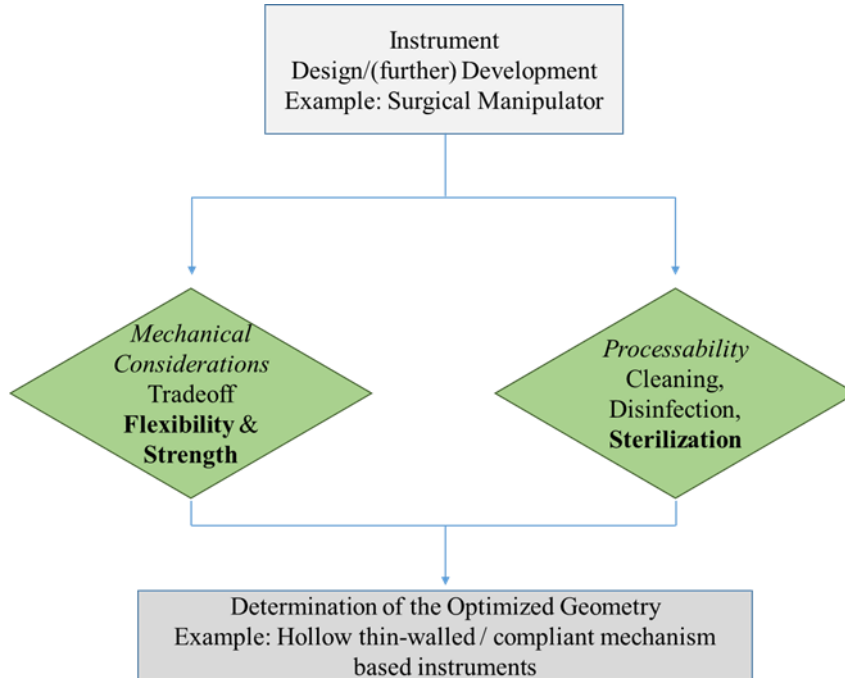


Figure 2.4: General solution process of the present work.

Regarding the mechanical solution process, a schematic illustration can be shown in Figure 2.5. The first step consists on the test specimen conception, the ones the experiments will be done with. In this specific step, considerations about the exact geometry that needs to be tested have to be deduced. This involves parameters of the compliant mechanism such as its length, L ; width, b ; and thickness, h ; which will be introduced in following sections. Once these design parameters have already been decided, a computer-aided design and manufacturing (CAD/CAM) software will be implemented for their design and they will be further manufactured by electrical discharge manufacturing (EDM) technique. Each structure will be subjected to the test, which entails a force-displacement sensor capable of measuring small increments of the force that is being applied to the structure along its displacement. Plastic deformation needs to be detected in order to define the model. A digital microscopic camera will provide information about the deflected angle plastic deformation takes place at in each mechanism. For the complete definition of the model, specific nitinol material properties need to be determined, such as the elastic modulus and the yield strength. Having defined the model that describes the behavior of the compliant mechanism, a validation will be carried out in order to ensure that the information provided is accurate and does reflect the real response of the structure. The experimentally obtained model is now able to render the optimal geometry of the mechanism, provided the requirements and constraints of the particular task where it is going to be applied.

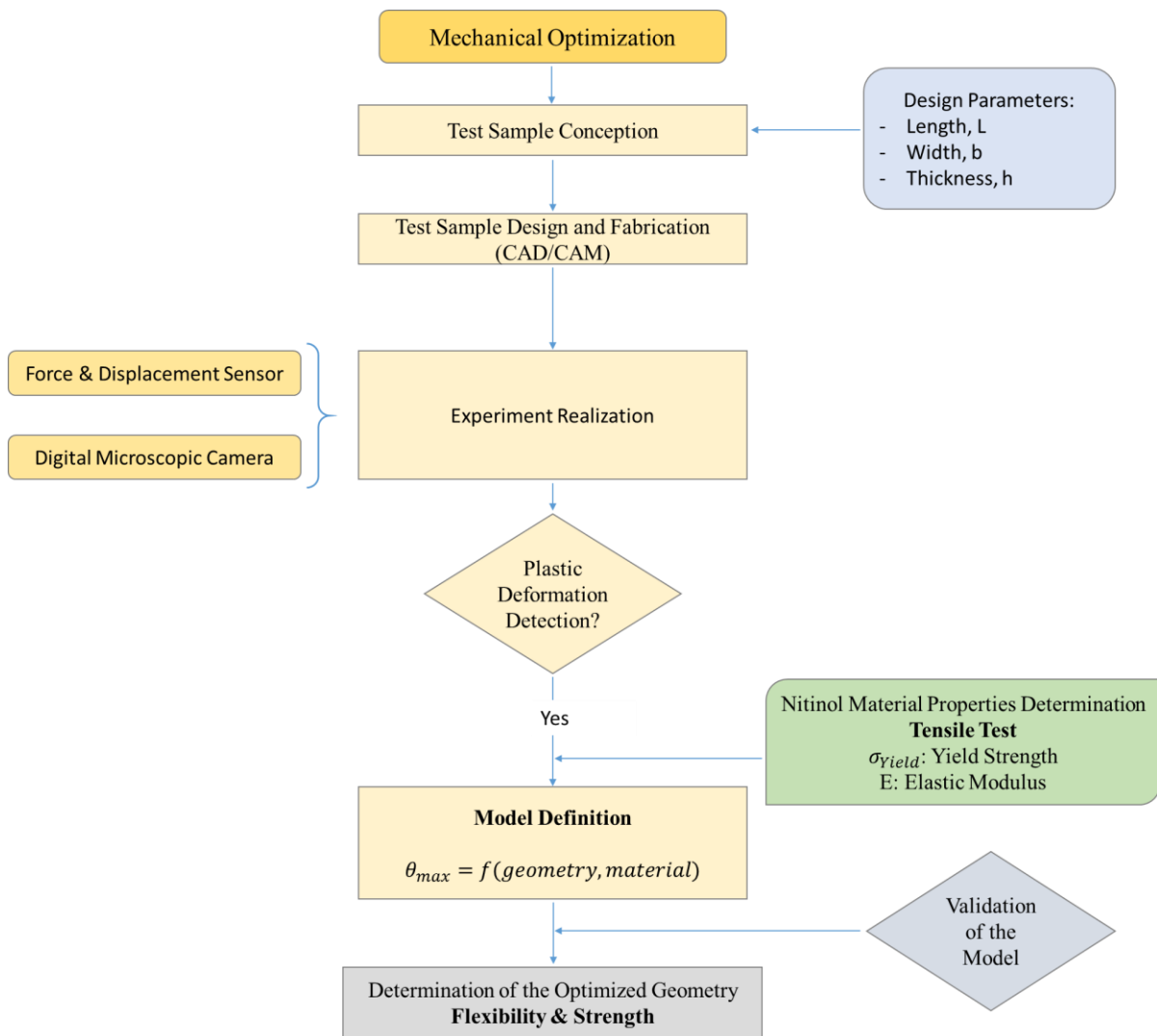


Figure 2.5. Solution process – Mechanical Characterization.

Figure 2.6 shows the solution process in terms of processability, which goes as follows: the first step is the test sample conception, including the selection of the correspondent structural configuration. These test samples are going to act as Process Challenge Devices (PCDs), thus requiring for an accurate design that will allow to set a limit on the geometry that can be properly sterilized. Deciding on their geometric parameters such as diameter and length will be the next step to be performed. Once the PCDs have been modeled, they will be processed with all the required steps, later on farther detailed. To validate the results, the use of different process monitoring indicators is required. This validation process entails the inoculation of the PCDs with bacterial solution and the verification of their sterilization through different measurement procedures. Based on these measurements, the next geometric parameters should be selected with the subsequent modeling of the new to-be-processed PCDs. Two different structural configurations will be tested, namely hollow tubes with both ends open and with one dead-end. By proceeding this way, a guideline will be written containing information regarding the processability of stainless hollow tubes with different lengths and inner diameters.

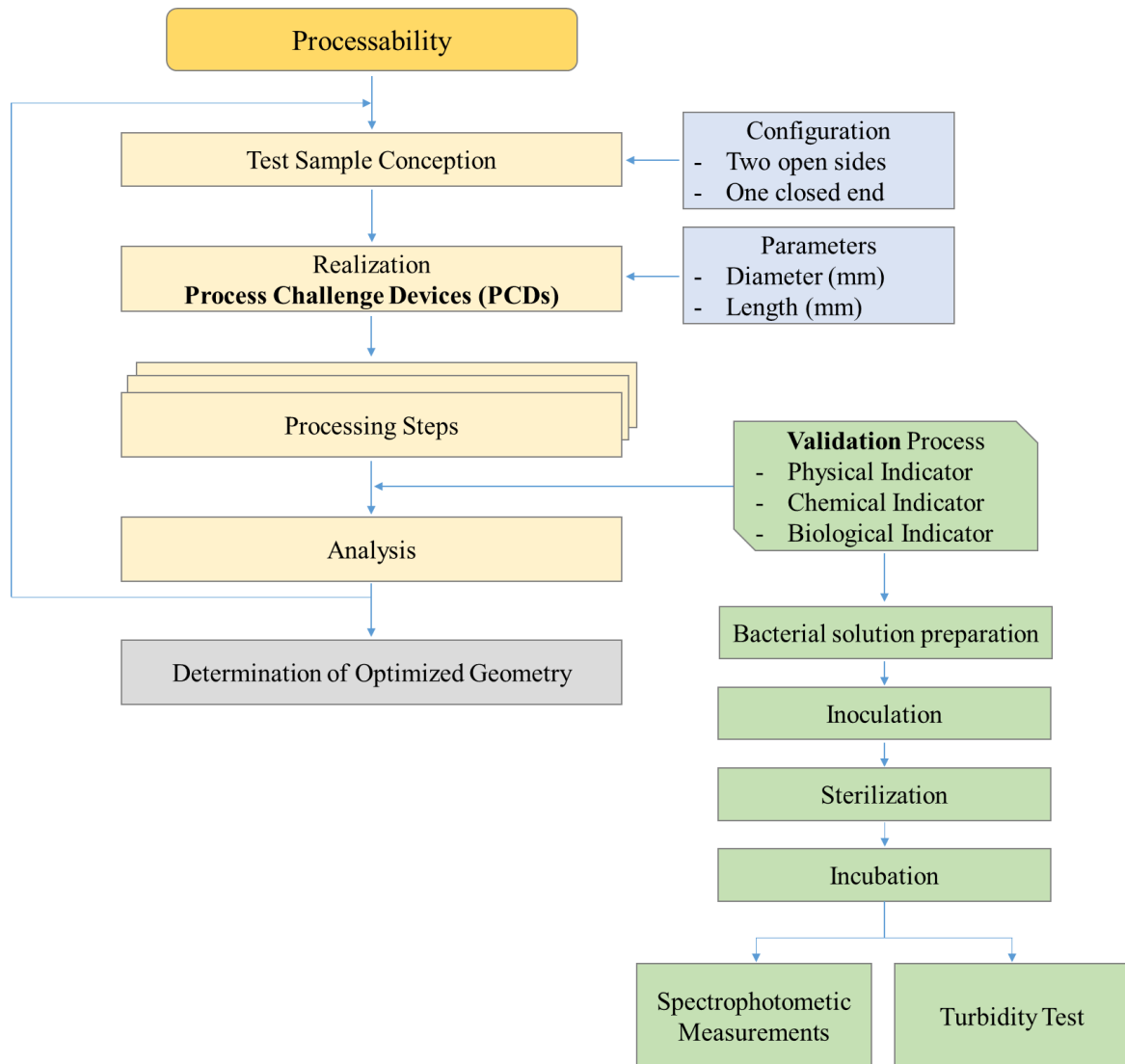


Figure 2.6: Solution process – Medical Processability.

2.6 Distinctive Features of the Solution

Analytical methods are mostly employed to define a model capable of describing the behavior of compliant mechanisms. In the present work, and because of the characteristics of the material being used, an experimental validation of the model was performed, aiming to obtain a model from a baseline equation, the classic beam theory equation, making it match the experimental data.

Information with regard to the geometry that can be safely and properly sterilized is of great interest when developing a new surgical instrument. However, no information regarding the steam processability of hollow thin-walled instruments with small inner diameters is yet available. For that reason, inner diameters smaller than 1 mm were selected and experimentally processed. Besides, no conclusive information about the behavior of steam sterilization over the geometry of the PCDs could be found in literature, which was also aimed to be analyzed with the present experiments.

2.7 Realization – Mechanical Characterization

This section details the process of defining the model which will afterwards be experimentally validated as well as the procedure of designing the compliant structure used for the tests. It describes the selected structure geometry and the different parameters defining it, whose effect is still to be determined. Finally, information regarding the performed tensile test is provided.

2.7.1 Definition of the Model

This section is going to present the definition of the model which seeks to predict the behavior of a nitinol compliant mechanism in terms of flexibility and strength.

As previously stated, when using compliant mechanisms, and due to the large deflections experienced by these mechanisms, geometric nonlinearities do take place. Compliant mechanisms are commonly modeled similar to cantilever beams undergoing large deformations (Aguirre *et al.*, 2011; Howell, 2001). Conventional linear beam theory, previously introduced in Section 1.2.3, provides a method of calculating the load-carrying and deflection characteristics of beams and is therefore used in the deflection and motion analysis of many simple mechanisms (Howell and Midha, 1994). However, since large deflections are now involved, the small-deflection assumption used to linearize the equations is no longer valid.

Maximum Deflection Angle for a Flexible Beam

Considering the rectangular-cross-section cantilever beam with a force F applied at the free end, the maximum deflection angle that the beam will undergo before failure, θ_{max} , can be obtained as follows.

Remembering the basic Bernoulli-Euler equation that connects the bending moment of the beam and its curvature,

$$M = EI \frac{d\theta}{ds} \quad (2.1)$$

, and after having made the small-deflection assumption, the deflection angle of the beam, or simply beam slope, can be written in terms of the coordinate along the undeflected beam axis, x , as

$$\theta = \frac{dy}{dx} \quad (2.2)$$

For the cantilever beam with a vertical end force the moment can be expressed as

$$M = F(L - x) \quad (2.3)$$

, being L the beam length. Equation (2.1) can then be reformulated as follows

$$F(L - x) = EI \frac{d\theta}{dx} \quad (2.4)$$

, or

$$\int d\theta = \frac{F}{EI} \int (L - x) dx \quad (2.5)$$

Solving the integration yields

$$\theta = \frac{F}{EI} \left(Lx - \frac{x^2}{2} \right) + C_1 \quad (2.6)$$

, where C_1 represents the constant of integration that can be solved applying the boundary conditions $\theta = 0$ at $x = 0$, thus resulting in

$$\theta = \frac{Fx}{2EI} (2L - x) \quad (2.7)$$

The maximum stress occurs at the fixed end of the beam, where $x = L$, therefore

$$\theta_{max} = \frac{FL^2}{2EI} \quad (2.8)$$

, where the moment of inertia, I , for a rectangular cross section is $I = \frac{bh^3}{12}$. Substituting this equation into equation (2.8) results in

$$\theta_{max} = \frac{6FL^2}{Ebh^3} \quad (2.9)$$

The failure of the beam, meaning plastic deformation, is considered when the maximum stress reaches the yield strength, σ_{yield} , which can be written as

$$\sigma_{yield} = \frac{6FL}{bh^2} \quad (2.10)$$

Rearranging to get the equation that defines the force, F , results in

$$F = \frac{\sigma_{yield} I}{L \frac{h}{2}} \quad (2.11)$$

Substituting the former equation into equation (2.9) results in the maximum deflection angle that the beam will undergo before failure:

$$\theta_{max} = \frac{\sigma_{yield} L}{E h} \quad (2.12)$$

Because of the assumption made above, equation (2.12) is only valid for linear deflections. The difference in analysis between linear and nonlinear deflections lies in the statement about the slope of the transverse deflection being small enough to approximate it as the undeflected beam axis, x .

To take into account the geometric nonlinearities and since the small-deflections assumption only involves the parameters which are related with the geometry, the equation provided in (2.12) is not valid anymore, but it provides us with information regarding the geometric parameters of the structure which will play a role in the final model predicting its behavior, which are mainly the beam length and thickness, as deducible from the equation above. These parameters will allow us to design the test samples, and after their experimental analysis, a final model will be defined.

2.7.2 Compliant Mechanism Test Sample Design

Once all the parameters that can have an influence are known, test samples need to be designed, so the model can be experimentally defined.

First of all, a monolithic compliant structure is proposed, like the ones our surgical manipulator is comprised of (see Figure 2.7). The surgical manipulator is manufactured in such a way that several of these compliant mechanisms are attached to one another, allowing the overtube and the arms to articulate or to bend and increasing thus the whole angle they are able to provide.



Figure 2.7: Functional prototype of the Double Arm Endoscopic Mini-Manipulator System (MiMed) based on compliant mechanisms in its overtube, as well as in its both arms.

The selected geometry of the compliant mechanism is illustrated in Figure 2.8. Six design parameters, namely the length L of the beam, its thickness h and its width b , the outer diameter D , the ring thickness t and the fillet radius r , are used to define the compliant specimen.

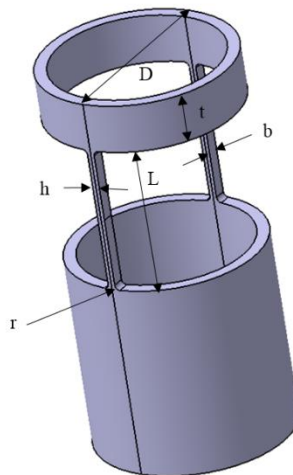


Figure 2.8: Geometry and representative parameters of the compliant mechanism.

For the assignment of numerical values to the parameters, following procedure was carried out. Prior to our surgical manipulator, a polyamide additively manufactured structure was designed to analyze and evaluate its behavior regarding the maximum deflected angle it could reach. This structure was also based on the same compliant mechanisms and its values for the beam were: 3 mm length, 0.6 mm thickness and 1 mm width, with an elastic modulus of 1.5 GPa.

Considering the complex geometry and such a small size of the manipulator, polyamide was discarded provided that not manufacturing method is yet accurate enough to obtain such complex structure. A titanium structure was then designed, aiming to keep the same behavior as the previously showed polyamide one. Considering the following formula and provided that the elastic modulus of the new material was 120 GPa, adjustments on the geometric values were made:

$$\theta = \frac{6 F l^2}{E b h^3} \quad (2.13)$$

Table 2.1: Values of the previous polyamide and titanium structures.

Material	Length L (mm)	Width b (mm)	Thickness h (mm)	Elastic Modulus (GPa)
Polyamide, p	3	1	0.6	1.5
Titanium, t	6	0.5	0.3	120

With the previous values, following ratio was achieved:

$$\frac{\theta_t}{\theta_p} = 0.8 \quad (2.14)$$

, which was acceptably close to the unity and therefore a similar behavior could be reached.

Taking the former parameters, the current surgical manipulator was built (see Figure 2.7), based on nitinol compliant mechanisms. The compliant mechanisms that conform the surgical manipulator are slightly different from the ones to be tested. There is an additional design parameter, the distance D just before the beginning of the slot, which prevents plastic deformation. This distance was eliminated for the final design of the specimens so they could be tested in such a way that larger angles were experienced by the parts, ensuring therefore that plastic deformation was going to be reached.

In light of the finally used numerical values for the surgical manipulator, and aiming to analyze the influence of each parameter, next values were adopted for the test samples.

Table 2.2: Geometric design parameters of the compliant structure: length L (mm), thickness h (mm) and width b (mm).

Length L (mm)	Width b (mm)	Thickness h (mm)
3	0.25	0.2
4	0.5	0.3
5	0.75	0.4
6	1	0.5
7		
8		

As seen in Figure 2.8, the designed compliant mechanism has a more extended length on one of their sides so that it can be fixed in the experimental setup. On their proximal end, a minimum length is there required for the contact point between the structure and the device applying the force, as we will see in following sections. This geometric value is represented by the ring thickness t and a value of 2 mm was picked, large enough not to lose the contact point during the deformation of the sample. A total length L_T of 16 mm was selected for all of the specimens, considering that this length had to cover the contact point length (2 mm) and the length L of the beam, which for the longest one made it already 10 mm, and also be able to provide left structure to be placed in the setup, for which 6 mm were chosen.

Since the outer diameter D of the sample is not affecting the model, a value of 8 mm was selected. Regarding the fillet radius r , the smallest possible value was given, but also a smooth transition was needed so the stresses will not become that high in this particular area, avoiding thus the break of the sample when high forces are being involved. Then, a final value of 0.2 mm was given.

The resulting compliant mechanisms, some of which can be seen in Figure 2.9, were modeled in CATIA and then manufactured by drilling and electrical discharge machining (EDM), which represents the appropriate technology for accurately manufacturing such complex geometrical designs. The fabrication was done from a nitinol tube.



(a)



(b)

Figure 2.9: Three test samples showing different geometric values for the parameters to be analyzed. (a) Length, L . (b) Width, b .

2.7.3 Tensile Test

As previously indicated, and in order to be able to experimentally validate the model, both strength and elastic properties of the material to be used are needed. These properties, namely Young's modulus and Yield strength, can be deduced from the proper tensile test.

The detailed dimensions of the three test specimens (Figure 2.10) used to carry out the assay are in concordance with the measurements based on ASTM standards, in particular with the one referenced as specimen shape D, which can be found in the technical drawing attached at the end of the document. The experimental setup along with its parts is illustrated in Figure 2.11, and one of the resulting stress-strain diagrams is also shown in Figure 2.12, being all of them provided in Appendix C – Nitinol Tensile Test. The machine used to perform the tensile test was a servo hydraulic Schenk Hydropulser with 160 kN traction/compression force.



Figure 2.10: Dog bone tension test specimens.

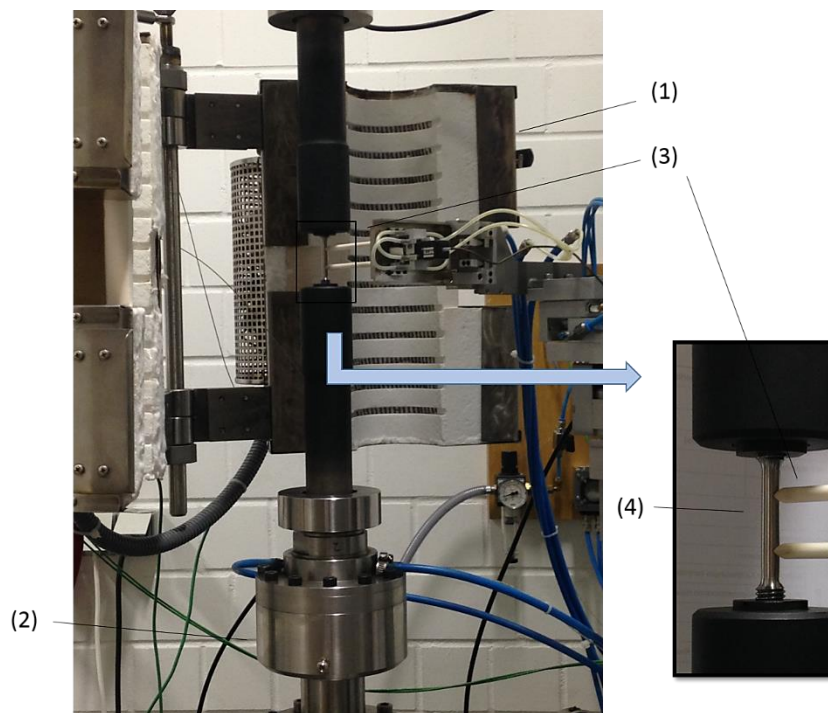


Figure 2.11: Experimental setup for the required tensile test with the corresponding dog bone specimen: (1) furnace, (2) servo hydraulic actuator, (3) thermocouples and (4) dog bone specimen.

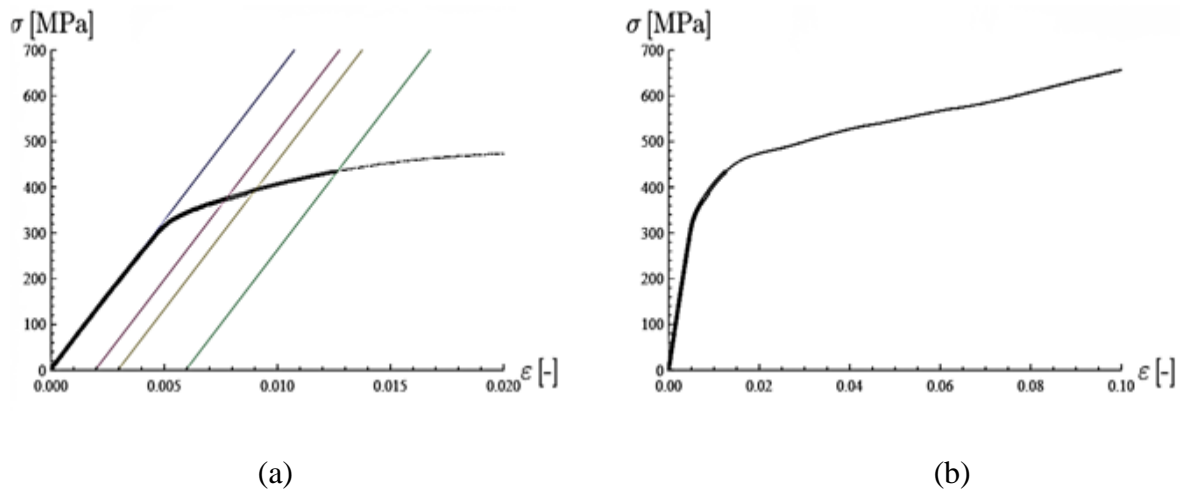


Figure 2.12: Stress-strain diagrams of one of the corresponding nitinol dog bone specimens: (a) detailed, (b) general.

The same test was performed three times in order to obtain reliable data, which we afterwards averaged out, as seen in the following table:

Table 2.3: Results of the three different tensile test and the average of the resulting values. Nitinol material properties, namely Elastic modulus, E , and Yield strength, σ_{yield} respectively.

	E (GPa)	σ_{yield} (MPa)
Test 1	65	375
Test 2	69	399
Test 3	65	378
Average	66.33	384

2.8 Realization – Medical Processability

This section discusses the conception procedure of the Process Challenge Devices. Processing and validation steps are exhaustively detailed, providing protocols and rigorous information on how to proceed.

2.8.1 Process Challenge Device Conception

One of the most critical geometries of surgical instruments in terms of reprocessability is the hollow one, to which both through holes and blind holes belong (Working Group Instrument Preparation, 2001a). As in Section 1.3.2 already stated, little to no information is available in

the literature regarding the sterilization of hollow thin-walled surgical instruments with small inner diameters. There is therefore a need of knowing whether such complex geometries can be properly reprocessed, provided that medical devices are increasingly becoming more complex and even smaller due to the demands imposed by non-invasive surgical techniques.

To assure reproducible conditions and to cover the not-yet investigated instrumentation with narrow lumens, suitable PCDs were conceived, capable of simulating the structural features that can interfere or even impede the sterilization process in real-life instrumentation. The final design should be able to simulate the requirements for the steam to penetrate them, and should be representative for this geometry in nowadays used or to be developed medical devices.

The final hollow instrument PCD can be seen in Figure 2.13 and it basically consists on a 1.4301 stainless steel capillary tube with a wall width of 0.1 mm. This tube would present a variable length and inner diameter, so that different geometries can be actually tested and more reliable and closer data can thus be obtained, when compared to the existing instrumentation.

The different values of the lengths of the tubes and their inner diameters were selected in such a way that there was a ratio between them. Both the inner diameter and the length were gradually increased from one sample to the next one, always keeping the same ratio, so an acceptable value could be found as the limit value on the geometry that can be safely processed. Finally following values were selected:

Table 2.4: Initially conceived geometrical values for the PCDs regarding length and diameter.

ID (mm)	OD (mm)	Length (mm)
0.4	0.4	20 40 60 80 100
0.3	0.5	30 60 90 120 150
0.4	0.6	40 80 120 160 200
0.5	0.7	50 100 150 200 250
0.6	0.8	60 120 180 240 300
0.7	0.9	70 140 210 280 350
0.8	1.0	80 160 240 320 400
0.9	1.1	90 180 270 360 450
1.0	1.2	100 200 300 400 450

A maximum length of 450 mm was chosen due to the ultrasonic cleaner and sterilizer dimensions, which would not allow to introduce longer items.



Figure 2.13: Different PCDs already packaged and ready for the sterilization process.

These PCDs were obtained from 1-meter-long 1.4301 stainless steel tubes with different inner diameters and manufacturing them into their final geometrical dimensions in terms of length with a grinding machine.



Figure 2.14: PCD finishing process with the grinding machine.

Once two-ends-open PCDs had already been evaluated and enough information regarding their processability had been acquired, PCDs with one end closed were to be tested. The way of closing them consisted on introducing a 2 mm long stainless steel wire with a similar diameter on one of their sides and with the help of a self-adjusting crimping pliers, like the ones showed in Figure 2.15, apply a force until no gaps were to be seen.



Figure 2.15: Self-adjusting crimping pliers used for the closing of one of the tube ends.

2.8.2 Processing Steps

The methodology carried out to perform the experiments is detailed in this section. Each of the processing steps to which each PCD will be put through, already introduced in previous sections, can be schematically seen in Figure 2.16.

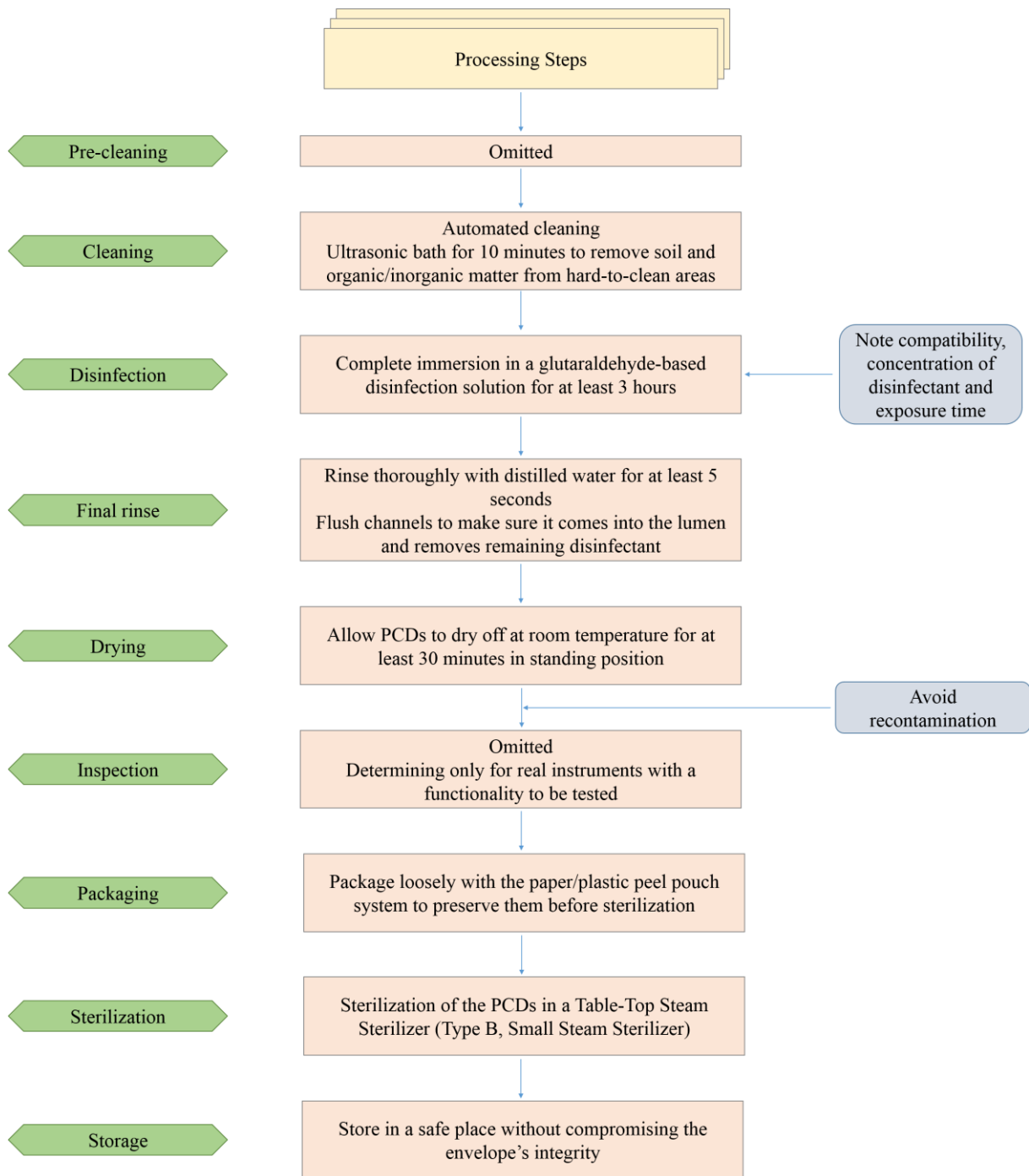


Figure 2.16: Schematic illustration of the processing steps.

Pre-cleaning

Pre-cleaning of medical devices in healthcare facilities is one of the most important steps in order to achieve a successful processing. It needs to be carried out with instruments that are heavily soiled with sputum, blood, or other material. If omitted, dried secretions and excretions can considerably interfere in following processes (Rutala *et al.*, 2008).

Prior to testing, PCDs have not previously been used, and the amount of gross soil is thus not that relevant. Starting with the cleaning step would be then sufficient.

Cleaning

Meticulous cleaning is required before high-level disinfection and sterilization, as documented in EN ISO 15883, in order to greatly remove organic and inorganic matter that can interfere in the provided results of such following processes. Inorganic contaminants are thought to decrease the efficiency by protecting the existing microorganisms due to an occlusion in salt crystals. Organic matter, on the other hand, when combined with a germicidal, used in the disinfection and sterilization steps, produces a chemical reaction ending with a less germicidal complex, decreasing thus its potential attacking ability (Rutala *et al.*, 2008).

Regarding the type of experiments we are about to carry out, we did select the ultrasonic bath as a cleaning method for the instruments processing. Among all the different available techniques, ultrasonic cleaning is one of the mechanical or automated cleaning methods recommended for metallic narrow-lumened instruments (Deutsche Gesellschaft für Sterilgutversorgung, 2006). The visible soil attached to the solid surfaces of the instruments is removed by cavitation bubbles that implode due to the high frequency pressure sound waves propagating through the liquid. This implosion taking place at the surfaces of the item produces the release of the adhering residues (Carter *et al.*, 2013). It is normally carried out using water, which can also be combined with detergents or enzymatic products (Rutala *et al.*, 2008).

When processing them, tubes have to be fully submerged, so that the cavitation bubbles can penetrate the lumens and clean their entire inner surfaces.

Instruments will be then processed in the Bandelin Sonorex Technik RM 40 UH cleaner with distilled water for the full recommended cycle time, 10 minutes.

Because of the small inner diameter of the tubes, brushing of internal channels cannot be performed, which is also a highly recommended step before proceeding with the disinfection, and additionally there is not yet a cleared method to quantify the degree in which cleaning methods help decrease contamination of such items.

Disinfection

In healthcare facilities, items are usually disinfected by liquid chemicals (Rutala *et al.*, 2008). Some of the factors affecting the disinfection process include prior cleaning, as already indicated above; type and level of microbial contamination; physical nature of the object, for instance hollow instruments; and concentration and exposure time to the disinfectant (Figure 2.16) (Rutala *et al.*, 2008). For a correct outcome, specimens must be entirely exposed to the germicide for the appropriate minimum contact time, although in general, longer contact times provide more effective results (Rutala *et al.*, 2008).

Because of their several advantages glutaraldehyde-based solutions are commonly used in healthcare facilities as a disinfection method, for medical equipment such as endoscopes among others; some of these advantages include their excellent biocidal properties, activity in the presence of organic matter and noncorrosive action to a wide range of materials (Rutala *et al.*, 2008).

Glutaraldehyde is known as a high-level disinfectant and chemical sterilant, which alters microorganism's RNA, DNA and protein synthesis.

The specific selected liquid chemical was a 4% diluted 5% glutaraldehyde-containing cleaning disinfectant Kohrsolin® extra (Bode Chemie GmbH, Hamburg, Germany) suitable for medical devices, which come under the Medical Device Directive. An exposure time of 3 hours was defined as the minimum required. Again, a total submersion of the PCDs is to be carried out.

Final rinse

A final rinse after disinfection is of great importance since it helps preventing adverse effects derived from the retained disinfectant, which can interfere in the efficiency of the subsequent sterilization process. Sterile or distilled water needs to be used to avoid recontamination with living organisms in tap water (Rutala *et al.*, 2008). Tubes need to be thoroughly rinsed with distilled running water and attention should be paid to the water flushing the holes and lumens repeatedly.

Each tube will thus be washed with distilled water for at least 5 seconds.

Drying

The previously cleaned and disinfected items need to be properly dried before being stored in their correspondent packages, otherwise wet surfaces will prevent the vacuum to be achieved and the cycle will not be properly occurred. Furthermore, the drying phase greatly decreases the probability of recontamination of the item by microorganisms that might be present in the water.

We will let the tubes dry in a standing position to facilitate the process for about 30 minutes at room temperature. Before continuing with the following step, confirmation that no water comes from none of the sides of each tube is required.

Inspection

Inspection of the PCDs will not be performed since, as previously stated, there is no possible way of verifying the cleanness achieved by the cleaning and disinfection part, nor is there any functionality to test, being these the main purposes of this step.

Packaging

Different options for the packaging of the instruments prior to sterilization are commercially available. The ones used for the current work are peel-open pouches, particularly heat-sealed plastic and paper pouches. These envelopes allow the penetration of the steam during the autoclave, protect against potential external contamination, prevent bacteria to penetrate them and maintain the sterility condition of the processed item after sterilization, and besides they are designed for light weight items, like the tubes to be sterilized. They also allow the user to select

the required length of the package, which perfectly suits our needs, since tubes up to 450 mm long will be used.

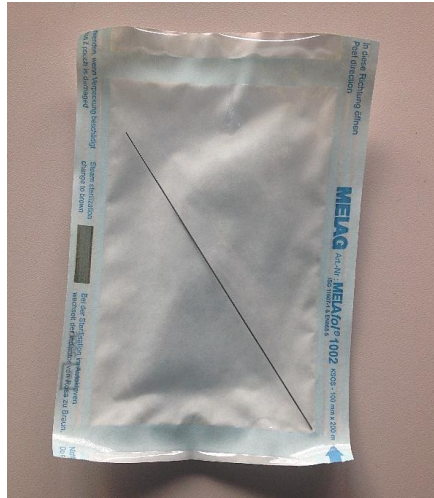


Figure 2.17: Heat-sealed plastic and paper peel-open pouch with one of the PCDs inside it.

Sterilization

After the lumens for each length and diameter had been prepared in their corresponding envelopes, the sterilization step is to be carried out.

This step represents the most important one and it needs to be performed for the medical devices categorized as critical one, such as the cystoscopes and thus our surgical manipulator, which is intended to have similar applications as cystoscopes.

As a sterilization technique we decided on moist heat (steam) sterilization. As regards EN ISO 17664, steam sterilization should always be the preferred technique for processing all critical and semi-critical items that are heat- and moisture-resistant, even if not necessarily required, statement also supported by (Fraise *et al.*, 2004; Rutala *et al.*, 2008). The main reason resides in its reliability, consistency and lethality, which leads to the largest margin of safety.

The particular device responsible for the sterilization was a WEBECO A50-B Table-Top Steam Sterilizer, which can be found for general, dental and surgical practices. It is designed and built according to the requirements of EN 13060 for Small Steam Sterilizers (type B) and it also complies with European Directive 93/42/EEC, the standards DIN 58946 and EN 554. It allows for two test programs, namely the vacuum test and the Bowie&Dick test, also known as Helix test according to EN 867-5. The A50-B model consists on a fractionated pre-vacuum sterilizer with following sterilization parameters:

- Standard program for instruments
- Pressure: 3 bar (abs.)
- Temperature: 134 °C

Storage

Following the sterilization phase, processed items should be safely stored. Safely storing them means not compromising the integrity of the envelope (e.g., puncture, bending, tears) and ensuring sterile items do not become wet, since moisture brings with it microorganisms from the air and surfaces. Since we do use heat-sealed plastic envelopes, as long as the seal is still intact, the package should be considered as not contaminated (Fraise *et al.*, 2004).

2.8.3 Validation Process

Sterilization is the process that comprises the destruction, inactivation or removal of all viable microorganisms, by exposing the product to a sterilizing agent. Quality assurance of the instruments undergoing sterilization being free of all viable microorganisms needs to be provided. This sterility assurance can be guaranteed by means of validating the process by which sterility is achieved. Any validation procedure must cover the evaluation of the physical performance of the sterilizer, as well as the biological one on the product being sterilized.

The validation of the sterilization process needs to be performed with the previously explained biological indicators (BI). Biological indicators are used to assess presence of steam. Several and different types exist but because of the special features of the current work, not all of them can be used. Narrow lumens cannot contain traditional biological indicators such as spore strips and self-contained BIs (Dufresne *et al.*, 2008), therefore a direct inoculation method was chosen. It consists on the direct inoculation of the lumen of the tube with a bacterial suspension. Additionally, if indirect inoculation method was to be used, that means the insertion of a previously inoculated carrier into the channel of the lumen, threads, wires or sutures for instance, some complications might appear such as the obstruction of the gas when trying to penetrate the lumen, which will no longer represent the real conditions (Dufresne *et al.*, 2008).

Assuring sterility with the biological indicators means being able to demonstrate the death of all available microorganisms defined as “the failure to grow and be detected in culture media previously known to support its growth”, what the validation process basically consists of (Fraise *et al.*, 2004). Other than the biological one, physical and chemical indicators are also used to monitor the sterilization process. As chemical indicator external autoclave tapes are used on the surface of the envelope, which confirm that the process occurred and the steam was able to make contact with this particular surface. On the other hand, mechanical indicators can be found on the display of the sterilizer, showing whether the physical parameters (temperature, pressure and time) were accurately achieved, and whether the sterilization process did take place in a correct manner or not.

Work Area Preparation

Before starting with the validation process, some basic steps needed to be taken into account, so the rest of the procedure can take place without major complications:

- The incubation shaker is started while preparing other materials and the temperature required by the specific procedure, 37 °C, is set.
- The work bench is disinfected with a proper disinfectant such as isopropanol.

- Each sample container is marked with the sample letter, date and other necessary information. Contaminating the inside of the sample container needs to be avoided in any way.

Inoculum Preparation

Preparing the inoculum is of great importance, since this represents the solution containing the bacteria with which the inoculation of the PCDs will take place.

1 Bacterial Strain

Suspensions of *Escherichia coli* (optical density: 0.159) were used to prepare the inoculation solution. They represent a type of bacteria with a great resistance to the steam sterilization technique and a greater challenge than the ones found in healthcare facilities.

2 Media Preparation

Preliminary to the test and in order for the bacteria to be able to grow, a proper medium is needed, as well as an adequate incubation period. Lysogeny broth (LB), also referred as liquid culture media, is a highly-referenced microbial growth medium used for the cultivation of *Escherichia coli*. This highly nutritious microbial broth contains peptides, amino acids and carbohydrates in a low-salt formulation. The formulations generally differ in the amount of sodium chloride, distinguishing between Lennox, Luria and Miller formulations. The exact ingredients, composition and directions for its preparation are:

Lysogeny broth-Lennox (LB)

Sodium chloride (NaCl)..... 5g

Tryptone/Peptone ex casein..... 5g

Yeast Extract..... 2.5g

pH (at 25°C) 7.3±0.2

The 12.5 g are then poured in 500 ml distilled water. The composition is well mixed and stirred to completely dissolve the lumps on the medium. The result is a yellow-coloured clear solution without any precipitate. The obtained media is sterilized by autoclaving at 121 °C and stored at at 2-8 °C.

Once we have the media in which the bacteria are going to be cultivated, the next step is the preparation of the inoculum as follows:

1. 50 ml of the LB broth are transferred into a sterile Erlenmeyer flask.
2. The bacteria are directly pipetted from the container into the flask.
3. The flask is placed into an incubation shaker and the bacteria are let incubate at 37 °C for at least 6 hours.

4. Half-hourly spectrophotometric measurements are carried out to ensure the bacteria has stopped growing, so that a stable value is kept.

Inoculation

All inoculations of the PCDs were performed aseptically in a sterile bench, also referred as laminar flow hood or biological safety cabinet. The inoculation refers to the step where all the specimens are contaminated with the bacteria solution. As already stated, a direct inoculation method was chosen.

From the previous processing procedure, the test specimens have already been sterilized, ensuring no bacteria can be found, rather than the one used for the inoculation step, and the way to keep on proceeding is as follows:

1. Each of the PCDs is pulled out from its correspondent sterile envelope.
2. The inner surface of the lumen of the PCD is flushed with a 0.25 mm outer diameter needle and a 1 ml injector containing the bacteria solution.
3. The tubes are allowed to dry at room temperature for at least 30 minutes.
4. Finally they are wrapped with paper/plastic peel pouch envelopes.

For the tubes which have an inner diameter narrower than 0.25 mm, a silicone adapter with a 0.33 mm inner diameter is used. It is attached to the end of the needle on one of its sides and to one of the ends of the tube on its other side. That way we can ensure that the whole content of the injector will penetrate the lumen.

Sterilization

The sterilization step during the validation process is identical to the one performed during the prior processing phase. The manner of proceeding is, though, slightly different, since the test sample used for the positive control is not sterilized for the second time, but directly transferred to the next step, as already indicated below, since the positive control represents a test sample previously inoculated and for the one a positive result is to be expected, thus meaning bacterial growth must be seen. Should it be placed in the incubator shaker and no bacterial growth is to be detected, we can therefore conclude that the process was not correctly performed. At this point, the entire experiment needs to be repeated.

In the validation phase no prior cleaning and disinfection are allowed, since just the efficacy of the sterilization process itself is being evaluated (Food and Drug Administration, Division of General and Restorative Devices, 1993).

Incubation

An incubation step follows the previous sterilization of the PCDs. After sterilization, possible remaining bacteria were incubated in liquid culture media (LB broth) for 48 hours at 37 °C and

assessed for growth of *Escherichia coli* microorganisms, thereby indicating a sterilization failure. This stage seeks to ensure that no bacteria remained alive after the sterilization process and it entails following steps:

1. Transfer 10ml of broth media to a sterile 15ml plastic tube
2. Mark the tube with a letter to identify it
3. Unpack the PCD from its envelope
4. Flush 1ml of sterile broth media to the lumen of the tube with a 0.25 mm outer diameter needle attached to a plastic injector, as done in the inoculation step with the bacteria solution, and mix it with the 10 ml broth media in the plastic tube
5. Measure the geometrical values of the PCD (length and inner diameter) and assign them to the corresponding letter of the tube it was placed in
6. Place the plastic tube into the incubator for 48 hours for a possible bacteria growth

Previous steps need to be performed for every PCD tested. In order not to mislead the results with recontamination of the test specimens, steps 1-3 require the use of a laminar flow hood.

Since we are only interested in knowing whether the inner surface of the lumens can be sterilized or not, we do not need to test their outer surface, meaning the inoculation and incubation phases refer only to the lumens. Besides, information about the processability of the tubes regarding their outer surface is already known thanks to previous sterilization tests, as we will explain in Chapter 3.

Analysis

The analysis stage entails the evaluation of the results obtained during the validation process. These results will give information about whether the test specimens are sterile or not. When microbial growth is detected, the product tested is considered non-sterile. Moreover, and since biological indicators have made direct contact with the product being tested, they will reflect the actual sterilizing conditions of the product itself and the geometry and structure which represent it, rather than just the ones in the sterilizing environment. If any microorganism remains after the sterilization process and it is placed into a broth containing the appropriate nutrients to support growth, the microorganism flourishes and the broth becomes turbid (Food and Drug Administration, 2014)(Fraise *et al.*, 2004). Turbidity, which is the result of many generations of cells having originated from a few ones, is thus a visual indicator of microbial growth, which can afterwards be quantified by a UV-VIS spectrophotometer by measuring values of absorbance or transmittance exhibited by the broth and comparing these values to the positive and negative controls used, as in the next pages further explained.

One of the most widely used methods for determining bacterial numbers is spectrophotometric analysis, which is based on turbidity and indirectly measures all existing bacteria. Spectrophotometry is a scientific method used to measure the light absorbed or transmitted by a chemical substance as a function of wavelength. This quantitative measurement is carried out by means of detecting the light beam's intensity passing through the sample, which will be calculated employing the Beer-Lambert law. The reading, called absorbance or optical density, indirectly

reflects the number of bacteria existent on the swab. In this case, the amount of absorbed light increases as the cell population increases. The simplified Beer-Lambert law's equation is expressed as follows:

$$A = \epsilon dc \quad (2.15)$$

, where

A = absorbance of the sample

ϵ = wavelength-dependent molar absorptivity or molar absorption coefficient ($\text{mol}^{-1} \text{ dm}^3 \text{ cm}^{-1}$)

c = concentration of the solution ($\text{mol} \text{ m}^{-3}$)

d = length of the solution the beam's light passes through (cm)

As increased turbidity in a culture is an index of bacterial growth and cell numbers (biomass), possible bacteria growth will be then checked for two consecutive days, meaning 24 and 48 hours after having been put into the incubator. After an incubation period of 24 hours, the first evaluation takes place. This evaluation consists on a qualitative and a quantitative analysis, meaning the turbidity test (see Figure 2.18) and the spectrophotometric measurement, respectively.



Figure 2.18: Qualitative measurement of the specimen's turbidity compared with the positive control.

To perform the spectrophotometric measurement, whose setup can be seen in Figure 2.19, following steps need to be carried out:

1. 100 μl of the inoculation solution contained in each of the 15 ml plastic tubes are pipetted in the well with the equivalent letter
2. Step 1 is repeated for the same tube three consecutive times, each sample contiguous to the previous one

- Steps 1-2 are repeated for each PCD
- Steps 1-2 are again repeated for the samples used for the positive and negative controls
- The measurement in the spectrophotometer is performed with the plate containing all samples



Figure 2.19: Spectrophotometer with a 96-well plate containing 100 μ l swabs of each PCD.

In addition to the previously described indicators and in order to increase the reliability of the results, often through a comparison between control measurements and the other measurements, appropriate negative and positive controls must be run simultaneously with the samples. Negative controls refer to the experiments that seek to confirm that the equipment or the aseptic techniques used were not comprised, for which no microbial growth should be seen. They ensure that there is no effect when no effect should actually take place. On the other hand, positive controls expect a phenomenon to take place, and should therefore verify the suitability for bacteria to grow when proper conditions are provided. For the positive control, the same exact procedure as with the PCDs is to be carried out, except for the validation step, in which no sterilization step is performed, thus making sure bacteria are not killed and a growth should be observed when placed into the incubator. The comparison between the results of both positive and negative controls and the ones obtained for each sample will allow to reject any hypothetical result obtained by accident.

Once results have been evaluated and analyzed, decisions about the geometric values of the following to-be-tested PCDs need to be made in order to plan the next round of experiments. To continue with, and knowing the limits on the values of the geometry that can be safely and properly sterilized regarding the tubes with both sides open, experiments will be set up for the next structural configuration of the PCDs, meaning dead-ended tubes.

3 Experiments

This chapter presents the experiments carried out within the scope of the current work, necessary to complete the required tasks (Section 2.2). The manner of proceeding and the results obtained with every test will be presented and thoroughly explained.

3.1 Experiment I – Mechanical Characterization

The first experiment refers to the mechanical part, which seeks to define a model capable of predicting the behavior of a nitinol compliant mechanism regarding flexibility and strength.

3.1.1 Determination of the Measurement Procedure

Problem

Because of the large deformations experienced by compliant mechanisms, plastic deformation has to be avoided so that the mechanism only works in the elastic region. In this regard, the largest deflection angle that a mechanism can provide before being plastically deformed needs to be analyzed. The analysis will provide the required information for the definition of the final model capable of predicting the compliant structure's behavior, for which different parameters of the mechanisms will be modified and evaluated, as in next sections further detailed.

Hypothesis

Regarding the conception of the model, modifying the width b of the compliant structure should not alter the results and thus its formulation, meaning that increasing and decreasing the width will provide the same maximum deflection angle for every test specimen, if length L and thickness h are preserved. On the other hand, varying the width b of the beam will have an effect on the applied force, which should become higher as the width increases, as expressed in equation (2.10).

Concerning the length and the thickness of the beam, they are no longer expected to be proportional or inversely proportional, respectively, to the maximum deflected angle that the mechanism can provide. Since the length of the beam is highly directly affected by the small-deflection assumption, it is then thought to have a considerable influence in the final model. Although less directly correlated with such assumption, the thickness of the beam is also a geometric parameter thought to have an effect on the behavior of the mechanism, which should provide wider angles as it decreases. However, the effect of the thickness is expected not to be as pronounced as the one with the length.

Materials

The previously conceived test samples (see Figure 2.9) will be tested in order to obtain information regarding their mechanical behavior in terms of flexibility and strength. The effect of modifying some of their geometric parameters over the model needs to be analyzed, so that a complete experimental validation can be carried out. These compliant structures have been manufactured using wire electric discharge machining (EDM), whereby very intricate and complex shapes are accurately obtained by using electrical discharges.

Besides, for the realization of the experiments, following measurement devices and softwares were employed, which can be seen in Figure 3.1:

- Double bending beam force sensor KD45 with nominal force range: $\pm 5\text{N}$, (ME-Meßsysteme GmbH, Hennigsdorf, Germany)
- Potentiometric displacement sensor 8710-50 with a measurement range: 0-50 mm (Burster Praezisionsmesstechnik GmbH & Co KG, Gernsbach, Germany)
- USB 9 million pixel digital microscope camera (Conrad Electronic SE, Germany)
- eScope software
- DIGIFORCE® 9310 monitor display and software

Experimental Parameters

The main aim of these experiments is to be able to detect the beginning of the plastic deformation, for what the deflected angles experienced by the compliant mechanism will be measured.

Changing values for some of the geometric parameters is thought to have an effect on the behavior of such mechanism. To analyze the particular effect of each of the parameters, several different values were chosen for each of them (see Table 2.2). The selected combinations resulted in 12 different samples, for which only one of the parameters will be modified, keeping the rest constant. Each of the combinations was tested twice, so the results could be reliable.

Table 3.1: Selection of the combination of parameters conforming the compliant structure used for the experiments.

Length L (mm)	Thickness h (mm)	Width b (mm)
3, 4, 5, 6, 7, 8	0.3	0.50
6	0.2, 0.3, 0.4, 0.5	0.50
6	0.3	0.25, 0.50, 0.75, 1.0

Method

The experimental definition of the model will be carried out by making use of a curve fitting tool called multiple regression, which a method used to correlate several independent variables, in our case beam length and thickness, with a dependent one, the maximum deflection angle experienced by the mechanism. It basically consists on matching a linear equation to the experimental data.

The mean values of the experimental data will be used for the curve fitting and, with the standard deviation, they will be plotted and compared to the values provided by the analytical formula given after the regression and with the ones of the classic beam theory equation (refer to equation (2.12)).

The error of the final analytical model in terms of degrees and the standard deviation will be also expressed for its final evaluation.

3.1.2 Experiment for Measuring the Advantages

Experimental Setup

The experimental setup (Figure 3.1) utilized to carry out the mechanical part comprises the following elements:

- Force sensor KD45 with a nominal force range: $\pm 5\text{N}$
- Displacement sensor
- Digital microscope camera
- Force-displacement monitor
- Polyamide 2200 (PA 2200) laser-sintered adapter
- PA 2200 laser-sintered screw cap
- Side screw (M3)

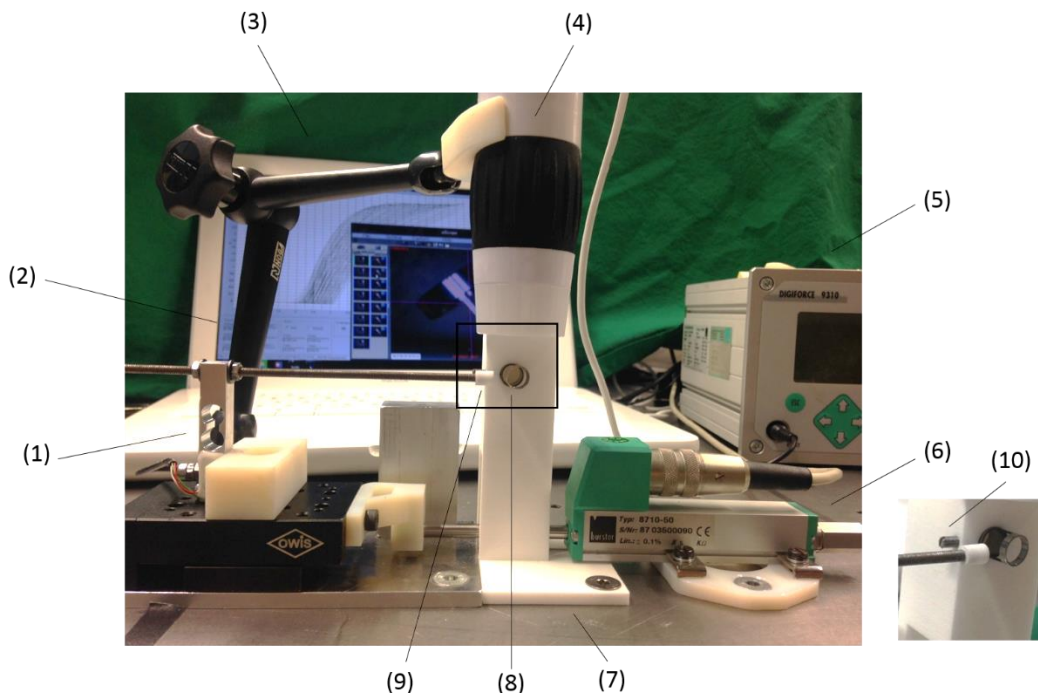


Figure 3.1: Experimental setup. (1) Force sensor. (2) Microscope camera stand. (3) Softwares. (4) Digital microscope camera. (5) Force-displacement monitor. (6) Displacement sensor. (7) Adapter. (8) Compliant mechanism. (9) Screw cap. (10) Side screw.

The force-displacement monitor provides information of the values obtained after performing the test, it allows the user to evaluate the resulting curves as well as to analyze and export all data. The eScope software will be used for capturing the images taken during the experiment.

The laser-sintered adapter has the function of accommodating the compliant structure which is about to be tested. The cap, on the other side, is put on the distal end of the screw that is going to be used to apply the force to the structure. It serves as an enlargement of the surface making contact with the specimen, so that the contact point between them is not going to be lost, no matter how large the deflection angle is. Both the adapter and the screw cap have been designed with CATIA, which is a CAD (Computer-Aided Design) software, and have been manufactured by the EOS Formiga P100 (EOS GmbH, Krailing, Deutschland), a selective laser sintering additive manufacturing machine.

Finally, a side screw was used in order to avoid the part to move while the experiment is being performed. It will therefore be loosened and tightened before and after the placement of each of the test samples.

Experiment Preparation and Realization

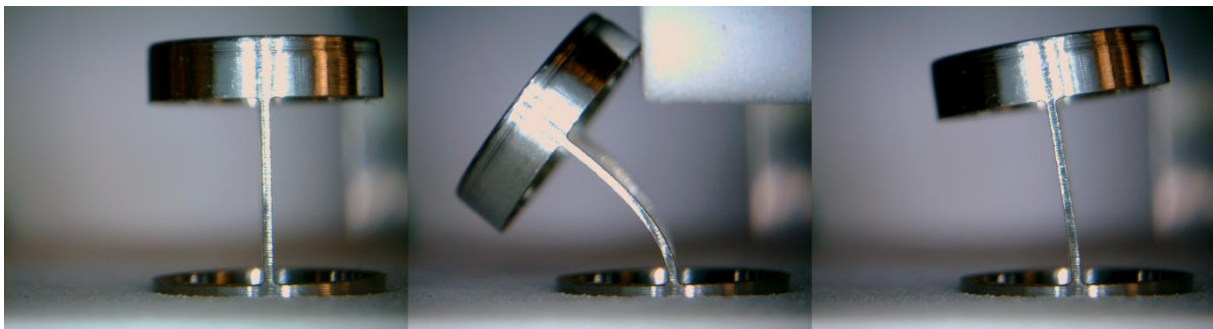
The mechanical experiments were performed at the Institute of Micro Technology and Medical Device Technology (MIMED) at the Technische Universität München and they covered the assay of 24 different structures, resulting of the combination of the different parameters to be evaluated. In order to demonstrate the reproducibility of the results, each combination of length L , width b and thickness h was tested twice, for which two different specimens were conceived. Once the structure was placed in the adapter and fixed at the correct orientation with the side screw, the experiment was ready to be initiated.

To begin with, a starting point was chosen, where there was no contact between the screw applying the force and the outer surface of the part (Figure 3.2), being this position within the measurement range of the sensor. Then the sensor was displaced until a safe position where certainly no plastic deformation had yet taken place. This specific position would change depending on the part being tested. Subsequently the sensor would be returned to its starting position and again gradually further displaced with the consequent deflection of the part, returning always to the starting position after each force/displacement increment. As soon as there was evidence of the plastic deformation of the mechanism, the experiment could be stopped.

Pictures were taken in the starting point as well as in every deflected position (Figure 3.2), which will allow afterwards to detect the particular step at which the plastic deformation started taking place and to calculate the specific angle it did happen at.



(a)



(b)

Figure 3.2: Pictures taken during the realization of the experiment: starting point, most deflected position and final remaining plastic deformation. Compliant mechanism with following measures: (a) $L = 3$ mm, $h = 0.3$ mm and $b = 0.5$ mm; (b) $L = 7$ mm, $h = 0.3$ mm and $b = 0.5$ mm.

The previously taken pictures were afterwards analyzed by detecting the position at which plastic deformation did take place. The measurement of this deflection angle was performed with a CAD software allowing to provide information about all samples, which would be used for the consequent experimental validation of the analytical model.

Results Deduction

With the previously calculated angles, the definition of the final model could be performed. First of all, the experimental data, represented with red crosses on the graphs, were plotted and several statements were then deduced.

To begin with, when evaluating the parameter b , beam width, it was shown that increasing or decreasing it did not change the most deflected angle experienced by the mechanism before reaching failure, as previously expected, meaning the final model will not include the effect of such parameter.

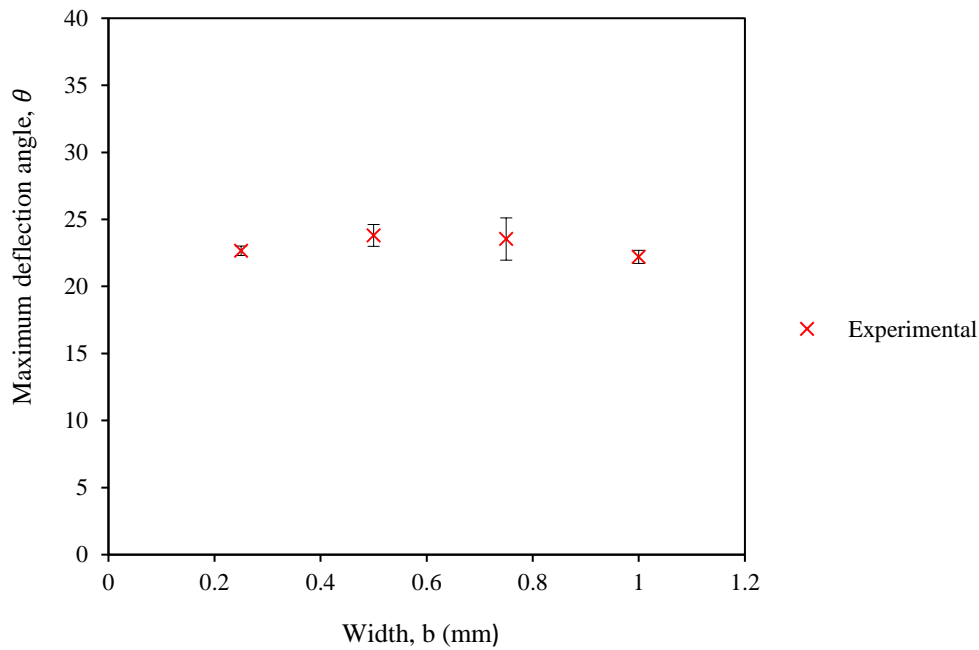


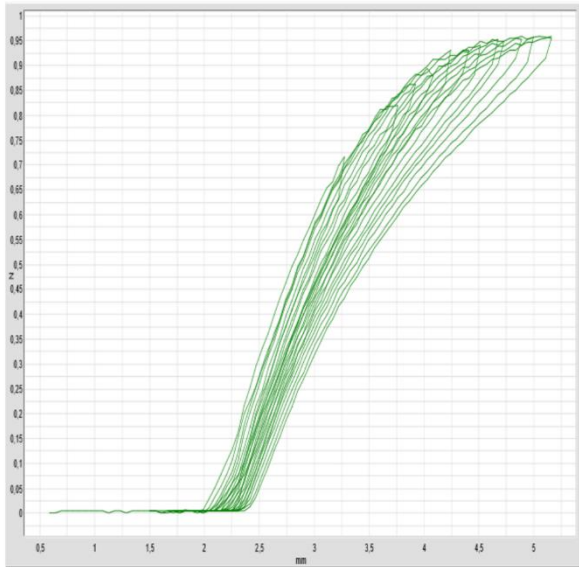
Figure 3.3: Experimental data regarding the maximum deflection angle in terms of the beam width parameter, b .

In addition, some other statements regarding the effect of the beam width could also be observed. When deflecting the mechanism, the force applied increases as the width of the compliant structure also increases (Figure 3.4), as already expected. This can be correlated with the blocked force provided by the surgical manipulator while operating. The wider the beam width of the flexure hinge, the higher the force the tumor can be resected with, which is of great interest, since really big tumors can be found in the bladder and therefore high forces are required for their en bloc resection.

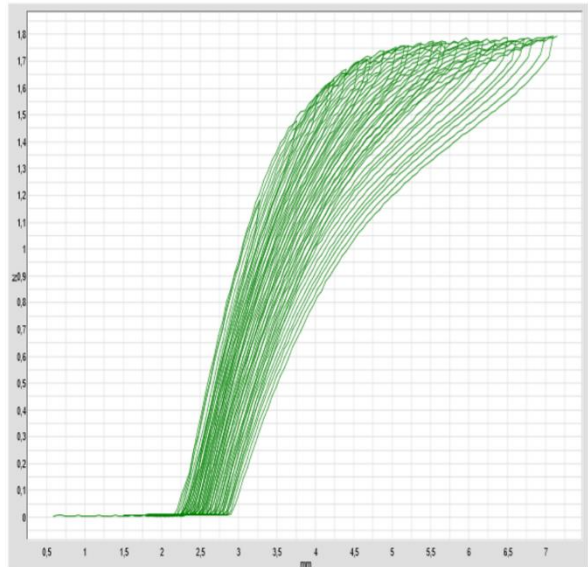
Regarding the geometric parameters beam length and thickness, when plotting the data, a linear tendency could be detected, and provided that the width of the beam was not affecting the yield angle, the multiple linear regression method was employed to approach a linear equation to the experimental data (Figure 3.5 and Figure 3.6), resulting into the final model:

$$\theta_{max} = 17,21^\circ + 2,92^\circ L - 34,72^\circ h \quad (3.1)$$

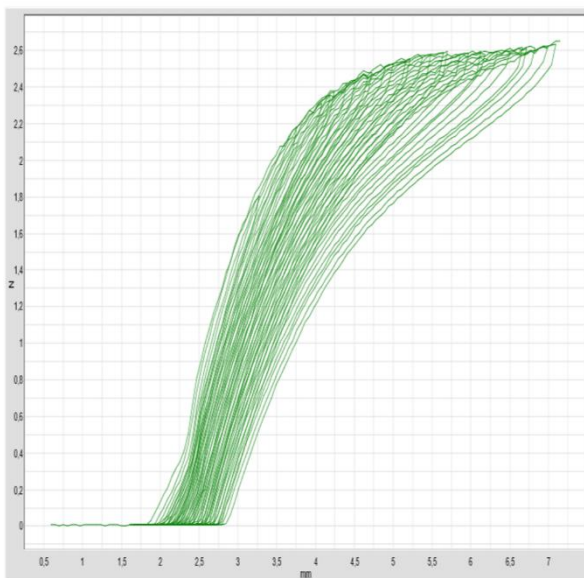
This model describes the behavior of the compliant mechanism and it can provide useful information about the limits of the elastic behavior of the structure regarding its geometric parameters with a mean error of $0.75^\circ \pm 0.72^\circ$.



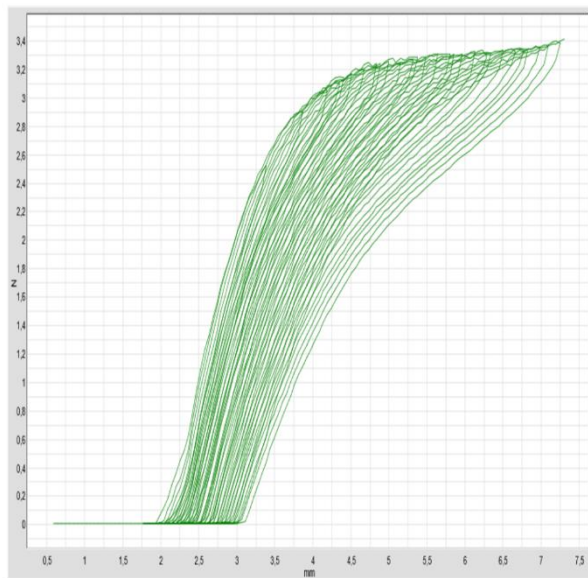
(a)



(b)



(c)



(d)

Figure 3.4: Readings of the force-displacement monitor display for the compliant mechanisms with different values of beam width b . (a) $b = 0.25$ mm. (b) $b = 0.50$ mm. (c) $b = 0.75$ mm. (d) $b = 1.0$ mm.

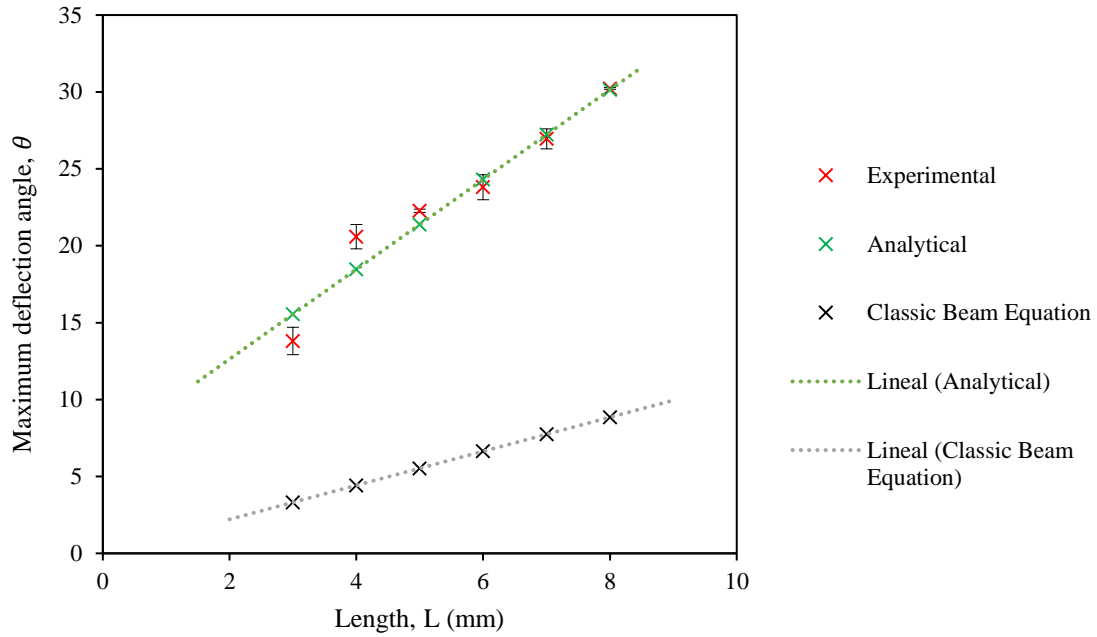


Figure 3.5: Experimental data regarding the maximum deflection angle in terms of the beam length parameter, L .

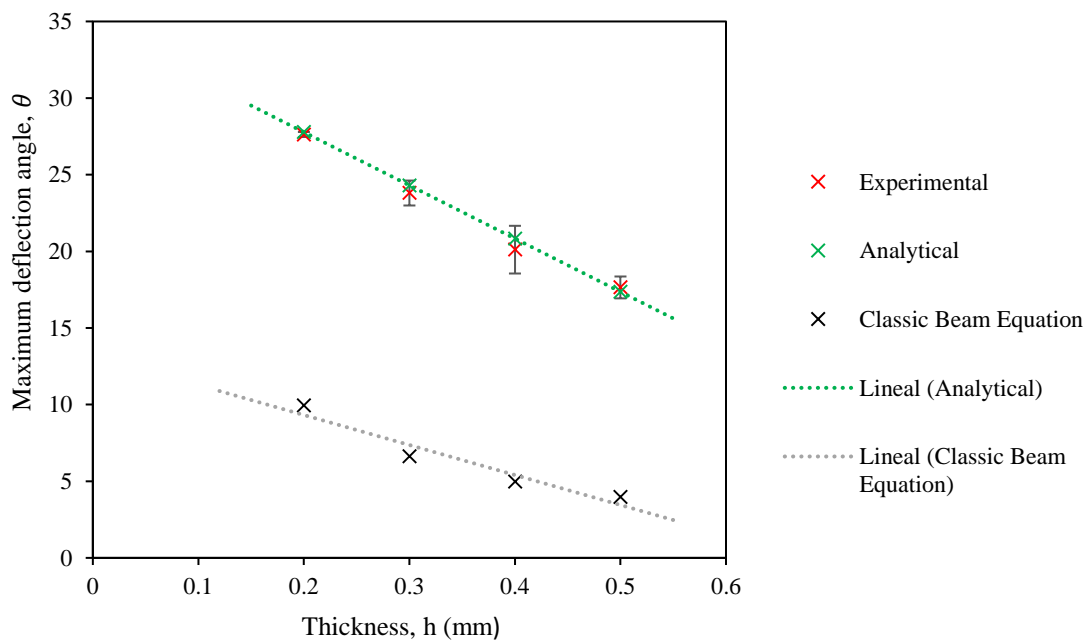


Figure 3.6: Experimental data regarding the maximum deflection angle in terms of the beam thickness parameter, h .

3.1.3 Summary of the Results

Multiple linear regression technique yielded a final model to predict the nitinol compliant mechanism's behavior in terms of the maximum deflection angle that the mechanism can provide before plastic deformation, which depends on both the beam length L and the beam thickness with a mean error of $0.75^\circ \pm 0.72^\circ$.

3.2 Experiment II – Medical Processability

3.2.1 Determination of the Measurement Procedure

Problem

Information about the processability of the stainless steel PCDs should be deduced from the following experiments, being these representative for the small-inner-diameter and thin-walled instruments. This information should be able to provide a limit on the geometry of the tubes that can be properly processed with the steam sterilization technique regarding the maximum length and the smallest inner diameter, so that a general guideline can be obtained for future needs.

Hypothesis

The processability of the PCDs depends on their length and size of their inner diameter, as well as with real-life surgical instrumentation. No conclusive information about the effect of these two parameters has yet been provided. As already mentioned, some studies affirmed that the wider the inner diameter of a tube, the harder to sterilize it, while some would claim exactly the opposite; and some others would say the effect of such parameters cannot be explained in a logical manner. Regarding the length, there is a general agreement, which states that the steam penetration decreases with increasing tube length.

On the basis that geometrical parameters do have an influence upon the processability of an item, we seek to obtain knowledge about the effect of these parameters in such small geometries, about which no information is available.

Materials

Besides the different PCDs used to perform the tests, several other materials and devices have also been utilized for the several steps carried out, which are listed below.

Processing Steps

- Bandelin Sonorex Technik RM 40 UH ultrasonic cleaner
- 4% diluted Kohrsolin glutaraldehyde-based disinfectant solution
- WEBECO A50-B table-top steam sterilizer
- Heat-sealed plastic/paper peel-open envelopes

Validation Steps

In addition to the previously mentioned ones for the processing steps, following materials and instruments were also employed for the validation part:

- 500 ml borosilicate glass beakers
- 300 ml Erlenmeyer flasks
- Escherichia coli (OD 0.159)
- 15 ml sterile falcon tubes
- 96-well plates
- Spectrophotometer
- Autoclavable 200 μ l pipette microtips
- 200 μ l adjustable pipette
- Biological safety cabinet
- Digital calliper

Experimental Parameters

The experimental parameters modified for the different tests were the length and the inner diameter of the PCDs. As in previous sections schematically illustrated, the change of such parameters was performed regarding the results of the prior tests, always seeking to obtain the limit on the geometry which can be safely sterilized.

Material, manufacturing process and protocols, meaning the way of proceeding in every step, were exactly the same for all experiments, so comparable results could be obtained.

In order to get information about the processability of the PCDs, quantitative and qualitative tests were carried out. Measuring the absorbance at 620 nm of every swab in the spectrophotometer refers to the quantitative measurement, while the qualitative test corresponds to checking their turbidity, especially after a period long enough for the bacteria to have stopped growing, being thus able to provide conclusive information.

Method

Three different spectrophotometric measurements of the absorbance of each swab at 620 nm were performed for each test sample in order to obtain a reliable result. The mean value and the standard deviation of such measurements were used for their evaluation. Exceeding a limit value on the spectrophotometric measurements was seen as a proof of nonsterility. The value selected as a limit was one high enough to already ensure bacterial growth. Comparison with the measurements of the positive and negative controls also helped ensuring that there were no misleading results.

3.2.2 Experiment for Measuring the Advantages

Experimental Setup

The totality of the sterilization experiments were carried out in a laboratory equipped with all previously mentioned needed devices.

The setup used for the validation phase of the sterilization process can be seen in Figure 3.7. It was performed in a biological safety cabinet with sterile materials, which are required in order not to contaminate the results.

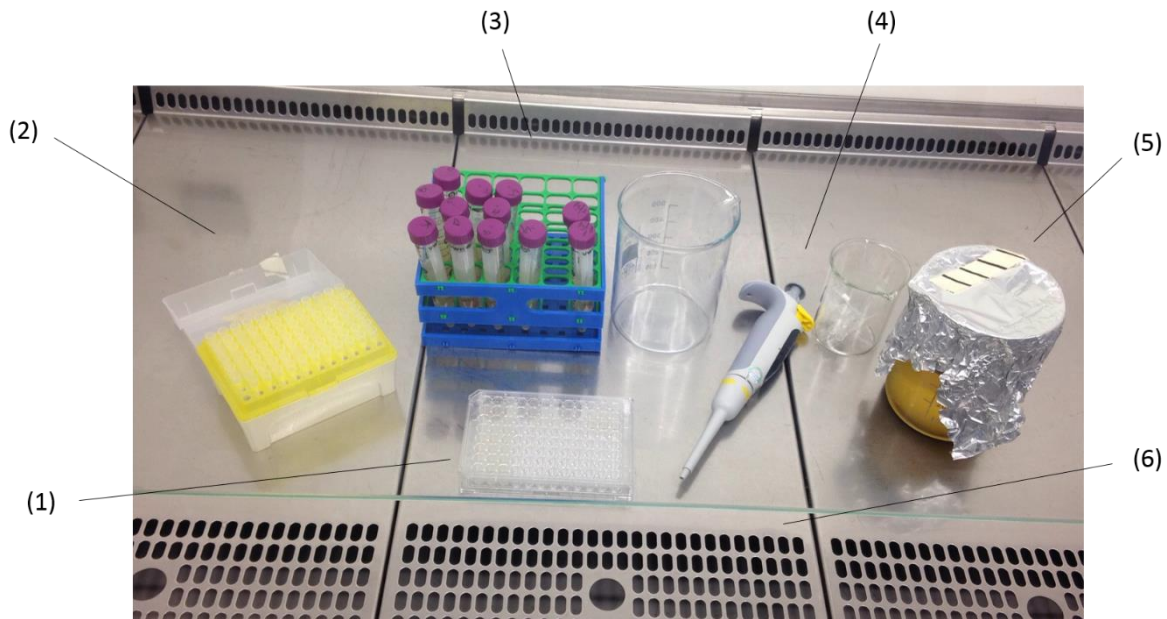


Figure 3.7: Setup for the analysis of the PCDs. (1) 96-well plate. (2) Autoclavable 200 µl pipette microtips. (3) 15 ml plastic tubes with inoculation solution. (4) 200 µl adjustable pipette. (5) Sterile broth solution. (6) Biological safety cabinet.

Experiment Preparation and Realization

The sterilization experiments were performed at the Institute of Medical Engineering (MedTech) at the Technische Universität München.

Once the initial values for the PCDs to be tested were decided, the experiments were performed. Several different ways of contaminating the inside of the lumen were tried, as well as for the recovery of the bacteria.

The first experiments covered a total of 45 different PCDs with the measures shown in Table 2.4. However, the initial way of proceeding was slightly different from the final one, extensively explained in Section 2.8.3. When inoculating the PCDs, they were simply submerged into the bacterial solution, assuming that solution would enter the lumen by natural means and also using a vortex mixer to help facilitating the process. When put into the incubation shaker, the tested tubes would be submerged into the growth solution and placed inside it and let incubate for 48 hours. After the incubation period, the 45 PCDs resulted to be all sterile, provided that no bacteria had grown into the solution were the PCDs had been put.

From literature, indirect inoculation of the lumens using a wire was then selected, which also proved not to be reliable since no bacterial growth was detected in the positive control, meaning no contamination was actually carried out.

In order to assess the processability of the samples and ensuring the inner surface of the lumen contacted the bacteria, a flushing step was introduced which, as previously stated, consisted on the injection of the media with a needle through the whole length of the lumen.

In order to obtain useful and detailed information about the limits on the geometry that could be safely processed, a total number of 60 PCDs with both ends open were finally tested following the methodology presented in Section 2.8.3, whose results will be discussed in the next section. Spectrophotometric measurements were performed 24 and 48 hours after placing the tubes with the swabs in the incubator. For those being still sterile and wanting to ensure bacteria would not grow at all, spectrophotometric measurements were also carried out one week after the experiments.

Regarding the 10 one-end-closed PCDs conceived, when performing the validation phase, it was observed that the methodology used to test the previous configuration was not suitable, since the flushing step could not be properly conducted and no other adequate method could be found. Therefore, no information in regard to the processability of dead-end PCDs was obtained.

Results Deduction

Following graphs show the results of the tested PCDs, particularly the values refer to the mean value of their spectrophotometric measurements. The standard deviation of the spectrophotometric measurements is plotted as a vertical line with a dash and a discontinuous line, denominated as sterility barrier (SB), is represented so the limit between sterile and nonsterile can be clearly delimited. Table 3.2 provides information about the geometric measurements of the different PCDs

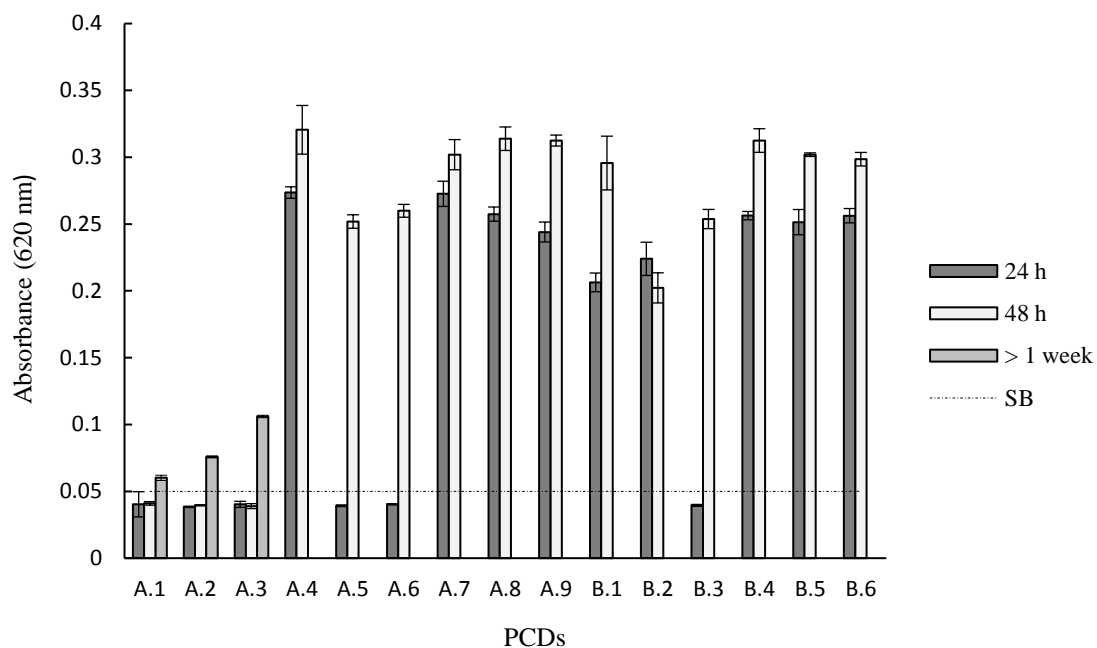


Figure 3.8: Sterilization results for inoculated lumens of different internal diameters and lengths 24h, 48 h and one week after performing the experiments – Part I.

The previous chart shows the sterilization results for the PCDs tested with inner diameters of 0.2 and 0.3 mm with their corresponding different lengths, selected during the entire procedure and determined by previous sterilizations results. All of the different spectrophotometric measurements exceed the value of 0.05, being defined as the sterilization barrier or limit, meaning they all turned out to be nonsterile after the experiments and its corresponding evaluation. For the samples showing no bacterial growth after 48 hours, namely A.1, A.2 and A.3, measurements were also performed one week after the realization of the experiment, showing in this case a slightly change in their measurements and leading to a value considered to be high enough to considerate them as nonsterile anymore. The reason for them to present a slower bacterial growth could be the smaller surface to which the bacteria can get attached to, meaning that a small number of bacteria would need more time to grow.

Regarding the second and the third parts of the experiments, all PCDs resulted to be nonsterile except for two. The PCDs tested in these parts comprised tubes with inner diameters from 0.4 and 0.8 mm with lengths in a range between 10 and 450 mm. The only two samples in which no bacterial growth was detected could be due to inaccuracies while performing any of the several steps of the entire process.

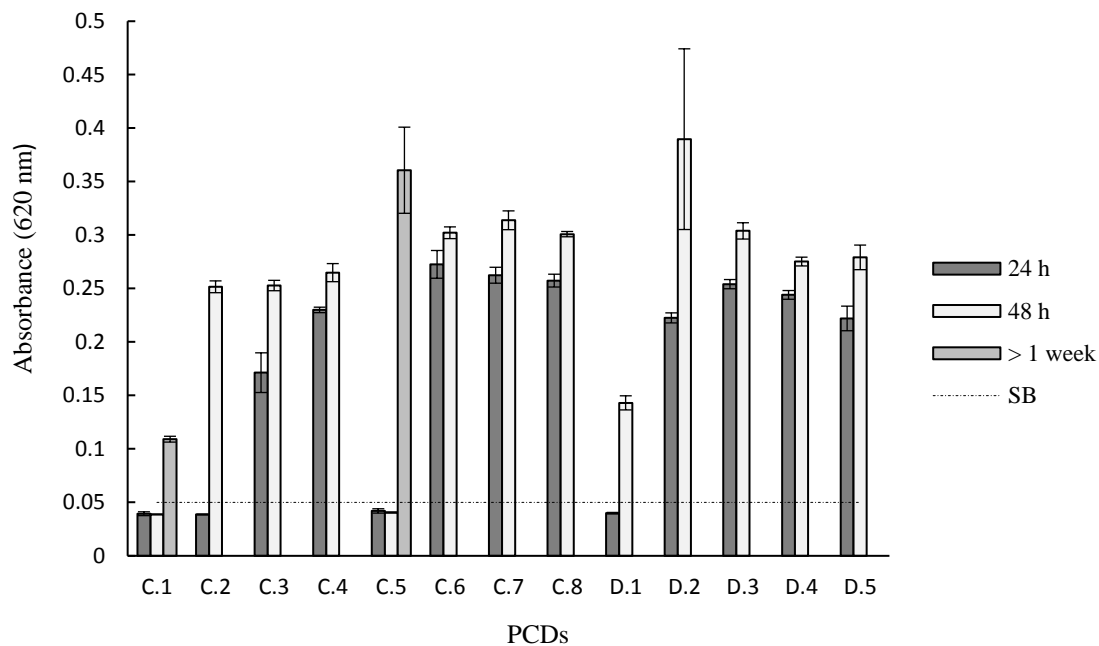


Figure 3.9: Sterilization results for inoculated lumens of different internal diameters 24h, 48 h and one week after performing the experiments – Part II.

The last round of experiments (Figure 3.11) showed more interesting results, since inner diameters wider than 4 mm proved to be sterile, both of the different samples, and tubes with inner diameters between 2 and 3 mm resulted to be harder to sterilize as their length decreased, for what no scientific explanation could yet be found. Besides, tubes with inner diameters of 0.9 and 1.0 mm resulted to be nonprocessable.

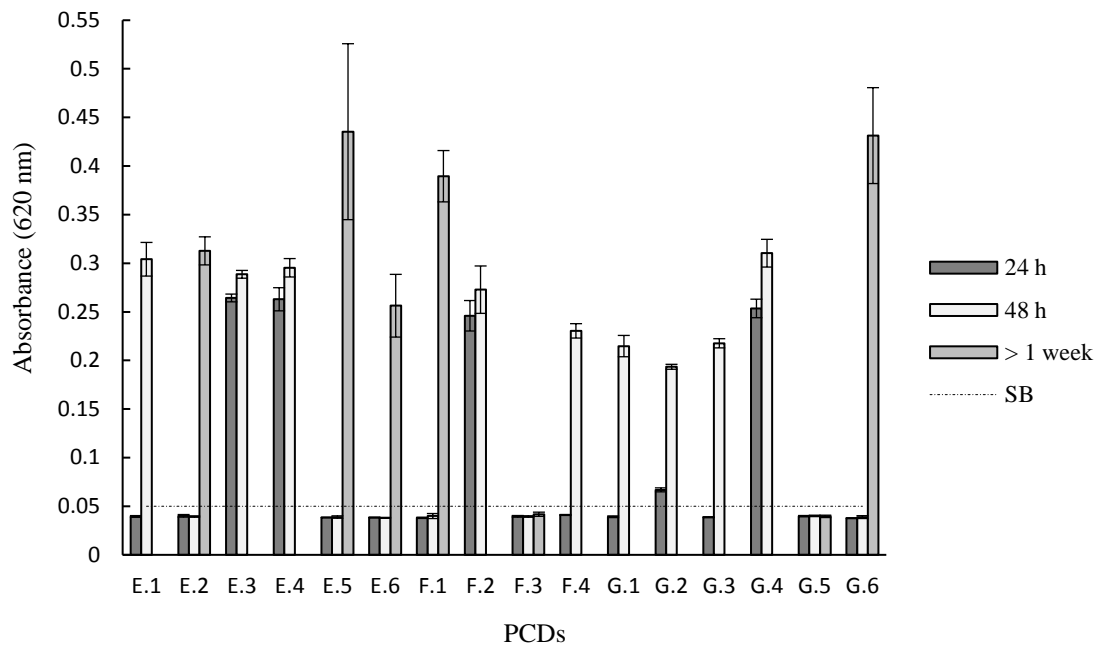


Figure 3.10: Sterilization results for inoculated lumens of different internal diameters 24h, 48 h and one week after performing the experiments – Part III.

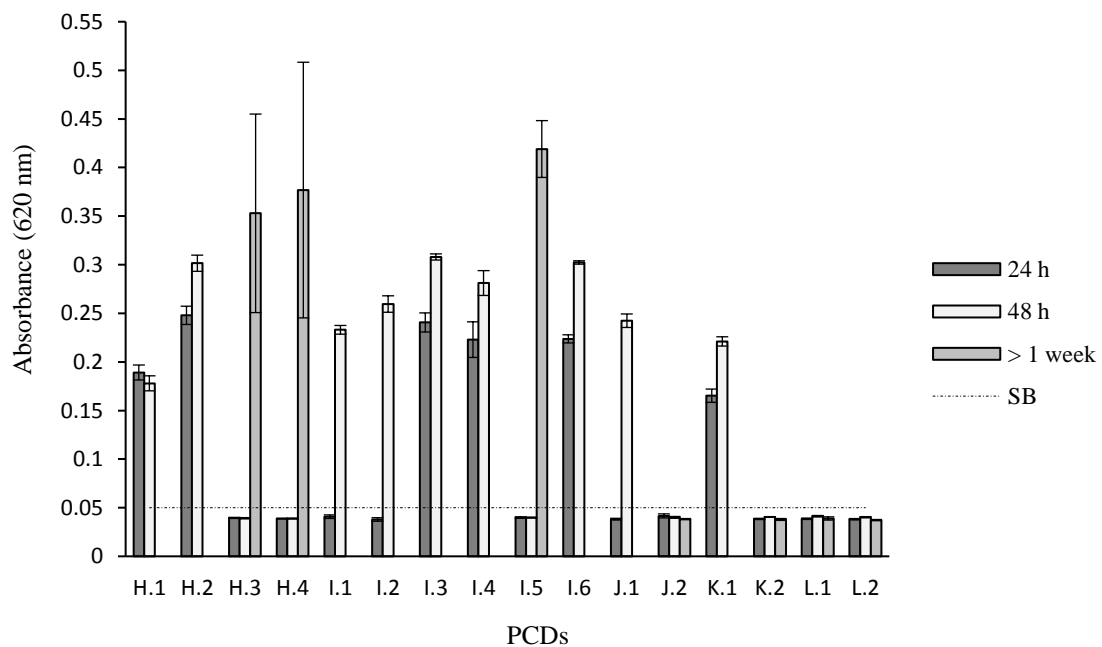


Figure 3.11: Sterilization results for inoculated lumens of different internal diameters 24h, 48 h and one week after performing the experiments – Part IV.

Regarding the negative and positive controls used to verify the results and to ensure that bacteria was actually able to grow in such conditions and that sterile swabs did not get contaminated during the procedure, it can be seen in Figure 3.12 that their state after one week of the realization of the experiments was the expected one, therefore the results obtained and plotted in the graphs showed above can be reliable.

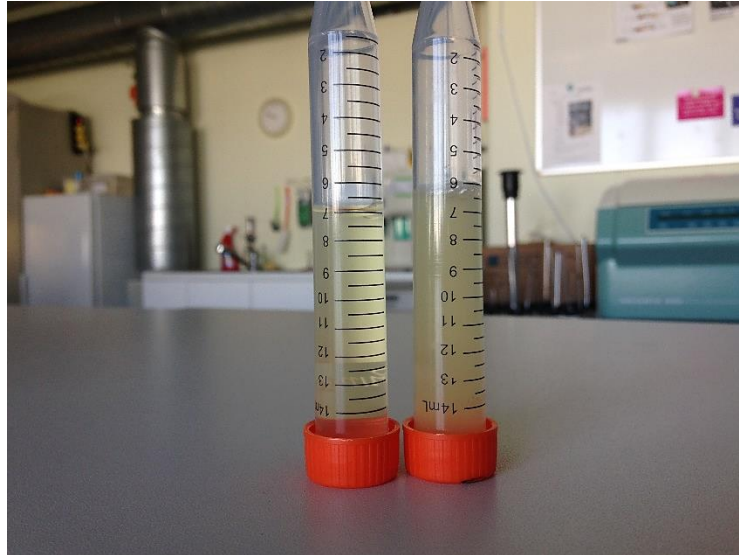


Figure 3.12: Negative and positive controls states one week after the realization of one of the rounds of the experiments.

Table 3.2: Specifications of the PCDs tested.

PCD	ID (mm)	Length (mm)	PCD	ID (mm)	Length (mm)
A.1	0.2	5	E.3	0.6	60
A.2	0.2	10	E.4	0.6	120
A.3	0.2	20	E.5	0.6	180
A.4	0.2	40	E.6	0.6	240
A.5	0.2	60	F.1	0.7	70
A.6	0.2	80	F.2	0.7	140
A.7	0.2	160	F.3	0.7	210
A.8	0.2	300	F.4	0.7	280
A.9	0.2	450	G.1	0.8	20
B.1	0.3	30	G.2	0.8	40
B.2	0.3	60	G.3	0.8	80
B.3	0.3	90	G.4	0.8	160
B.4	0.3	150	G.5	0.8	240
B.5	0.3	300	G.6	0.8	320
B.6	0.3	450	H.1	0.9	90
C.1	0.4	10	H.2	0.9	180
C.2	0.4	20	H.3	0.9	270
C.3	0.4	40	H.4	0.9	360
C.4	0.4	80	I.1	1.0	25
C.5	0.4	120	I.2	1.0	50
C.6	0.4	160	I.3	1.0	100
C.7	0.4	320	I.4	1.0	200
C.8	0.4	450	I.5	1.0	300
D.1	0.5	50	I.6	1.0	400
D.2	0.5	100	J.1	2	100
D.3	0.5	150	J.2	2	200
D.4	0.5	300	K.1	3	150
D.5	0.5	450	K.2	3	300
E.1	0.6	15	L.1	5	200
E.2	0.6	30	L.2	5	400

3.2.3 Summary of the Results

Following table summarizes the results of the sterilization experiments. The green color represents that the PCD resulted to be sterile after the experiment, while, on the other hand, the red color indicates that the tube was not able to be steam processed.

Inner Diameter (mm)	Length (mm)
0,2	5-10-20-40-60-80-160-300-450
0,3	30-60-90-150-300-450
0,4	10-20-40-80-120-160-320-450
0,5	50-100-150-300-450
0,6	15-30-60-120-180-240
0,7	70-140-210-280
0,8	20-40-80-160-240-320
0,9	90-180-270-360
1,0	25-50-100-200-300-400
2,0	100-200
3,0	150-300
5,0	200-400

4 Summary and Outlook

To sum up, major conclusions and further work will be specified. Regarding the mechanical characterization of the nitinol compliant mechanism a final model depending on the beam length and thickness was experimentally obtained for a range of geometric values adapted to the needs of our surgical manipulator and providing a mean error of $0.75^{\circ} \pm 0.72^{\circ}$. This model describes the behavior of such structure in terms of strength and flexibility, and, particularly, it gives the maximum deflection angle that the mechanism can experience before failure, namely plastic deformation. The final validation of the numerical model should still need to be performed, considered as part of the further work to be done.

According to the results obtained in the present thesis, and regarding the medical processability of a surgical instrument, we were able to find a proper direct inoculation method for such small and complex geometry, which cannot incorporate traditional measurement techniques, consisting on a flushing step where the inner surface of the lumen is contaminated. We also deduced that small diameters are harder to sterilize than larger ones, and, specifically, narrow lumens with inner diameters smaller than 1 mm could not be steam sterilized. Statements regarding inner diameter lumens between 1 and 2 mm showed a trend in which longer lumens were easier to sterilize, which should be further investigated with a more extended number of test samples. Concerning lumens with internal diameters of 5 mm, sterility results of the representative samples for such geometric values did not present bacterial growth, considered then as sterile geometries.

As a conclusion, relevant information could be obtained from the present work, which could be used to further improve the design of the surgical manipulator and to provide information related to its medical processability in terms of steam sterilization techniques.

References

- Aguirre, M.E., Hayes, G.R., Meiom, G.R., Frecker, M.I., Muhlstein, C.L. and Adair, J.H. (2011), “Optimal Design and Fabrication of Narrow-Gauge Compliant Forceps”, *Journal of Mechanical design*, Vol. 133 No. 8, 081005.
- Antoniou, S.A. and Bartsch, D.K. (2012), “NOTES: Current Status and Recent Developments”, *Viszeralmedizin*, Vol. 28 No. 6, pp. 388–394.
- ASP, Johnson & Johnson, *Sterilizer Brochure*.
- Babjuk, M. (2009), “Transurethral Resection of Non-muscle-invasive Bladder Cancer”, *European Urology Supplements*, Vol. 8 No. 7, pp. 542–548.
- Bajo, A., Pickens, R.B., Herrell, S.D. and Simaan, N. (2013), “Constrained motion control of multisegment continuum robots for transurethral bladder resection and surveillance”, in *2013 IEEE International Conference on Robotics and Automation, Karlsruhe, Germany, 06/05/2013 - 10/05/2013*, IEEE, pp. 5837–5842.
- Biscarini, A., Mazzolai, G. and Tuissi, A. (2008), “Enhanced Nitinol Properties for Biomedical Applications”, *Recent Patents on Biomedical Engineering*, Vol. 1 No. 3, pp. 180–196.
- Borchers, U. and Mielke, M. (2004), “How material, length, wall thickness and diameter of hollow devices affect the inactivation behaviour of biological indicators when subjected to moist heat treatment.”, Vol. 12 No. 5, pp. 314–323.
- Borneff-Lipp, M., Kaetzke, A. and Dürr, M. (2008), “Evaluation of Low Temperature Hydrogen Peroxide Plasma (LTS) Sterilization. Results of Three Different Technologies”, *Central Service*, Vol. 16 No. 1, pp. 35–42.
- British Columbia Ministry of Health (2011), *Best Practice Guidelines for Cleaning, Disinfection and Sterilization in Health Authorities*.
- Cao, L., Dolovich, A.T., Schwab, A.L., Herder, J.L. and Zhang, W.C. (2015), “Toward a Unified Design Approach for Both Compliant Mechanisms and Rigid-Body Mechanisms: Module Optimization”, *Journal of Mechanical design*, Vol. 137 No. 12, p. 122301.
- Carter, A., Biering, H. and Gebel, J. (2013), “Guideline for Validation of Manual Cleaning and Manual Chemical Disinfection of Medical Devices”, *Zentral Sterilisation*.
- Cronin, J.A., Frecker, M.I. and Mathew, A. (2008), “Design of a Compliant Endoscopic Suturing Instrument”, *Journal of Medical Devices*, Vol. 2 No. 2, p. 25002.
- de Bruijn, A.C.P. and van Drongelen, A.W. (2005), “Performance Evaluation of Hospital Steam Sterilisers Using the European Helix Test”, *Zentral Sterilisation*, Vol. 13 No. 1, pp. 26–33.
- Deutsche Gesellschaft für Sterilgutversorgung (2006), “Empfehlungen des AK „Qualität“ (45): Aufbereitung englumiger Medizinprodukte (1)”, *Zentral Sterilisation*, pp. 311–313.
- Dion, M. and Parker, W. (2013), “Steam Sterilization Principles”, *Pharmaceutical Engineering*, Vol. 33 No. 6, pp. 1–8.
- Dufresne, S., Hewitt, A. and Robitaille, S. (2004), “Ozone Sterilization. Another Option for Healthcare in the 21st Century”, *American journal of infection control*, Vol. 32 No. 3, E26-E27.

- Dufresne, S., Leblond, H. and Chaunet, M. (2008), "Relationship between lumen diameter and length sterilized in the 125L ozone sterilizer", *American journal of infection control*, Vol. 36 No. 4, pp. 291–297.
- Erdman, A.G., Sandor, G.N. and Kota, S. (2001), *Mechanism design: Analysis and synthesis*, 4th ed, Prentice Hall, Upper Saddle River, N.J.
- Food and Drug Administration, Division of General and Restorative Devices (1993), *Guidance on Premarket Notification [510(k)] Submissions for Sterilizers Intended for Use in Health Care Facilities.*, Rockville, MD.
- Food and Drug Administration (FDA) (2014), *Pharmaceutical Microbiology Manual - FDA*.
- Fraise, A.P., Lambert, P.A. and Maillard, J.-Y. (2004), *Russell, Hugo & Ayliffe's Principles and Practice of Disinfection, Preservation & Sterilization*, Blackwell Publishing Ltd, Oxford, UK.
- Frecker, M.I., Ananthasuresh, G.K., Nishiwaki, S., Kikuchi, N. and Kota, S. (1997), "Topological Synthesis of Compliant Mechanisms Using Multi-Criteria Optimization", *Journal of Mechanical design*, Vol. 119 No. 2, pp. 238–245.
- Frecker, M.I., Powell, K.M. and Haluck, R. (2005), "Design of a Multifunctional Compliant Instrument for Minimally Invasive Surgery", *Journal of Biomechanical Engineering*, Vol. 127 No. 6, pp. 990–993.
- Gillen, S., Kleeff, J., Kranzfelder, M., Shrikhande, S.V., Friess, H. and Feussner, H. (2010), "Natural orifice transluminal endoscopic surgery in pancreatic diseases", *World Journal of Gastroenterology*, Vol. 16 No. 31, p. 3859.
- Goemann, J., Kaiser, U. and Menzel, R. (2001), "Air removal from porous and hollow goods using different steam sterilization processes", *Zentral Sterilisation*, Vol. 9 No. 3, pp. 177–186.
- Goldman, R.E., Bajo, A., MacLachlan, L.S., Pickens, R., Herrell, S.D. and Simaan, N. (2013), "Design and performance evaluation of a minimally invasive telerobotic platform for transurethral surveillance and intervention", *IEEE transactions on biomedical engineering*, Vol. 60 No. 4, pp. 918–925.
- Herrell, S.D., Webster, R. and Simaan, N. (2014), "Future robotic platforms in urologic surgery. Recent developments", *Current opinion in urology*, Vol. 24 No. 1, pp. 118–126.
- Hertzberg, R.W. (1989), *Deformation and fracture mechanics of engineering materials*, 3. ed., Wiley, New York.
- Hole, J.W. (1981), *Human Anatomy and Physiology*, McGraw-Hill Education, Dubuque.
- Howell, L.L. (2001), *Compliant mechanisms*, Wiley, New York.
- Howell, L.L., Magleby, S.P. and Olsen, B.M. (2013), *Handbook of Compliant Mechanisms*, John Wiley & Sons Ltd, Oxford, UK.
- Howell, L.L. and Midha, A. (1994), "A Method for the Design of Compliant Mechanisms With Small-Length Flexural Pivots", *Journal of Mechanical design*, Vol. 116 No. 1, pp. 280–290.
- Hoyos, J.V.D.G. and Kopinga, K. (2015), "Steam penetration in thin-walled channels and helix shaped Process Challenge Devices.", *Zentralsterilisation*.
- Jurewicz, M. and Soloway, M.S. (2014), "Approaching the optimal transurethral resection of a bladder tumor", *Turkish journal of urology*, Vol. 40 No. 2, pp. 73–77.

- Kaiser, D., Kaiser, U. and Vogel, H. (2006), “A quantitative description of air removal from hollow devices in steam sterilization processes”, *Central Service*, Vol. 14 No. 4, pp. 275–288.
- Kaiser, U. and Gömann, J. (1998), “Investigation of air removal from hollow devices in steam sterilization processes.”, *Central Service*, Vol. 6, pp. 401–413.
- Kirk, B., Smith, A. and Winter, S. (2016), “Performance of Hollow Load Process Challenge Devices (HLPCDs) for the determination of air removal and steam penetration in porous load steam sterilization processes: Part 1–The evolution of HLPCDs in standards and a review of the current supporting published evidence.”, *Zentral Sterilisation*, pp. 308–314.
- Kommission für Krankenhaushygiene und Infektionsprävention (KRINKO) and Bundesinstitutes für Arzneimittel und Medizinprodukte (BfArM) (2012), “Anforderungen an die Hygiene bei der Aufbereitung von Medizinprodukten. Empfehlung der Kommission für Krankenhaushygiene und Infektionsprävention (KRINKO) beim Robert Koch-Institut (RKI) und des Bundesinstitutes für Arzneimittel und Medizinprodukte (BfArM)”, *Bundesgesundheitsblatt, Gesundheitsforschung, Gesundheitsschutz*, Vol. 55 No. 10, pp. 1244–1310.
- Kota, S., Lu, K.J., Kreiner, Z., Trease, B., Arenas, J. and Geiger, J. (2005), “Design and Application of Compliant Mechanisms for Surgical Tools”, *Journal of Biomechanical Engineering*, Vol. 127 No. 6, p. 981.
- Kramer, M.W., Wolters, M., Cash, H., Jutzi, S., Imkamp, F., Kuczyk, M.A., Merseburger, A.S. and Herrmann, T.R.W. (2015), “Current evidence of transurethral Ho: YAG and Tm: YAG treatment of bladder cancer: update 2014”, *World Journal of Urology*, Vol. 33 No. 4, pp. 571–579.
- Kremmel, M., Laudner, W. and Task Group (Länderarbeitskreis) «Open Questions in Reprocessing» (2011), “Testing the performance of process challenge devices (PCDs) used to check air removal from hollow instruments and effectiveness of sterilisation in steam sterilisation processes”, *Zentral Sterilisation*, Vol. 2, pp. 100–104.
- Lagoudas, D.C. (2011), *Shape memory alloys: Modeling and engineering applications*, Springer, New York, London.
- Liu, J., Hall, B., Frecker, M. and Reutzel, E.W. (2013), “Compliant articulation structure using superelastic NiTiNOL”, *Smart Materials and Structures*, Vol. 22 No. 9, p. 94018.
- Lu, K.-J. and Kota, S. (2005), “An Effective Method of Synthesizing Compliant Adaptive Structures using Load Path Representation”, *Journal of Intelligent Material Systems and Structures*, Vol. 16 No. 4, pp. 307–317.
- Miller, D.A. and Lagoudas, D.C. (2000), “Thermomechanical characterization of NiTiCu and NiTi SMA actuators: influence of plastic strains.”, *Smart Materials and Structures*, Vol. 9 No. 5, pp. 640–652.
- Patel, N., Darzi, A. and Teare, J. (2015), “The endoscopy evolution. 'the superscope era'”, *Frontline gastroenterology*, Vol. 6 No. 2, pp. 101–107.
- Pemberton, R.J., Tolley, D.A. and van Velthoven, R.F. (2006), “Prevention and management of complications in urological laparoscopic port site placement”, *European urology*, Vol. 50 No. 5, pp. 958–968.
- Ray, E.R. and O'Brien, T.S. (2007), “Should urologists be spending more time on the golf course?”, *BJU International*, Vol. 100 No. 4, pp. 728–729.

- Rutala, W.A. and Weber, D.J. (1998), "Clinical Effectiveness of Low-Temperature Sterilization Technologies", *Infection Control and Hospital Epidemiology*, Vol. 19 No. 10, pp. 798–804.
- Rutala, W.A. and Weber, D.J. (2004), "Disinfection and sterilization in health care facilities: what clinicians need to know.", *Clinical infectious diseases*, Vol. 39 No. 5, pp. 702–709.
- Rutala, W.A., Weber, D.J. and Healthcare Infection Control Practices Advisory Committee (HICPAC) (2008), "Guideline for Disinfection and Sterilization in Healthcare Facilities, 2008", *Guidelines for environmental infection control in health-care facilities. MMWR*, Vol. 52 No. 10, pp. 1–48.
- Shang, J., Noonan, D.P., Payne, C., Clark, J., Sodergren, M.H., Darzi, A. and Yang, G.Z. (2011), "An Articulated Universal Joint Based Flexible Access Robot for Minimally Invasive Surgery", *2011 IEEE International Conference on Robotics and Automation*, pp. 1147–1152.
- Shoup, T.E. (1972), "On the Use of the Nodal Elastica for the Analysis of Flexible Link Devices", *ASME Journal of Engineering for Industry*, Vol. 94 No. 3, pp. 871–875.
- Shoup, T.E. and McLarnan, C.W. (1971), "On the Use of Undulating Elastica for the Analysis of Flexible Link Mechanisms.", *ASME Journal of Engineering for Industry*, Vol. 93 No. 1, pp. 263–267.
- Smith, J.A. (1989), "Laser treatment of urologic cancers", *Seminars in Surgical Oncology*, Vol. 5 No. 1, pp. 30–37.
- Stewart, B.W. and Wild, C.P. (2014), *World Cancer Report 2014*, International Agency for Research on Cancer, WHO.
- Su, H.J. (2009), "A pseudorigid-body 3R model for determining large deflection of cantilever beams subject to tip loads.", *Journal of Mechanisms and Robotics*, Vol. 1 No. 2, p. 21008.
- Swanstrom, L.L., Kozarek, R., Pasricha, P.J., Gross, S., Birkett, D., Park, P.-O., Saadat, V., Ewers, R. and Swain, P. (2005), "Development of a new access device for transgastric surgery", *Journal of gastrointestinal surgery official journal of the Society for Surgery of the Alimentary Tract*, Vol. 9 No. 8, 1129-36; discussion 1136-7.
- Thompson, C.C., Ryou, M., Soper, N.J., Hungess, E.S., Rothstein, R.I. and Swanstrom, L.L. (2009), "Evaluation of a manually driven, multitasking platform for complex endoluminal and natural orifice transluminal endoscopic surgery applications (with video)", *Gastrointestinal endoscopy*, Vol. 70 No. 1, pp. 121–125.
- Ukai, R., Kawashita, E. and Ikeda, H. (2000), "A new technique for transurethral resection of superficial bladder tumor in 1 piece", *The Journal of urology*, Vol. 163 No. 3, pp. 878–879.
- van Doornmalen, J.P.C.M., Verschueren, M. and Kopinga, K. (2013), "Penetration of water vapour into narrow channels during steam sterilization processes", *Journal of Physics D: Applied Physics*, Vol. 46 No. 6, p. 65201.
- Vitiello, V., Lee, S.-L., Cundy, T.P. and Yang, G.-Z. (2013), "Emerging robotic platforms for minimally invasive surgery", *IEEE reviews in biomedical engineering*, Vol. 6, pp. 111–126.
- Wilby, D., Thomas, K., Ray, E., Chappell, B. and O'Brien, T. (2009), "Bladder cancer: New TUR techniques", *World Journal of Urology*, Vol. 27 No. 3, pp. 309–312.

-
- Working Group Instrument Preparation (2001a), “Sterilisability of Reusable Surgical Instruments. Part 1: General Introduction – PCD Designing Process – Experimental Design”, *Zentral Sterilisation*, Vol. 9 No. 6, pp. 425–437.
- Working Group Instrument Preparation (2001b), “Sterilisability of Reusable Surgical Instruments. Part 2: Study Results – Implications for Working Practices in the CSSD”, *Zentral Sterilisation*, Vol. 10 No. 2, pp. 100–109.
- Wu, M.H. (2002), “Fabrication of Nitinol Materials and Components. Trans Tech Publications”, *Materials Science Forum*, Vol. 394, pp. 285–292.
- Yoshida, M., Furukawa, T., Morikawa, Y., Kitagawa, Y. and Kitajima, M. (2010), “The developments and achievements of endoscopic surgery, robotic surgery and function-preserving surgery”, *Japanese journal of clinical oncology*, Vol. 40 No. 9, pp. 863–869.
- Young, J.H. (1993), “Sterilization of various diameter dead-ended tubes”, *Biotechnology and bioengineering*, Vol. 42 No. 1, pp. 125–132.

LIST OF FIGURES

Figure 1.1: Transurethral Resection of Bladder Tumors (TURBT). (Source: Bajo <i>et al.</i> , 2013).	3
Figure 1.2: En bloc resection technique of a bladder tumor. (A), (B) A superficial circular incision around the tumor is initially made, keeping a margin of the resection site. (C) The tumor is then en bloc resected with the aid of the instruments. (D) Finally the base of the tumor is coagulated by the laser fiber, as well as the remaining adhesions. (Source: Kramer <i>et al.</i> , 2015).	4
Figure 1.3: Mechanisms. (a) Rigid-body mechanism (RBM). (b) Fully compliant mechanism (CM). (Source: Cao <i>et al.</i> , 2015).	6
Figure 1.4: Prototype of the fully compliant and monolithic kidney gripper and manipulator in its inactive and gripping mode, respectively. (Source: Kota <i>et al.</i> , 2005).	6
Figure 1.5: The scissors-forceps end-effector design at its neutral, grasping and cutting positions. (Source: Frecker <i>et al.</i> , 2005).	6
Figure 1.6: Compliant suturing device. (a) Prototype. (b) Suture of a porcine stomach. (Source: Cronin <i>et al.</i> , 2008).	7
Figure 1.7: Compliant forceps for NOTES. (a) Prototype. (b) Optimal designs. (Source: Aguirre <i>et al.</i> , 2011).	7
Figure 1.8: Compliant articulation structure. (a) Integration of a surgical tool tip. (b) Designs of the compliant structure to be tested. (Source: Liu <i>et al.</i> , 2013).	7
Figure 1.9: Stress-strain diagram of a typical tensile test. (Source: Hertzberg, 1989).	10
Figure 1.10: Flexible cantilever beam. (Source: Howell, 2013).	11
Figure 1.11: Flexible cantilever beam with a moment applied at its free end. (Source: Beam Deflection Formulae).	12
Figure 1.12: Large deflection of a cantilever beam. (Source: Su, 2009).	13
Figure 1.13: Basic computational procedure. (Source: Frecker <i>et al.</i> , 1997).	15
Figure 1.14: Illustration of a general compliant mechanism and the beam element used for its discretization by the chain algorithm. (Source: Howell, 2001, p. 261).	16
Figure 1.15: (a) Cantilever beam element with a force applied at one of its ends. (b) Representation of the beam element with the pseudo-rigid-body model. (Source: Howell, 2001, p.146).	17
Figure 1.16: Schematic illustration for the ‘load path representation’ procedure. (Source: Lu and Kota, 2005).	18
Figure 1.17: Module optimization model of a four-bar mechanism. (Source: Cao <i>et al.</i> , 2015).	19
Figure 1.18: Processing steps for a medical product or device.	21
Figure 1.19: Schematic illustration of the pressure inside a sterilization chamber. Phase I: removal of air and penetration of steam. Phase II: sterilization. Phase III: exhaust and drying. (Source: van Doornmalen <i>et al.</i> , 2013).	23

Figure 1.20: Representation of different critical features of a MIS scissors including: hollow instrument, sliding metal/metal surface, insulation, thread and gap features (Source: Working Group Instrument Preparation, 2001a).	25
Figure 1.21: Commercially available Process Challenge Devices (PCDs). (a) Steri-Record® Compact-PCD® provided by gke GmbH. (b) ISP® Helix Test System provided by Sentry Medical.	26
Figure 1.22: Schematic illustration of a Helix PCD with its components: 1. Capsule where the indicator is hosted. 2. Gasket to close the capsule. 3. Chemical or biological indicator. 4. Connector between the tube and the capsule. 5. Open end where the steam enters. 6. Tube along which the steam penetration takes place. (Source: de Bruijn and van Drongelen, 2005).	27
Figure 1.23: “Hollow PCD Instrument” simulating lumens accessible from one or both ends with a length of 500 mm and a 0.5 mm inner diameter. (Source: Working Group Instrument Preparation, 2001a).	27
Figure 2.1: Surgical manipulator attached to the actuation unit used to reproduce the movements at the preliminary experiment about surgical workspace coverage.	35
Figure 2.2: Experimental setup with the first marking configuration (a) and the final one (b).	36
Figure 2.3: Solution structure for the work regarding the mechanical characterization and the medical processability of a surgical instrument.	38
Figure 2.4: General solution process of the present work.	39
Figure 2.5. Solution process – Mechanical Characterization.	40
Figure 2.6: Solution process – Medical Processability.	41
Figure 2.7: Functional prototype of the Double Arm Endoscopic Mini-Manipulator System (MiMed) based on compliant mechanisms in its overtube, as well as in its both arms.	45
Figure 2.8: Geometry and representative parameters of the compliant mechanism.	45
Figure 2.9: Three test samples showing different geometric values for the parameters to be analyzed. (a) Length, L. (b) Width, b.	48
Figure 2.10: Dog bone tension test specimens.	49
Figure 2.11: Experimental setup for the required tensile test with the corresponding dog bone specimen: (1) furnace, (2) servo hydraulic actuator, (3) thermocouples and (4) dog bone specimen.	49
Figure 2.12: Stress-strain diagrams of one of the corresponding nitinol dog bone specimens: (a) detailed, (b) general.	50
Figure 2.13: Different PCDs already packaged and ready for the sterilization process.	52
Figure 2.14: PCD finishing process with the grinding machine.	52
Figure 2.15: Self-adjusting crimping pliers used for the closing of one of the tube ends.	53
Figure 2.16: Schematic illustration of the processing steps.	54
Figure 2.17: Heat-sealed plastic and paper peel-open pouch with one of the PCDs inside it.	57
Figure 2.18: Qualitative measurement of the specimen’s turbidity compared with the positive control.	62

Figure 2.19: Spectrophotometer with a 96-well plate containing 100 μ l swabs of each PCD.	63
Figure 3.1: Experimental setup. (1) Force sensor. (2) Microscope camera stand. (3) Softwares. (4) Digital microscope camera. (5) Force-displacement monitor. (6) Displacement sensor. (7) Adapter. (8) Compliant mechanism. (9) Screw cap. (10) Side screw.....	66
Figure 3.2: Pictures taken during the realization of the experiment: starting point, most deflected position and final remaining plastic deformation. Compliant mechanism with following measures: (a) $L = 3$ mm, $h = 0.3$ mm and $b = 0.5$ mm; (b) $L = 7$ mm, $h = 0.3$ mm and $b = 0.5$ mm.....	68
Figure 3.3: Experimental data regarding the maximum deflection angle in terms of the beam width parameter, b	69
Figure 3.4: Readings of the force-displacement monitor display for the compliant mechanisms with different values of beam width b . (a) $b = 0.25$ mm. (b) $b = 0.50$ mm. (c) $b = 0.75$ mm. (d) $b = 1.0$ mm.	70
Figure 3.5: Experimental data regarding the maximum deflection angle in terms of the beam length parameter, L	71
Figure 3.6: Experimental data regarding the maximum deflection angle in terms of the beam thickness parameter, h	71
Figure 3.7: Setup for the analysis of the PCDs. (1) 96-well plate. (2) Autoclavable 200 μ l pipette microtips. (3) 15 ml plastic tubes with inoculation solution. (4) 200 μ l adjustable pipette. (5) Sterile broth solution. (6) Biological safety cabinet.....	74
Figure 3.8: Sterilization results for inoculated lumens of different internal diameters and lengths 24h, 48 h and one week after performing the experiments – Part I.....	75
Figure 3.9: Sterilization results for inoculated lumens of different internal diameters 24h, 48 h and one week after performing the experiments – Part II.....	76
Figure 3.10: Sterilization results for inoculated lumens of different internal diameters 24h, 48 h and one week after performing the experiments – Part III.	77
Figure 3.11: Sterilization results for inoculated lumens of different internal diameters 24h, 48 h and one week after performing the experiments – Part IV.	77
Figure 3.12: Negative and positive controls states one week after the realization of one of the rounds of the experiments.....	78

LIST OF TABLES

Table 1.1: Spaulding classification of medical devices.	20
Table 1.2: Summary of advantages of commonly used sterilization technologies.	22
Table 1.3: Summary of data regarding limiting geometric values obtained with different processing techniques.	30
Table 1.4: Processing of real surgical instruments tested with different sterilization techniques.....	31
Table 1.5: Summary of disadvantages of commonly used sterilization technologies.	33
Table 2.1: Values of the previous polyamide and titanium structures.	46
Table 2.2: Geometric design parameters of the compliant structure: length L (mm), thickness h (mm) and width b (mm).	46
Table 2.3: Results of the three different tensile test and the average of the resulting values. Nitinol material properties, namely Elastic modulus, E, and Yield strength, σ_{yield} respectively.	50
Table 2.4: Initially conceived geometrical values for the PCDs regarding length and diameter.	51
Table 3.1: Selection of the combination of parameters conforming the compliant structure used for the experiments.	65
Table 3.2: Specifications of the PCDs tested.	79

Appendix A – Nitinol Material Certificate

This Appendix contains the certificate of the material used for the compliant mechanism.

Materialzertifikat



Memry GmbH
Am Kesselhaus 5
79576 Weil am Rhein
phone +49 7621 913410
fax +49 7621 91341 127
www.memry.com

Legierung	NiTi-Alloy	S	
Artikel	Stange		
Lieferdatum	12.05.2016		
Herstelldatum	07.03.2016		
Kunde	Technische Universität München		

chemische Zusammensetzung Herstellerangabe											
Ni [wt-%]	Ti [wt-%]	Cr [wt-%]	Cu [wt-%]	Fe [wt-%]	Nb [wt-%]	Co [wt-%]	C [ppm]	O [ppm]	H [ppm]	N+O [ppm]	others [wt-%]
55,96	bal	0,0046	0,0007	0,0130	0,0001	0,0002	335	351	<50	368	<0,2

Rohmaterial per ASTM	metallurgische Eigenschaften Gußzustand		
	Einschlüsse	Flächenanteil [%]	Korngröße
F2063-12	19,05	1,14	6

Umwandlungstemperatur Gußzustand							
Umwandlungstemperatur, vollständig geglühter Zustand	As [°C]	Apeak [°C]	Af [°C]	Ms [°C]	Mpeak [°C]	Mr [°C]	
	-21	-12	-7				

Kaltumformung			
Anlage			
Art der Umformung	<input type="radio"/> Ziehen	<input type="radio"/> Walzen	<input checked="" type="radio"/> Keine
Umformgrad (log)	keine		

Wärmebehandlung nach Kaltumformung	
Behandlung	Heiß verformt
Oberflächenbehandlung	spitzenlos geschliffen

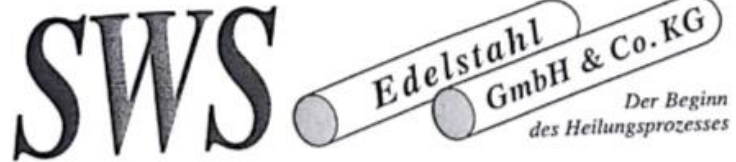
Geometrie	
Durchmesser	12,7 mm
Länge	0,88 m

Eigenschaften (im Lieferzustand)			
Eigenschaften	Wert	Einheit	
Zugfestigkeit	937,6	MPa	
Bruchdehnung	18	%	
Plastische Dehnung	k.A.	%	
Obere Plateauspannung	k.A.	MPa	
Untere Plateauspannung	k.A.	MPa	
Aktiver Af	k.A.	°C	

Appendix B – Stainless Steel Material Certificate

This Appendix contains the certificate of the material used for the Process Challenge Devices.

Carl-Benz-Str. 32
78576 Emmingen
Tel.: 0 74 65 - 92 03 04
Fax: 0 74 65 - 92 03 06
Email: mail@sw-stahl.de
Internet: sw-stahl.de



SWS Edelstahl GmbH & Co. KG · Carl-Benz-Str. 32 · 78576 Emmingen-Liptingen

Prüfbescheinigung

Firma
SWS Edelstahl GmbH & Co. KG
Carl-Benz-Straße 32
DE 78576 Emmingen-Liptingen 1

Nr. 2016/2542
DIN 50049
EN 10204 3.1
Blatt 1 von 1

Auftragsdaten		Erzeugnis-Nr.	Lieferzustand				
Ihr Auftrag Nr.	Datum	89/3477.005	entspr. Auftragsbestätigung				
988239	15.06.2016	Liefercharge: 160754					
Artikel: Präzisionsfeinrohr							
Abmessung	Tol.D _A [mm]	Tol.D _I [mm]					
0,70 x 0,100 mm	+0/-0,02	+0,02/-0					
Ist - Werte	D _A [mm]	D _I [mm]					
	0,685-0,689	0,51					
Mechanische Eigenschaften							
Härte	Rm [N/mm ²]	Ra (innen) [µm]	Ra (ausen) [µm]				
zughart	1355,11	0,654-0,849	0,137-0,351				
Chemische Analyse:							
Schmelz-Nr.:	0661	Entspricht Werkstoff: 1.4301					
C %	Si %	Mn %	P %	S %	Cr %	Ni %	N %
0,021	0,410	1,370	0,023	0,001	18,300	9,500	0,050

Appendix C – Nitinol Tensile Test

This Appendix contains the information related to the nitinol tensile tests.

4 Probenform

4 Specimen shape

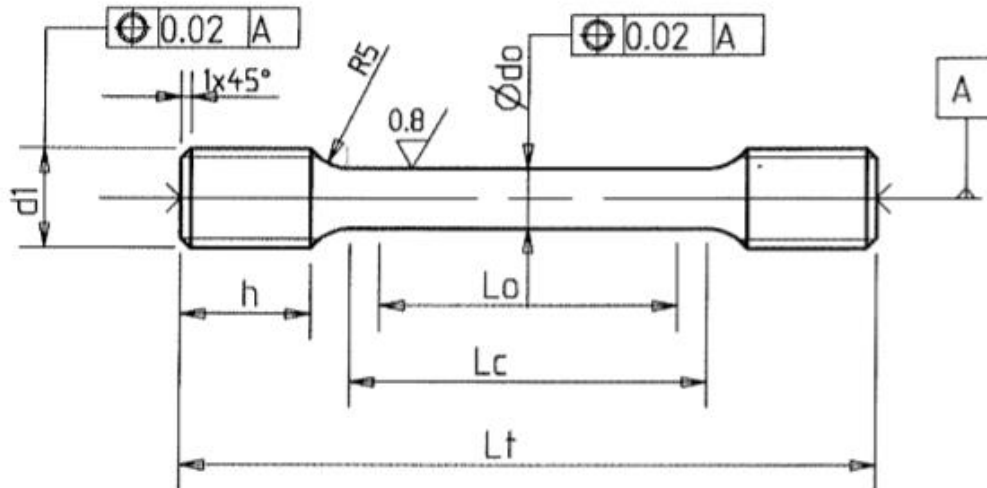


Tabelle 1

Kennung ID	d_0 +0.1	d_1 8g (1)	h +0.5	L_0 +0.5	L_c +0.5	L_t +0.8	Werkstoffauswahl/ Material selection	
							Kerbunempfindlich/ Notch insensitive	Kerbempfindlich (2) Notch sensitiv (2)
A	3	M5	6,5	15	18	37	x	
B	4	M6	7,5	20	24	45	x	
C	5	M8	9,5	25	30	56	x	
D (3)	6	M10	13	30	36	70	x	
E	8	M12	14,5	40	48	85	x	
F	10	M16	15,5	50	60	100	x	
G	5	M10	8,7	25	30	56		x
H	6	M12	12,4	30	36	70		x

(1) Für nationale Hersteller gilt DIN 332-1. Für ausländische Hersteller gilt ISO 6411-A2 / For non-German Manufacturers apply ISO 6411-A2.

(2) Z.B. für TiAl, e.g. for TiAl.

(3) Für Zeitstand- und Kriechversuche mit Dehnungsmessung. For stress rupture- and creep tests with strain measurement.

5 Bemerkungen

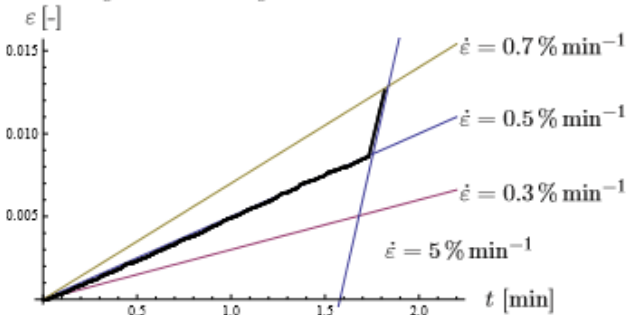
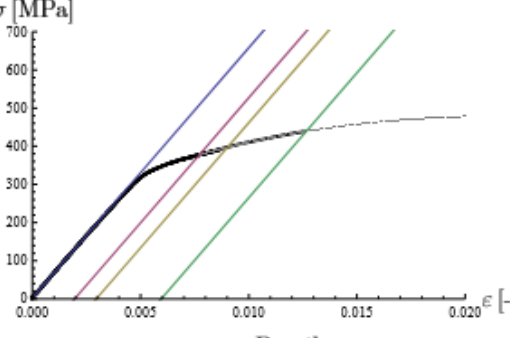
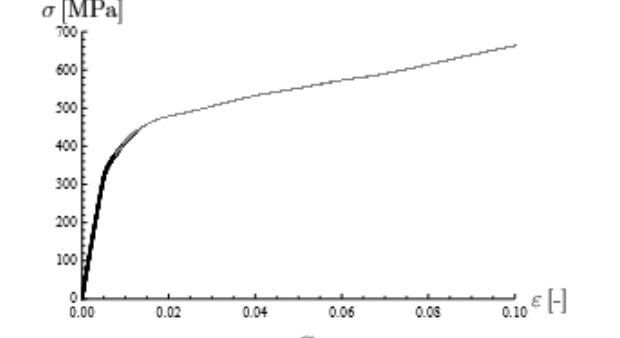
- Durchmesser im Zentrum 0.02-0.03 kleiner als am Ende des Bereichs
- bei geschweißten Proben ist die Lage der Schweißnaht mittig, ± 0.5
- Übergänge kontinuierlich

5 Notes

- the diameter must taper such that it is 0.02-0.03 larger at gage section ends than at the center
- for weld specimens, weld must be located within ± 0.5 of gage section centerline.
- continuous transitions

MPA MASCHINENBAU TUMÜNCHEN		Warmzugversuch	VNr. WZe20170504e
Bearbeiter:	C. Kremaszky	Unterschrift:	
Datum:	2017-05-04		
<i>Prüfparameter</i>		<i>Ergebnis</i>	
Prüf-Nr:	MT21075	Elastizitätsmodul:	65 GPa
Proben-Nr:	1	0,1% Dehngrenze:	353 MPa
Anfangsquerschnitt:	29.03 mm ²	0,2% Dehngrenze:	375 MPa
Probengesamtlänge:	- mm	Zugfestigkeit:	661 MPa
Korr. Versuchslänge:	42 mm	Bruchdehnung A ₅ :	- %
Prüftemperatur:	RT	Brucheinschnürung Z:	- %
<i>Dehnungsentwicklung</i>			
<p style="text-align: center;">Umschalten von Dehnung auf Wegregelung</p>			
<i>Spannungs-Dehnungs-Diagramm (schwarz: Dehnungsaufnehmer; grau: über Maschinenweg berechnet)</i>			
<p style="text-align: center;">Detail</p>		<p style="text-align: center;">Gesamt</p>	
<i>Bemerkungen:</i>			
Bruch erfolgte nicht innerhalb der Messlänge - keine Auswertung der Bruchdehnung.			

MPA MASCHINENBAU TU MÜNCHEN	Warmzugversuch	VNr. WZe20170504d	
Bearbeiter: Datum:	C. Krempaszky 2017-05-04	Unterschrift:	
<i>Prüfparameter</i>		<i>Ergebnis</i>	
Prüf-Nr:	MT21075	Elastizitätsmodul:	69 GPa
Proben-Nr:	2	0,1% Dehngrenze:	382 MPa
Anfangsquerschnitt:	28.27 mm ²	0,2% Dehngrenze:	399 MPa
Probengesamtlänge:	- mm	Zugfestigkeit:	663 MPa
Korr. Versuchslänge:	39 mm	Bruchdehnung A ₅ :	- %
Prüftemperatur:	RT	Brucheinschnürung Z:	- %
<i>Dehnungsentwicklung</i>			
<p style="text-align: center;">Umschalten von Dehnungs auf Wegregelung</p>			
<i>Spannungs-Dehnungs-Diagramm (schwarz: Dehnungsaufnehmer; grau: über Maschinenweg berechnet)</i>			
<p style="text-align: center;">Detail</p>		<p style="text-align: center;">Gesamt</p>	
<i>Bemerkungen:</i>			
Bruch erfolgte nicht innerhalb der Messlänge - keine Auswertung der Bruchdehnung.			

MPA <small>MASCHINENBAU TU MÜNCHEN</small>	Warmzugversuch		VNr. WZe20170504c
Bearbeiter: Datum:	C. Kremaszky 2017-05-04	Unterschrift:	
Prüfparameter Prüf-Nr: MT21075 Proben-Nr: 3 Anfangsquerschnitt: 28.75 mm ² Probengesamtlänge: - mm Korr. Versuchslänge: 42 mm Prüftemperatur: RT		Ergebnis Elastizitätsmodul: 65 GPa 0,1% Dehngrenze: 356 MPa 0,2% Dehngrenze: 378 MPa Zugfestigkeit: 668 MPa Bruchdehnung A ₅ : - % Brucheinschnürung Z: - %	
Dehnungsentwicklung  <p style="text-align: center;">Umschalten von Dehnung auf Wegregelung</p>			
Spannungs-Dehnungs-Diagramm (schwarz: Dehnungsaufnehmer; grau: über Maschinenweg berechnet)			
 <p style="text-align: center;">Detail</p>		 <p style="text-align: center;">Gesamt</p>	
Bemerkungen: Bruch erfolgte nicht innerhalb der Messlänge - keine Auswertung der Bruchdehnung.			